NASA CR-54884
PWA-2933

FINAL REPORT
COMPRESSOR RESEARCH PACKAGE FOR RESEARCH AND DEVELOPMENT OF HIGH PERFORMANCE AXIAL-FLOW TURBOMACHINERY

written by
R. Cohen, W. K. Gilroy, R. D. Marchant

approved by
P. Bolan

prepared for

NATIONAL AERONAUTICS AND SPACE ADMINISTRATION

CONTRACT NAS3-4179

Pratt & Whitney Aircraft DIVISION OF UNITED AIRCRAFT CORPORATION

Requests for copies of this report
should be referred to:

National Aeronautics and Space Administration
Scientific and Technical Information Facility
P.O. Box 33, College Park, Maryland 20740

NASA CR-54884
PWA-2933

FINAL REPORT
COMPRESSOR RESEARCH PACKAGE FOR RESEARCH AND DEVELOPMENT OF HIGH PERFORMANCE AXIAL-FLOW TURBOMACHINERY

written by

R. Cohen, W. K. Gilroy, R. D. Marchant

approved by

P. Bolan

March 1967

prepared for

NATIONAL AERONAUTICS AND SPACE ADMINISTRATION

CONTRACT NAS 3-4179

Technical Management
NASA Lewis Research Center
Cleveland, Ohio

Space Power System Division
Jack A. Heller

Fluid System Components Division
Consultant - Calvin L. Ball

Pratt & Whitney Aircraft DIVISION OF UNITED AIRCRAFT CORPORATION

#46

FINAL REPORT

COMPRESSOR RESEARCH PACKAGE FOR RESEARCH AND DEVELOPMENT OF HIGH PERFORMANCE AXIAL-FLOW TURBOMACHINERY

written by

R. Cohen, W. K. Gilroy, R. D. Marchant

approved by
P. Bolan

ABSTRACT

The National Aeronautics and Space Administration is conducting an evaluation of candidate Brayton-cycle turbomachinery configurations. As part of this program, Pratt & Whitney Aircraft has designed a turbine-compressor incorporating a single-stage axial-flow turbine driving a six-stage axial-flow compressor supported on gas bearings. A compressor research package was provided to permit evaluation of the aerodynamic performance of the compressor. The compressor research package incorporates oil-lubricated rolling-contact bearings. The aerodynamic design of the axial-flow compressor and the mechanical design of the compressor research package are discussed, and the results of mechanical testing are presented.

FOREWORD

This report was produced in accordance with NASA Contract NAS3-4179 under the technical management of Jack A. Heller and in consultation with Calvin L. Ball, NASA Lewis Research Center, Cleveland, Ohio. It describes the design and mechanical testing of the compressor research package produced in accordance with Article I, Section A of the contract.

TABLE OF CONTENTS

LIST OF FIGURES

LIST OF FIGURES (Cont'd)

LIST OF TABLES

I. SUMMARY

The compressor research package is a test rig intended to provide aerodynamic performance data for the Brayton-cycle axial flow compressor. This compressor is a six-stage unit having a tip diameter of approximately 3.5 inches and was designed to provide a high efficiency potential.

The compressor research package provides a convenient mechanical configuration for aerodynamic testing. The unit with unbladed rotor has been constructed and tested mechanically to twenty per cent over its design speed. The complete unit was assembled and delivered to the National Aeronautics and Space Administration.

II. INTRODUCTION

The National Aeronautics and Space Administration is conducting an evaluation program of candidate Brayton-cycle turbomachinery configurations. As part of this program, Pratt & Whitney Aircraft has designed a turbine-compressor incorporating a single-stage axial-flow turbine driving a six-stage axial-flow compressor supported on gas bearings. A compressor research package was provided to permit evaluation of the aerodynamic performance of the compressor. The compressor research package incorporates oil-lubricated rolling-contact bearings.

The compressor for the turbine-compressor was designed to provide high efficiency and reliability potential. The specific compressor design conditions for the turbine-compressor were as follows:

working fluid	argon	total pressure ratio	2.30
flow rate (lb/sec)	0.611	operating life (hours)	10,000
inlet total temperature (°R)	536	rotational speed (rpm)	50,000
inlet total pressure (psia)	6.0	maximum speed (rpm)	60,000

The rotational speed was selected to provide low compressor aerodynamic losses, low bearing losses, and margin from critical speeds.

The compressor research package incorporates the aerodynamic compressor configuration of the turbine-compressor. The design point for the compressor research package had a slightly different inlet gas temperature than the turbine-compressor. Therefore, the design conditions for the compressor research package were slightly different to provide proper aerodynamic similarity. The design conditions for the compressor research package were:

working fluid	argon	total pressure ratio	2.30
flow rate (lb/sec)	0.621	rotational speed (rpm)	49,250
inlet total temperature (°R)	520	maximum speed (rpm)	59,100
inlet total pressure (psia)	6.0		

Particular compressor research package design objectives included high mechanical integrity, versatility, and ease of assembly and disassembly. The package is capable of operating at inlet pressures as high as 15 psia. The complete compressor research package is shown in Figures 1 and 2.

The discussion that follows begins with a description of the compressor blading and aerodynamic design, followed by a description of the compressor research package design. The results of the mechanical tests of the compressor research package are presented and a description of certain component development tests is included.

III. COMPRESSOR AERODYNAMIC DESIGN

The basic objective in the design of the Brayton-cycle axial-flow compressor was to provide a machine of high efficiency at the design operation conditions. Of particular importance, in an axial compressor of the small size and type required, is attention to effects of Reynolds number on viscous losses, clearance losses and exit ducting losses. To minimize the Reynolds number effects, conservatively loaded airfoils of reasonable size are required. Clearance losses are reduced by providing the minimum clearances consistent with mechanical integrity. Low velocities and reasonable diffusion rates are necessary to minimize exit duct losses.

The design of the Brayton-cycle axial-flow compressor involved the selection of a significant number of design variables. First the gas triangles were selected and then airfoils were chosen to produce the desired gas behavior. Included in the gas triangle selection is the specification of rotor speed, the number of compressor stages, and the inner and outer wall geometry.

Gas Triangle Selection

Since the turbine drives the compressor directly, the shaft rotational speed is one of the first design considerations. Initial analysis indicated that efficient turbines could be designed over a reasonable range of rotational speeds. Therefore, the compressor design was the governing factor in the speed selection.

The first compressor parameter reviewed was the design rotational speed. Compressor speeds in the range from 50,000 to 60,000 rpm were examined, based on an assumption of constant axial velocity of 305 ft/sec and constant mean diameter through a 5-stage machine. A constant swirl angle radially of 75 degrees leaving the inlet guide vanes was employed. The following tabulation indicates the effects of speed on the blade length, blade loading in terms of the static pressure rise, $\Delta p/q$, and efficiency increment.

Speed, rpm	Constant Mean Diameter, inches	Blade Length, inches In	Avg.	Out	Loading, $\Delta p/q$ R	M	T	Efficiency, Increment, per cent
						rotor		
50,000	3.42	0.72	0.60	0.48	0.51	0.42	0.34	base
						stator		
					0.47	0.38	0.31	
						rotor		
60,000	2.85	0.82	0.70	0.57	0.55	0.42	0.32	+0.9
						stator		
					0.52	0.38	0.26	

The higher speed offers some benefit in efficiency and a small advantage in blade length but at increased loading at the blade and vane roots. The reduction in compressor inner diameter with the resultant mechanical arrangement and the reduced critical speed, as well as the potential increase in bearing losses at the higher speed, indicated that 50,000 rpm is the best compressor speed. However, this study included a reduction in compressor diameter as speed was increased. The situation with a constant inner diameter was also examined at the two speeds with the following result.

Speed, rpm	Constant Inner Diameter, inches	Blade Length, inches In	Avg.	Out	Loading, $\Delta p/q$ R	M	T	Efficiency Increment, per cent
						rotor		
					0.52	0.45	0.38	
50,000	2.54	0.72	0.61	0.50		stator		base
					0.54	0.42	0.34	
						rotor		
					0.45	0.35	0.28	
60,000	2.54	0.72	0.61	0.50		stator		-0.3
					0.47	0.35	0.28	

The higher speed produced higher velocities relative to the blades, resulting in Mach number losses in the compressor. Also the high speed would produce higher bearing losses and would require operation closer to the critical speed (bent shaft). Therefore, 50,000 rpm was the final selection for the compressor design speed.

A compressor with a constant inner diameter provides longer blades and some advantages in mechanical design compared with a constant mean or tip diameter. The above tabulations indicate that a constant inner diameter selection increases blade and vane loading, particularly stator root loading. Therefore, two design parameters were evaluated for constant inner diameter machines to reduce rotor and stator loadings: the number of stages and the radial swirl distribution leaving the inlet guide vanes. A six-stage machine with a constant inner diameter of 2.54 inches and the same axial velocity as before was used as the basis of comparison. First the radial swirl distribution was examined with the following result:

Swirl Angle, degrees R	Swirl Angle, degrees T	Loading, $\Delta p/q$ R	Loading, $\Delta p/q$ M	Loading, $\Delta p/q$ T	Efficiency Increment, per cent
			rotor		
		0.46	0.40	0.33	
75	75		Stator		base
		0.46	0.35	0.28	
			rotor		
		0.42	0.38	0.34	
90	75		stator		+0.4
		0.39	0.30	0.22	

The 90 to 75-degree swirl variation from root to tip was selected and the effects of the number of stages were examined.

Number of Stages	Loading, $\Delta p/q$ R	Loading, $\Delta p/q$ M	Loading, $\Delta p/q$ T	Efficiency Increment, per cent
		rotor		
	0.49	0.44	0.40	
5		stator		0
	0.48	0.37	0.28	
		rotor		
	0.42	0.38	0.34	
6		stator		base
	0.39	0.30	0.22	
		rotor		
	0.38	0.33	0.30	
7		stator		-0.2
	0.32	0.24	0.17	

The predicted efficiency variation between five, six, and seven stages is very small, but the rotor and stator loadings are reduced significantly as the number of stages is increased. Since this compressor operates at low Reynolds number, the six-stage compressor was selected to obtain more conservative loadings and greater design margin than a five-stage configuration would provide.

The six-stage design has higher rotor and stator loadings at the root than at

the tip. A radial total pressure variation, maintained at each stator discharge, five per cent higher at the root than at the mean diameter, was evaluated in an effort to reduce the root loadings, with the following result:

Radial Total Pressure Variation		Loading, $\Delta p/q$ R	M	T	Efficiency Increment, per cent
uniform	rotor	0.42	0.38	0.34	base
	stator	0.39	0.30	0.22	
5% higher at root	rotor	0.38	0.38	0.34	+0.05
	stator	0.31	0.30	0.31	

The negative total pressure slope provides a significant reduction in root loading, particularly in the stators, with practically no change in efficiency. Therefore, the five per cent negative slope was selected for the first four stages, but was reduced in the last two stages to present a more uniform profile to the radial diffuser.

The selection of axial velocity is particularly important in the design of the Brayton-cycle compressor because of the strong influence of exit diffuser and scroll losses on the overall performance of the compressor. Figure 3 indicates the loss in compressor efficiency flange to flange, as a function of the Mach number leaving the last stator and entering the diffuser. The axial velocity level also affects the rotor and stator loading, the blade and vane length, and the airfoil Reynolds numbers. Therefore an increase in axial velocity level through the machine was evaluated with the following results:

Axial Velocity, ft/sec In	Out	Blade Length, inches In	Avg.	Out		Loading, $\Delta p/q$ R	M	T	Efficiency Increment, per cent
305	305	0.72	0.61	0.50	rotor	0.38	0.38	0.34	base
					stator	0.31	0.30	0.31	
335	335	0.67	0.56	0.46	rotor	0.37	0.37	0.36	-0.6
					stator	0.29	0.27	0.27	

A major portion of the reduction in efficiency as axial velocity is increased is due to an increase in the diffuser and scroll losses. Therefore, the 305 ft/sec level was selected at the discharge of the compressor. In order to realize some of the advantages of higher axial velocity without introducing exit losses, a stagewise variation in axial velocity was examined with adjustment in stage loading to hold the loading levels nearly uniform.

Axial Velocity, ft/sec		Blade Length, inches			Loading, $\Delta p/q$			Efficiency Increment, per cent
In	Out	In	Avg.	Out	R	M	T	
						rotor		
305	305	0.72	0.61	0.50	0.38	0.38	0.34	base
						stator		
					0.31	0.30	0.31	
						rotor		
404	305	0.60	0.55	0.50	0.36	0.38	0.38	-0.1
						stator		
					0.29	0.28	0.29	
						rotor		
540	305	0.50	0.50	0.50	0.36	0.39	0.40	-0.6
						stator		
					0.30	0.30	0.31	

The highest inlet axial velocity corresponding to a constant blade height through the machine, involves efficiency penalties due to Mach number effects and increased stage loading as the mean diameter is reduced. Some increase in axial velocity produces a significant increase in the stator Reynolds numbers, therefore, 404 ft/sec was selected for the inlet axial velocity.

In selecting the design velocity triangles, relatively high design losses have been employed. If very low losses were assumed in the design and if the machine actually were to produce larger losses, the exit blade length would be short and the exit velocity would be high. The overall result would be excessive diffuser and scroll losses. Conversely, if high losses are employed in the design and if lower losses are encountered, the exit velocity will be lower than the design value. The result will provide a two fold gain: lower losses in the exhaust system, coupled with the lower losses in the compressor. The radial loss distributions used in the compressor design are presented in Figures 4 and 5.

Since high design losses were assumed in the design of the compressor, they do not provide a correct basis for the estimated compressor efficiency. The anticipated level of efficiency is 82.5 per cent. The compressor efficiencies, both to scroll exit flange and to the diffuser inlet, are presented in Table 1.

TABLE 1

Estimated Performance

inlet flange total pressure	6.0 psia
inlet flange total temperature	536°R
scroll exit flange total pressure	13.8 psia
scroll exit flange total temperature	793°R
flow	0.611 lb/sec
speed	50,000 rpm
pressure ratio, total-to-total, inlet flange to scroll exit flange	2.3
efficiency, total-to-total, inlet flange to scroll exit flange	82.5 per cent
pressure ratio, total-to-total, inlet flange to compressor exit	2.365
efficiency, total-to-total, inlet flange to compressor exit	85.8 per cent
pressure ratio, total-to-static, inlet flange to compressor exit	2.28
efficiency, total-to-static, inlet flange to compressor exit	84.4 per cent

The design thermodynamic conditions between each row in the compressor are presented in Table 2. Figure 6 indicates the nomenclature employed in this table. The design gas triangles are presented in Table 3. These design conditions include the effects of the radial loss distributions presented in Figures 4 and 5. The gas properties used in developing the compressor design were based on:

NASA TR R-132, 1962, "Estimated Viscosities and Thermal Conductivities of Gases at High Temperatures", by R. A. Svehla

"Tables of Thermodynamic and Transport Properties of Air, Argon, Carbon Dioxide, Carbon Monoxide, Hydrogen, Nitrogen, Oxygen, and Steam", by J. Hilsenroth and others, Pergamon Press, 1960, (formerly NBS Circular 564)

The actual and effective flow areas for each row in the compressor are presented in Table 4. This table includes the actual root and tip diameters of each blade and vane row and the effective diameters allowing for the wall boundary layer growth.

TABLE 2

Mean Design Thermodynamic Conditions

Mean at Inlet to Each Row

Row	P_o, psfa	T_o, °R	P_s, psfa	T_s, °R	Corrected Flow lb/sec	Corrected Speed, rpm	Axial Velocity ft/sec	Stage Work Btu/lb
IGV	864	536	829.8	527.4			231.5	
R_1	855	536	750.5	508.8	1.535	49,182	407.9	
S_1	1056	588	887.8	548.8	1.302		399.1	6.51
R_2	1046	588	929.7	561.1	1.314	46,957	407.5	
S_2	1248	636	1073.9	599.1	1.145		392.5	5.95
R_3	1238	636	1118.1	610.8	1.155	45,150	393.5	
S_3	1440	680	1271.0	646.9	1.026		374.1	5.48
R_4	1430	680	1315.9	657.8	1.034	43,665	369.2	
S_4	1636	722	1472.8	692.1	0.931		354.5	5.20
R_5	1627	722	1517.1	702.0	0.936	42,376	348.8	
S_5	1840	763	1682.7	735.7	0.851		333.3	5.05
R_6	1831	763	1726.9	744.9	0.855	41,222	328.3	
S6	2048	801	1895.7	777.1	0.784		317.4	4.87
diffuser	2039	801	1941.6	786.0			311.4	
scroll exit	1987	801	1980.0	800			82	

TABLE 3

Gas Velocities and Angles Entering Each Row

Per Cent of Effective Area	0	20	40	60	80	100
Inlet Guide Vane						
act. dia. vane inlet	4.100	4.368	4.629	4.885	5.135	5.380
C_m (ft/sec)	264.8	249.3	236.9	226.6	217.7	209.7
C_u (ft/sec)	0	0	0	0	0	0
α (degrees	90.0	90.0	90.0	90.0	90.0	90.0
Rotor 1						
dia. rotor inlet	2.569	2.837	3.081	3.308	3.52	3.72
C_{x1}	412.7	411.8	409.5	406.0	401.5	396.2
U_1	560.5	618.9	672.3	721.7	768	811.6
C_{u1}	2.2	26.3	48.2	68.3	86.8	103.9
W_{u1}	558.3	592.6	624.1	653.4	681.2	707.6
W_1	694.3	721.6	746.5	769.2	790.6	811.1
β_1	36.47	34.80	33.27	31.86	30.52	29.24
α_1	89.7	86.35	83.29	80.45	77.80	75.30
M_1 relative	0.675	0.701	0.725	0.748	0.768	0.788
M_1 absolute	0.401	0.401	0.401	0.400	0.399	0.398
C_1	412.7	412.6	412.3	411.7	410.8	409.6
Stator 1						
dia. stator inlet	2.57	2.825	3.058	3.275	3.478	3.67
C_{x2}	444.6	439.6	412.6	382	348.7	308.2
U_2	560.7	616.2	667.1	714.4	758.8	800.7
C_{u2}	408.7	308.8	296.6	290.9	292.2	326.6
W_{u2}	152.0	307.4	370.5	423.6	466.6	474.1
W_2	469.9	536.5	554.5	570.3	582.5	565.4
β_2	71.13	55.03	48.08	42.05	36.77	33.03
α_2	47.41	54.92	54.29	52.72	50.04	43.34
M_2 relative	0.439	0.504	0.519	0.533	0.543	0.524
M_2 absolute	0.564	0.504	0.476	0.449	0.424	0.416
C_2	603.9	537.2	508.1	480.1	454.9	449.1
Rotor 2						
dia. rotor inlet	2.571	2.812	3.034	3.241	3.436	3.62
C_{x1}	463.1	434.2	415.6	394.6	374.4	356.6
U_1	560.9	613.5	662.0	707.2	749.6	789.8
C_{u1}	2.9	27.6	48.6	65.9	80.5	93.2
W_{u1}	558.0	585.9	613.4	641.2	669.1	696.6

TABLE 3 (Cont'd)

W_1	725.1	729.3	740.9	752.9	766.7	782.5
β_1	39.69	36.54	34.12	31.61	29.23	27.11
α_1	89.65	86.36	83.33	80.51	77.86	75.35
$M_{1\,relative}$	0.663	0.675	0.686	0.697	0.709	0.718
$M_{1\,absolute}$	0.424	0.403	0.387	0.370	0.354	0.338
C_1	463.1	435.1	418.4	400.1	383.0	368.6
<u>Stator 2</u>						
dia. stator inlet	2.572	2.805	3.021	3.222	3.411	3.59
C_{x2}	465.0	441.1	408.6	374.5	339.0	293.7
U_2	561.1	612.0	659.0	702.9	744.1	783.2
C_{u2}	360.5	275.9	276.2	280.9	288.3	326.8
W_{u2}	200.7	336.1	382.8	422.0	455.8	456.4
W_2	506.4	554.6	559.9	564.2	568.0	542.8
β_2	66.66	52.69	46.87	41.59	36.64	32.76
α_2	52.22	57.98	55.95	53.13	49.62	41.94
$M_{2\,relative}$	0.447	0.498	0.502	0.505	0.507	0.478
$M_{2\,absolute}$	0.519	0.467	0.442	0.419	0.397	0.387
C_2	588.3	520.3	493.2	468.1	445.0	439.4
<u>Rotor 3</u>						
dia. rotor inlet	2.573	2.798	3.007	3.202	3.386	3.56
C_{x1}	457.3	422.3	403.1	383.8	365.0	346.9
U_1	561.3	610.5	656.0	698.6	738.6	776.7
C_{u1}	3.2	26.9	47.0	63.9	78.2	90.3
W_{u1}	558.1	583.6	609.1	634.7	660.5	686.3
W_1	721.5	720.4	730.3	741.7	754.5	768.9
β_1	39.33	35.89	33.50	31.16	28.93	26.82
α_1	89.6	86.36	83.36	80.55	77.91	75.40
$M_{1\,relative}$	0.625	0.638	0.648	0.658	0.668	0.671
$M_{1\,absolute}$	0.396	0.375	0.360	0.345	0.331	0.313
C_1	457.3	423.2	405.8	389.1	373.3	358.5
<u>Stator 3</u>						
dia. stator inlet	2.574	2.797	3.003	3.196	3.377	3.550
C_{x2}	455.1	423.7	391.5	358.4	323.8	280.0
U_2	561.6	610.1	655.1	697.2	736.8	774.5
C_{u2}	334.0	256.6	257.5	261.0	268.6	305.2
W_{u2}	227.6	353.5	397.6	436.2	468.3	469.3
W_2	508.8	551.8	558.0	564.5	569.4	546.4
β_2	63.43	50.16	44.56	39.41	34.66	30.83
α_2	53.73	58.80	56.67	53.94	50.32	42.53
$M_{2\,relative}$	0.427	0.476	0.481	0.486	0.489	0.460
$M_{2\,absolute}$	0.474	0.427	0.404	0.382	0.361	0.349
C_2	564.5	495.3	468.6	443.3	420.7	414.2

TABLE 3 (Cont'd)

Rotor 4

dia. rotor inlet	2.576	2.796	2.999	3.190	3.369	3.54
C_{x1}	439.5	401.5	381.2	360.1	341.0	321.1
U_1	562.0	609.9	654.3	695.9	735.1	772.3
C_{u1}	3.5	25.7	44.4	59.8	72.8	83.3
W_{u1}	558.5	584.2	609.9	636.1	662.3	689.0
W_1	710.7	708.9	719.2	730.8	745.0	760.4
β_1	38.20	34.50	32.01	29.52	27.24	24.98
α_1	89.55	86.34	83.36	80.58	77.95	75.45
$M_{1\,relative}$	0.588	0.605	0.615	0.625	0.635	0.636
$M_{1\,absolute}$	0.364	0.343	0.328	0.312	0.297	0.277
C_1	439.5	402.3	383.8	365.0	348.7	331.7

Stator 4

dia. stator inlet	2.577	2.796	2.998	3.188	3.367	3.537
C_{x2}	440.5	405.2	371.1	337.5	297.2	252.8
U_2	562.2	609.9	654.1	695.5	734.6	771.7
C_{u2}	323.1	243.7	242.5	245.6	248.9	285.5
W_{u2}	239.1	366.2	411.6	449.9	485.7	486.2
W_2	501.2	546.1	554.2	562.5	569.5	548.0
β_2	61.51	47.90	42.04	36.87	31.46	27.47
α_2	53.74	58.98	56.84	53.96	50.06	41.52
$M_{2\,relative}$	0.403	0.455	0.462	0.468	0.473	0.444
$M_{2\,absolute}$	0.439	0.394	0.370	0.348	0.322	0.309
C_2	546.3	472.8	443.3	417.4	387.6	381.4

Rotor 5

dia. rotor inlet	2.579	2.796	2.998	3.187	3.365	3.534
C_{x1}	426.7	383.3	359.1	336.5	308.8	289.4
U_1	562.7	610.0	654.0	695.2	734.1	771.0
C_{u1}	3.7	24.7	41.8	55.8	65.7	74.9
W_{u1}	558.9	585.4	612.2	639.4	668.3	696.1
W_1	703.2	699.6	709.9	722.5	736.2	754.0
β_1	37.36	33.22	30.39	27.76	24.80	22.57
α_1	89.50	86.32	83.36	80.59	77.98	75.50
$M_{1\,relative}$	0.559	0.578	0.587	0.598	0.608	0.607
$M_{1\,absolute}$	0.339	0.317	0.299	0.261	0.261	0.241
C_1	426.7	384.1	361.5	341.1	315.7	298.9

TABLE 3 (Cont'd)

Stator 5

dia. stator inlet	2.58	2.796	2.997	3.185	3.362	3.531
C_{x2}	404.6	376.2	347.4	318.8	287.1	246.0
U_2	562.9	610.0	653.8	694.8	733.6	770.3
C_{u2}	287.3	227.0	233.7	240.3	250.6	287.6
W_{u2}	275.6	383.0	420.1	454.6	483.0	482.7
W_2	489.4	536.8	545.1	555.3	561.9	541.7
β_2	55.74	44.49	39.59	35.04	30.73	27.01
α_2	54.63	58.90	56.08	53.00	48.88	40.54
$M_{2\,relative}$	0.379	0.434	0.441	0.449	0.452	0.424
$M_{2\,absolute}$	0.384	0.355	0.339	0.322	0.307	0.296
C_2	496.2	439.3	418.6	399.2	381.1	378.5

Rotor 6

dia. rotor inlet	2.582	2.797	2.997	3.184	3.360	3.528
C_{x1}	376.8	350.2	335.8	320.8	306.3	291.9
U_1	563.3	610.2	653.7	694.5	733.1	769.7
C_{u1}	3.6	22.7	39.1	53.1	65.0	75.3
W_{u1}	559.7	587.5	614.6	641.5	668.0	694.4
W_1	674.7	683.9	700.4	717.2	734.7	753.3
β_1	33.95	30.80	28.65	26.57	24.64	22.80
α_1	89.46	86.30	83.36	80.61	78.01	75.54
$M_{1\,relative}$	0.517	0.548	0.563	0.576	0.588	0.586
$M_{1\,absolute}$	0.289	0.281	0.272	0.261	0.251	0.235
C_1	376.8	350.9	338.1	325.2	313.1	301.4

Stator 6

dia. stator inlet	2.584	2.797	2.996	3.182	3.358	3.525
C_{x2}	376.4	356.3	330.7	303.9	274.3	235.2
U_2	563.7	610.3	653.6	694.2	732.6	769.0
C_{u2}	296.8	225.1	225.3	228.2	234.5	272.0
W_{u2}	266.9	385.2	428.4	466.1	498.0	497.0
W_2	461.4	524.7	541.1	556.5	568.5	550.0
β_2	54.66	42.77	37.67	33.10	28.85	25.32
α_2	51.75	57.72	55.74	53.10	49.47	40.84
$M_{2\,relative}$	0.345	0.412	0.426	0.437	0.445	0.417
$M_{2\,absolute}$	0.359	0.331	0.315	0.299	0.283	0.273
C_2	479.3	421.4	400.1	380.0	360.9	359.7
dia. stator exit	2.672	2.878	3.070	3.251	3.423	3.586
C_{x3}	358.7	332.3	318.4	304.6	291.3	281.3
C_{u3}	0	0	0	0	0	0
α_3	90	90	90	90	90	90
$M_{3\,absolute}$	0.266	0.259	0.249	0.238	0.227	0.212

TABLE 4

Actual and Effective Flow Areas

Row	Actual Diameters Entering Root	Actual Diameters Entering Mean	Actual Diameters Entering Tip	Actual Area Entering, sq ft	Avg. Act. Length, inches	Actual Hub/Tip Entering	Effective Diameter Entering, inches Root	Effective Diameter Entering, inches Tip	Effective Area Entering, sq ft	Flow Factor Entering
IGV	4.10	4.74	5.38	0.06618						1.0
R_1	2.545	3.145	3.744	0.04112	0.5873	0.680	2.569	3.72	0.0395	1.0417
S_1	2.545	3.120	3.695	0.03913	0.5628	0.689	2.570	3.67	0.0374	1.0455
R_2	2.545	3.096	3.646	0.03717	0.5433	0.698	2.571	3.62	0.0354	1.0496
S_2	2.545	3.081	3.617	0.03602	0.5288	0.704	2.572	3.59	0.0342	1.053
R_3	2.545	3.067	3.588	0.03488	0.5193	0.709	2.573	3.56	0.0330	1.0567
S_3	2.545	3.062	3.579	0.03453	0.515	0.711	2.574	3.55	0.0326	1.0594
R_4	2.545	3.058	3.571	0.03422	0.5125	0.713	2.576	3.54	0.0322	1.0643
S_4	2.545	3.057	3.569	0.03414	0.5118	0.713	2.577	3.537	0.0320	1.0667
R_5	2.545	3.057	3.568	0.03410	0.5110	0.713	2.579	3.534	0.0318	1.0712
S_5	2.545	3.056	3.566	0.03403	0.5103	0.714	2.580	3.531	0.0317	1.0736
R_6	2.545	3.055	3.565	0.03399	0.5098	0.714	2.582	3.528	0.0315	1.0782
S_6	2.545	3.055	3.564	0.03395	0.5033	0.714	2.584	3.525	0.0314	1.0829
S_6 Exit	2.632	3.129	3.626	0.03391	0.5032		2.672	3.586	0.03135	1.0875

Airfoil Design

The objective in the airfoil selections is to provide blade and vane geometries that will produce the desired gas velocity vectors with minimum losses. A major consideration in the Brayton-cycle compressor design was the operating Reynolds numbers. At higher Reynolds numbers conventional compressors generally indicate some efficiency advantage at the design condition for NACA 6-digit airfoils compared with NACA 4-digit airfoils. For the low Reynolds numbers encountered in this design, airfoils designed to extend the region of laminar boundary layer flow, such as the NACA 6-digit series, increase the possibility of laminar separation. Therefore NACA 4-digit airfoils were selected to provide higher performance potential in this application. An airfoil thickness of nine per cent was selected throughout the machine except in the first and second stage blades, where seven per cent thickness was employed to increase the critical Mach number margin.

The blade and vane chords were selected to provide as high Reynolds numbers as possible, for aspect ratios in the neighborhood of one. The airfoil spacings were selected to provide conservative blade and vane loadings. The design incidence was selected to provide peak efficiency at design conditions. Experimental information indicates a necessary adjustment to the cascade minimum loss incidence angle to achieve peak efficiency in the compressor. In the first two stages the inlet angle is 1 1/2 degrees lower than the inlet angle for cascade minimum loss, while in the last stage the gas angle is 3 degrees higher than the angle for cascade minimum loss. The airfoils selected incorporate increased camber at the blade roots and the stator roots and tips to accommodate the loss profile anticipated and to maintain the energy of the gas near the walls.

Each blade and vane design is described in Table 5 and the airfoil loadings, incidence angles, Reynolds numbers and anticipated deviation angles in Table 6. The inlet guide vane design is also included in these tables. The nomenclature employed in these tables is defined in Figure 7.

The structural design of the compressor blades provides a generous design margin. The blades are made of AMS 4928, a high-strength titanium alloy containing aluminum and vanadium. The centrifugal stresses and unrestrained bending stresses at the design speed of 50,000 rpm are quite low in respect to the allowable stress of approximately 50,000 psi. The blade stresses are summarized in Table 7.

TABLE 5

Blade and Vane Design

Per Cent of Average Actual Length	0	20	40	60	80	100
Inlet Guide Vane						
diameter, actual exit	2.708	2.965	3.222	3.478	3.735	3.992
leading edge angle, α_2*	90.0	89.83	89.57	89.13	88.42	87.55
trailing edge angle, α_3*	90.0	93.28	96.82	100.48	104.12	107.75
camber, θ*	0.0	3.45	7.25	11.35	15.70	20.20
chord angle, α_{ch}	90.0	91.93	93.92	95.93	97.84	99.65
gap/chord ratio, τ/b average	0.4723	0.5092	0.5453	0.5806	0.6150	0.6487
thickness/chord ratio, t/b	0.11	0.11	0.11	0.11	0.11	0.11
chord, b	1.850	1.851	1.855	1.860	1.868	1.877
no. of vanes, Z	12	12	12	12	12	12
airfoil type	NACA 4-digit airfoil with max. camber at 40% of chord					
angle to centerline	20.61°	20.61°	20.61°	20.61°	20.61°	20.61°
Rotor 1						
diameter, avg. actual	2.545	2.780	3.015	3.25	3.485	3.7195
leading edge angle, β_1*	27.50	33.4	34.65	34.60	34.45	34.10
trailing edge angle, β_2*	85.00	66.9	58.0	50.2	42.50	34.9
camber angle, θ*	57.50	33.5	23.35	15.6	8.05	0.80
chord angle, α_{ch}	61.10	53.3	48.6	43.96	39.27	34.6
gap/chord ratio, τ/b	0.5694	0.622	0.6745	0.7271	0.7796	0.8322
thickness/chord ratio, t/b	0.07	0.07	0.07	0.07	0.07	0.07
chord, b	0.61	0.61	0.61	0.61	0.61	0.61
no. of blades, Z	23	23	23	23	23	23
airfoil type	NACA 4-digit airfoil with max. camber at 40% of chord					
Stator 1						
diameter	2.545	2.77	2.995	3.22	3.445	3.6705
leading edge angle, α_2*	45.10	53.50	52.86	51.03	47.93	40.25
trailing edge angle, α_3*	101.66	96.71	92.40	89.45	87.11	85.16
camber angle, θ*	56.56	43.21	39.54	38.42	39.18	44.91
chord angle, α_{ch}	78.10	79.05	76.33	73.82	71.17	66.76
gap/chord ratio, τ/b	0.6663	0.667	0.6676	0.6682	0.6687	0.6692
thickness/chord ratio, t/b	0.09	0.09	0.09	0.09	0.09	0.09
chord, b	0.60	0.6523	0.7046	0.757	0.8093	0.8616
no. of vanes, Z	20	20	20	20	20	20
airfoil type	NACA 4-digit airfoil with max. camber at 40% of chord					

TABLE 5 (Cont'd)

Blade and Vane Design

Rotor 2

diameter, avg. actual	2.545	2.762	2.980	3.197	3.414	3.6315
leading edge angle, β_1*	32.90	37.98	37.44	35.25	33.25	31.85
trailing edge angle, β_2*	79.40	63.60	56.10	49.05	42.00	35.05
camber angle, θ*	46.50	25.62	18.66	13.80	8.75	3.20
chord angle, α_{ch}	60.30	53.27	48.64	43.55	38.50	33.78
gap/chord ratio, τ/b	0.5694	0.618	0.6668	0.7153	0.7639	0.8125
thickness/chord ratio, t/b	0.07	0.07	0.07	0.07	0.07	0.07
chord, b	0.54	0.54	0.54	0.54	0.54	0.54
no. of blades, Z	26	26	26	26	26	26
airfoil type	NACA 4-digit airfoil with max. camber at 40% of chord					

Stator 2

diameter, avg. actual	2.545	2.757	2.968	3.18	3.391	3.6025
leading edge angle, α_2*	50.3	56.78	54.95	51.45	47.0	37.6
trailing edge angle, α_3*	99.7	95.20	91.75	89.30	87.50	85.88
camber angle, θ*	49.4	38.42	36.80	37.85	40.50	48.28
chord angle, α_{ch}	79.3	79.57	76.81	73.92	71.0	66.0
gap/chord ratio, τ/b	0.6663	0.6663	0.6662	0.6662	0.6661	0.6661
thickness/chord ratio, t/b	0.09	0.09	0.09	0.09	0.09	0.09
chord, b	0.50	0.5416	0.5832	0.6248	0.6664	0.708
no. of vanes, Z	24	24	24	24	24	24
airfoil type	NACA 4-digit airfoil with max. camber at 40% of chord					

Rotor 3

diameter, avg. actual	2.545	2.753	2.96	3.168	3.376	3.5835
leading edge angle, β_1*	33.8	37.25	36.75	34.65	32.75	31.15
trailing edge angle, β_2*	75.0	60.70	53.50	47.20	40.50	32.80
camber angle, θ*	41.20	23.45	16.75	12.55	7.75	1.65
chord angle, α_{ch}	58.20	51.27	46.80	42.17	37.40	32.15
gap/chord ratio, τ/b	0.5694	0.6159	0.6624	0.7088	0.7553	0.8018
thickness/chord ratio, t/b	0.09	0.09	0.09	0.09	0.09	0.09
chord, b	0.54	0.54	0.54	0.54	0.54	0.54
no. of blades, Z	26	26	26	26	26	26
airfoil type	NACA 4-digit airfoil with max. camber at 40% of chord					

Stator 3

diameter, avg. actual	2.545	2.751	2.957	3.163	3.369	3.575
leading edge angle, α_2*	46.98	54.22	52.99	49.82	45.07	34.7
trailing edge angle, α_3*	100.34	95.57	92.35	89.62	87.67	86.97
camber angle, θ*	53.36	41.35	39.36	39.80	42.60	52.27
chord angle, α_{ch}	78.25	78.72	76.34	73.42	70.25	65.35

TABLE 5 (Cont'd)

Blade and Vane Design

gap/chord ratio, τ/b	0.6663	0.6661	0.6660	0.6659	0.6658	0.6657
thickness/chord ratio, t/b	0.09	0.09	0.09	0.09	0.09	0.09
chord, b	0.50	0.5406	0.5812	0.6218	0.6624	0.703
no. of vanes, Z	24	24	24	24	24	24
airfoil type	NACA 4-digit airfoil with max. camber at 40% of chord					

Rotor 4

diameter, avg. actual	2.545	2.75	2.955	3.16	3.365	3.570
leading edge angle, β_1*	30.55	33.40	33.05	30.85	29.25	28.28
trailing edge angle, β_2*	75.40	59.70	52.40	45.90	38.20	29.20
camber angle, θ*	44.85	26.30	19.35	15.05	8.95	0.92
chord angle, α_{ch}	57.03	49.08	44.65	39.88	34.63	28.82
gap/chord ratio, τ/b	0.5694	0.6153	0.6612	0.7070	0.7529	0.7988
thickness/chord ratio, t/b	0.09	0.09	0.09	0.09	0.09	0.09
chord, b	0.54	0.54	0.54	0.54	0.54	0.54
no. of blades, Z	26	26	26	26	26	26
airfoil type	NACA 4-digit airfoil with max. camber at 40% of chord					

Stator 4

diameter, avg. actual	2.545	2.75	2.954	3.159	3.364	3.5685
leading edge angle, α_2*	46.60	52.10	50.40	47.60	43.20	32.90
trailing edge angle, α_3*	100.20	96.15	92.85	90.20	88.23	86.80
camber angle, θ*	53.60	44.05	42.45	42.60	45.63	53.90
chord angle, α_{ch}	78.00	78.13	75.52	72.78	69.80	64.40
gap/chord ratio, τ/b	0.6663	0.6661	0.6658	0.6657	0.6656	0.6654
thickness/chord ratio, t/b	0.09	0.09	0.09	0.09	0.09	0.09
chord, b	0.50	0.5404	0.5808	0.6212	0.6616	0.702
no. of vanes, Z	24	24	24	24	24	24
airfoil type	NACA 4-digit airfoil with max. camber at 40% of chord					

Rotor 5

diameter, avg. actual	2.545	2.749	2.954	3.158	3.363	3.567
leading edge angle, β_1*	30.85	32.30	30.65	28.10	25.70	23.35
trailing edge angle, β_2*	67.20	54.50	48.80	43.50	37.50	31.30
camber angle, θ*	36.35	22.20	18.15	15.40	11.80	7.95
chord angle, α_{ch}	52.43	45.58	41.51	37.34	32.77	28.10
gap/chord ratio, τ/b	0.5694	0.6151	0.6609	0.7066	0.7524	0.7981
thickness/chord ratio, t/b	0.09	0.09	0.09	0.09	0.09	0.09
chord, b	0.54	0.54	0.54	0.54	0.54	0.54
no. of blades, Z	26	26	26	26	26	26
airfoil type	NACA 4-digit airfoil with max. camber at 40% of chord					

TABLE 5 (Cont'd)

Blade and Vane Design

Stator 5

diameter, avg. actual	2.545	2.749	2.953	3.157	3.361	3.5655
leading edge angle, α_2*	47.05	49.98	50.02	46.90	42.12	30.85
trailing edge angle, α_3*	100.25	96.42	92.95	90.27	88.59	87.39
camber angle, θ*	53.20	46.44	42.93	43.37	46.47	56.54
chord angle, α_{ch}	78.22	77.35	75.42	72.53	69.51	63.95
gap/chord ratio, τ/b	0.6663	0.6661	0.6659	0.6659	0.6658	0.6658
thickness/chord ratio, t/b	0.09	0.09	0.09	0.09	0.09	0.09
chord, b	0.50	0.5402	0.5804	0.6206	0.6608	0.701
no. of vanes, Z	24	24	24	24	24	24
airfoil type	NACA 4-digit airfoil with max. camber at 40% of chord					

Rotor 6

diameter, avg. actual	2.545	2.749	2.953	3.157	3.361	3.5645
leading edge angle, β_1*	25.45	26.65	25.50	24.05	22.55	20.95
trailing edge angle, β_2*	66.60	56.80	49.70	43.30	36.60	28.60
camber angle, θ*	41.15	30.15	24.20	19.25	14.05	7.65
chord angle, α_{ch}	49.82	44.59	39.96	35.58	30.98	25.55
gap/chord ratio, τ/b	0.5694	0.615	0.6607	0.7063	0.752	0.7976
thickness/chord ratio, t/b	0.09	0.09	0.09	0.09	0.09	0.09
chord, b	0.54	0.54	0.54	0.54	0.54	0.54
no. of blades, Z	26	26	26	26	26	26
airfoil type	NACA 4-digit airfoil with max. camber at 40% of chord					

Stator 6

diameter, avg. actual	2.5885	2.79	2.991	3.192	3.394	3.595
leading edge angle, α_2*	41.80	47.50	45.35	42.20	36.35	24.60
trailing edge angle, α_3*	102.46	100.95	100.80	101.50	103.05	105.50
camber angle, θ*	60.66	53.45	55.45	59.30	66.70	80.90
chord angle, α_{ch}	77.15	78.80	77.80	76.75	74.95	70.70
gap/chord ratio, τ/b	0.6777	0.6761	0.6746	0.6733	0.6723	0.6713
thickness/chord ratio, t/b	0.09	0.09	0.09	0.09	0.09	0.09
chord, b	0.50	0.5402	0.5804	0.6206	0.6608	0.701
no. of vanes, Z	24	24	24	24	24	24
airfoil type	NACA 4-digit airfoil with max. camber at 40% of chord					

TABLE 6

Blade and Vane Loading

Per Cent Inlet Effective Area	0	20	40	60	80	100
Inlet Guide Vane						
diameter, inlet actual	4.011	4.299	4.568	4.823	5.064	5.295
incidence = $\alpha^* - \alpha$	0	-0.19	-0.49	-0.96	-1.57	-2.45
distance to minimum loss angle of attack $\Delta\alpha = \alpha_{min} - \alpha_2$	0.0	0.0	0.0	0.0	0.0	0.0
Reynolds number	102,500	102,200	100,700	98,700	96,600	94,200
diameter, exit effective	2.760	3.045	3.305	3.546	3.772	3.984
deviation = $\alpha_3^* - \alpha$	0.0	0.0	+0.15	+0.36	+0.52	+0.74
Rotor 1						
diameter, inlet	2.569	2.837	3.081	3.308	3.52	3.72
incidence = $\beta_1^* - \beta_1$	-7.9	-0.9	1.4	2.7	3.9	4.9
distance to minimum loss angle of attack $\Delta\beta = \beta_{min} - \beta_1$	-4.0	-0.4	1.2	1.2	1.2	1.5
critical Mach number	0.6563	0.7263	0.7479	0.7675	0.7919	0.8304
throat/pitch area ratio (o/τ)	0.5907	0.6184	0.6060	0.5868	0.5509	0.5534
Reynolds number	91,000	94,500	97,800	100,800	103,700	106,300
loading criteria:						
$\Delta P/Q = \dfrac{P_2 - P_1}{1/2\ \rho_1 W_1^2}$	0.385	0.404	0.405	0.402	0.397	0.393
D factor $= 1 - \dfrac{W_2}{W_1} + \dfrac{\tau}{b}\dfrac{\Delta W_u}{2 W_1}$	0.492	0.382	0.374	0.369	0.370	0.422
pressure loss coefficient $Zp = \dfrac{P_{o_{1\,rel}} - P_{o_{2\,rel}}}{1/2\ \rho_1 W_1^2}$	0.2241	0.0758	0.0701	0.0719	0.0841	0.1661
diameter exit	2.57	2.825	3.058	3.275	3.478	3.67
deviation = $\beta_2^* - \beta_2$	11.4	9.8	8.5	7.7	5.9	3.2
Stator 1						
diameter inlet	2.57	2.825	3.058	3.275	3.478	3.67
incidence = $\alpha_2^* - \alpha_2$	-0.5	-1.15	-1.80	-2.70	-2.70	-3.0
distance to minimum loss angle of attack $\Delta\alpha = \alpha_{min} - \alpha_2$	2.5	1.4	1.0	1.1	1.8	2.5

TABLE 6 (Cont'd)

Blade and Vane Loading

critical Mach number	0.6341	0.6624	0.6716	0.6744	0.6678	0.6592
throat/pitch area ratio (o/τ)	0.7413	0.7739	0.7712	0.7596	0.7313	0.6992
Reynolds number	77,300	77,900	79,800	81,100	81,900	84,900
loading criteria:						
$\Delta P/Q = \dfrac{P_3 - P_2}{1/2\ \rho_2 C_2^2}$	0.305	0.297	0.275	0.257	0.239	0.201
D factor $= 1 - \dfrac{C_3}{C_2} + \dfrac{\tau}{b}\ \dfrac{\Delta C_u}{2\ C_2}$	0.440	0.351	0.327	0.311	0.302	0.340
pressure loss coefficient						
$Zp = \dfrac{P_{o_{2A}} - P_{o_{3A}}}{1/2\ \rho_2 C_2^2}$	0.1392	0.0630	0.0601	0.0601	0.0624	0.1427
diameter exit	2.571	2.812	3.034	3.241	3.436	3.62
deviation $= \alpha_3^* - \alpha_3$	11.50	9.50	8.50	8.70	9.30	10.20
<u>Rotor 2</u>						
diameter inlet	2.571	2.812	3.034	3.241	3.436	3.62
incidence $= \beta_1^* - \beta_1$	-5.8	+1.6	+2.9	+3.2	+3.9	+4.8
distance to minimum loss angle of attack $\Delta\beta = \beta_{min} - \beta_1$	-4.0	0.0	1.3	1.4	1.1	1.5
critical Mach number	0.6860	0.7477	0.7596	0.7702	0.7836	0.8054
throat/pitch area ratio (o/τ)	0.6238	0.6373	0.6145	0.5838	0.5305	0.5291
Reynolds number	84,100	88,200	89,700	91,000	92,800	92,300
loading criteria:						
$\Delta P/Q = \dfrac{P_2 - P_1}{1/2\ \rho_1 W_1^2}$	0.355	0.376	0.386	0.392	0.394	0.400
D factor $= 1 - \dfrac{W_2}{W_1} + \dfrac{\tau}{b}\ \dfrac{\Delta W_u}{2\ W_1}$	0.443	0.347	0.350	0.356	0.366	0.430
pressure loss coefficient						
$Zp = \dfrac{P_{o_{1\,rel}} - P_{o_{2\,rel}}}{1/2\ \rho_1 W_1^2}$	0.2194	0.0758	0.0701	0.0717	0.0829	0.1636
diameter exit	2.572	2.805	3.021	3.222	3.411	3.59
deviation $= \beta_2^* - \beta_2$	9.7	8.9	7.8	6.6	5.5	3.6

TABLE 6 (Cont'd)

Blade and Vane Loading

Stator 2

diameter inlet		2.572	2.805	3.021	3.222	3.411	3.59
incidence $= \alpha_2^* - \alpha_2$		-0.6	-1.2	-1.8	-2.4	-2.95	-3.5
distance to minimum loss angle of attack $\Delta\alpha = \alpha_{min} - \alpha_2$		2.5	1.3	1.0	1.2	1.7	2.5
critical Mach number		0.6486	0.6729	0.6765	0.6750	0.6656	0.6534
throat/pitch area ratio	(o/τ)	0.7689	0.7899	0.7794	0.7612	0.7270	0.6878
Reynolds number		63,000	64,500	66,600	67,400	68,500	68,600
loading criteria:							
$\Delta P/Q = \frac{P_3 - P_2}{1/2\, \rho_2\, C_2^2}$		0.286	0.289	0.274	0.259	0.243	0.209
D factor $= 1 - \frac{C_3}{C_2} + \frac{\tau}{b}\frac{\Delta C_u}{2\, C_2}$		0.410	0.334	0.320	0.312	0.306	0.350
pressure loss coefficient $Zp = \frac{P_{o_{2A}} - P_{o_{3A}}}{1/2\, \rho_2 C_2^2}$		0.1375	0.0630	0.0601	0.0601	0.0616	0.1400
diameter exit		2.573	2.798	3.007	3.202	3.386	3.56
deviation $= \alpha_3^* - \alpha_3$		9.5	8.0	8.15	8.5	9.6	10.8

Rotor 3

diameter inlet		2.573	2.798	3.007	3.202	3.386	3.56
incidence $= \beta_1^* - \beta_1$		-4.7	+1.5	2.8	3.1	3.7	4.5
distance to minimum loss angle of attack $\Delta\beta = \beta_{min} - \beta_1$		-5.0	-2.1	-0.5	-0.6	-0.3	0
critical Mach number		0.6776	0.7340	0.7443	0.7554	0.7660	0.7961
throat/pitch area ratio	(o/τ)	0.5973	0.5990	0.5778	0.5467	0.4928	0.491
Reynolds number		83,700	90,100	92,000	93,500	94,300	91,500
loading criteria:							
$\Delta P/Q = \frac{P_2 - P_1}{1/2\, \rho_1\, W_1^2}$		0.363	0.375	0.382	0.386	0.388	0.398
D factor $= 1 - \frac{W_2}{W_1} + \frac{\tau}{b}\frac{\Delta W_u}{2\, W_1}$		0.427	0.334	0.333	0.335	0.342	0.402

TABLE 6 (Cont'd)

Blade and Vane Loading

pressure loss coefficient						
$Zp = \dfrac{P_{o_{1\,rel}} - P_{o_{2\,rel}}}{1/2\ \rho_1 W_1^2}$	0.1915	0.0658	0.0601	0.0601	0.0713	0.1413
diameter exit	2.574	2.797	3.003	3.196	3.377	3.55
deviation = $\beta_2^* - \beta_2$	9.0	8.8	7.7	7.0	5.8	3.2
Stator 3						
diameter inlet	2.574	2.797	3.003	3.196	3.377	3.55
incidence = $\alpha_2^* - \alpha_2$	-5.0	-4.5	-4.3	-4.7	-5.35	-6.0
distance to minimum loss angle of attack $\Delta\alpha = \alpha_{min} - \alpha_2$	-0.5	-1.1	-0.7	-0.6	-0.4	+0.5
critical Mach number	0.6402	0.6678	0.6713	0.6705	0.6607	0.6443
throat/pitch area ratio (o/τ)	0.7527	0.7814	0.7709	0.7533	0.7168	0.6684
Reynolds number	60,400	63,400	65,100	66,100	66,500	65,000
loading criteria:						
$\Delta P/Q = \dfrac{P_3 - P_2}{1/2\ \rho_2 C_2^2}$	0.280	0.289	0.279	0.270	0.260	0.234
D factor = $1 - \dfrac{C_3}{C_2} + \dfrac{\tau}{b}\dfrac{\Delta C_u}{2\ C_2}$	0.401	0.331	0.321	0.316	0.314	0.364
pressure loss coefficient						
$Zp = \dfrac{P_{o_{2A}} - P_{o_{3A}}}{1/2\ \rho_2 C_2^2}$	0.1361	0.0629	0.0601	0.0601	0.0611	0.1377
diameter exit	2.576	2.796	2.999	3.19	3.369	3.54
deviation = $\alpha_3^* - \alpha_3$	10.0	8.50	8.40	8.70	9.70	11.5
Rotor 4						
diameter inlet	2.576	2.796	2.999	3.19	3.369	3.54
incidence = $\beta_1^* - \beta_1$	-7.0	-0.9	0.8	1.0	2.0	3.4
distance to minimum loss angle of attack $\Delta\beta = \beta_{min} - \beta_1$	-6.0	-3.0	-1.3	-1.3	-2.1	-1.0
critical Mach number	0.6733	0.7267	0.7386	0.7490	0.7682	0.7976
throat/pitch area ratio (o/τ)	0.5668	0.5673	0.5454	0.5124	0.4563	0.4469
Reynolds number	82,400	92,900	93,500	95,000	96,100	92,000

TABLE 6 (Cont'd)

Blade and Vane Loading

loading criteria:						
$\Delta P/Q = \frac{P_2 - P_1}{1/2\ \rho_1\ W_1^2}$	0.361	0.366	0.371	0.373	0.373	0.384
D factor $= 1 - \frac{W_2}{W_1} + \frac{\tau}{b}\ \frac{\Delta W_u}{2\ W_1}$	0.424	0.326	0.322	0.321	0.325	0.385
pressure loss coefficient						
$Zp = \frac{P_{o_{1\ rel}} - P_{o_{2\ rel}}}{1/2\ \rho_1\ W_1^2}$	0.1873	0.0657	0.0601	0.0601	0.0708	0.1390
diameter exit	2.577	2.796	2.998	3.188	3.367	3.537
deviation $= \beta_2^* - \beta_2$	9.5	10.0	9.10	8.0	6.6	3.3
Stator 4						
diameter inlet	2.577	2.796	2.998	3.188	3.367	3.537
incidence $= \alpha_2^* - \alpha_2$	-6.95	-6.95	-6.95	-6.95	-6.85	-6.4
distance to minimum loss angle of attack $\Delta\alpha = \alpha_{min} - \alpha_2$	-1.0	-2.8	-2.6	-2.3	-1.2	0.0
critical Mach number	0.6405	0.6608	0.6646	0.6638	0.6524	0.6432
throat/pitch area ratio (o/τ)	0.7534	0.7708	0.7608	0.7426	0.7025	0.6628
Reynolds number	59,000	62,400	62,500	63,900	62,800	60,600
loading criteria:						
$\Delta P/Q = \frac{P_3 - P_2}{1/2\ \rho_2\ C_2^2}$	0.275	0.287	0.283	0.279	0.282	0.260
D factor $= 1 - \frac{C_3}{C_2} + \frac{\tau}{b}\ \frac{\Delta C_u}{2\ C_2}$	0.399	0.330	0.324	0.323	0.331	0.386
pressure loss coefficient						
$Zp = \frac{P_{o_{2A}} - P_{o_{3A}}}{1/2\ \rho_2\ C_2^2}$	0.1345	0.0629	0.0601	0.0601	0.0606	0.1351

TABLE 6 (Cont'd)

Blade and Vane Loading

diameter exit	2.579	2.796	2.998	3.187	3.365	3.534
deviation = $\alpha_3^* - \alpha_3$	10.0	9.0	8.9	9.3	10.2	11.5
Rotor 5						
diameter inlet	2.579	2.796	2.998	3.187	3.365	3.534
incidence = $\beta_1^* - \beta_1$	-6.2	-1.3	-0.4	0.0	0.9	1.1
distance to minimum loss angle of attack $\Delta\beta = \beta_{min} - \beta_1$	-6.0	-3.3	-2.2	-0.8	0.5	-2.0
critical Mach number	0.6919	0.7342	0.7405	0.7410	0.7457	0.7657
throat/pitch area ratio (o/τ)	0.5490	0.5318	0.5090	0.4745	0.4052	0.4012
Reynolds number	81,600	93,000	95,100	96,800	97,200	92,000
loading criteria:						
$\Delta P/Q = \frac{P_2 - P_1}{1/2\,\rho_1 W_1^2}$	0.373	0.369	0.373	0.373	0.373	0.385
D factor = $1 - \frac{W_2}{W_1} + \frac{\tau}{b}\frac{\Delta W_u}{2 W_1}$	0.420	0.323	0.323	0.323	0.332	0.393
pressure loss coefficient $Z_p = \frac{P_{o_1 rel} - P_{o_2 rel}}{1/2\,\rho_1 W_1^2}$	0.1836	0.0655	0.0601	0.0601	0.0704	0.1368
diameter exit	2.58	2.796	2.997	3.185	3.362	3.531
deviation = $\beta_2^* - \beta_2$	8.7	8.4	8.2	7.8	6.8	5.4
Stator 5						
diameter inlet	2.58	2.796	2.997	3.185	3.362	3.531
incidence = $\alpha_2^* - \alpha_2$	-6.9	-6.6	-6.5	-6.60	-6.90	-7.5
distance to minimum loss angle of attack $\Delta\alpha = \alpha_{min} - \alpha_2$	-1.5	-2.5	-2.2	-1.8	-1.0	-0.5
critical Mach number	0.6373	0.6616	0.6639	0.6619	0.6500	0.6342

TABLE 6 (Cont'd)

Blade and Vane Loading

throat/pitch area ratio (o/τ)	0.7469	0.7719	0.7595	0.7386	0.6969	0.642
Reynolds number	53,600	59,800	61,800	63,000	63,500	58,200
loading criteria:						
$\Delta P/Q = \frac{P_3 - P_2}{1/2\,\rho_2\,C_2^2}$	0.306	0.307	0.295	0.283	0.270	0.242
D factor $= 1 - \frac{C_3}{C_2} + \frac{\tau}{b}\,\frac{\Delta C_u}{2\,C_2}$	0.416	0.344	0.336	0.330	0.328	0.376
pressure loss coefficient						
$Zp = \frac{P_{o_{2A}} - P_{o_{3A}}}{1/2\,\rho_2\,C_2^2}$	0.1330	0.0628	0.0601	0.0601	0.0602	0.1327
diameter exit	2.582	2.797	2.997	3.184	3.360	3.528
deviation $= \alpha_3^* - \alpha_3$	10.2	9.3	8.9	9.4	10.6	12.05

<u>Rotor 6</u>

diameter inlet	2.582	2.797	2.997	3.184	3.360	3.528
incidence $\beta_1^* - \beta_1$	-8.0	-4.3	-3.4	-2.7	-2.1	-1.5
distance to minimum loss angle of attack $\Delta\beta = \beta_{min} - \beta_1$	-6.0	-4.0	-3.1	-2.8	-3.5	-5.5
critical Mach number	0.6783	0.7152	0.7258	0.7371	0.7535	0.7726
throat/pitch area ratio (o/τ)	0.5042	0.4904	0.4736	0.4502	0.3889	0.3861
Reynolds number	78,900	93,700	96,000	98,300	99,900	93,400
loading criteria:						
$\Delta P/Q = \frac{P_2 - P_1}{1/2\,\rho_1\,W_1^2}$	0.390	0.368	0.364	0.359	0.355	0.367
D factor $= 1 - \frac{W_2}{W_1} + \frac{\tau}{b}\,\frac{\Delta W_u}{2\,W_1}$	0.442	0.325	0.317	0.311	0.313	0.374

TABLE 6 (Cont'd)

Blade and Vane Loading

pressure loss coefficient						
$Zp = \dfrac{P_{o_{1\,rel}} - P_{o_{2\,rel}}}{1/2\ \rho_1 W_1^2}$	0.1798	0.0654	0.0601	0.0601	0.0700	0.1347
diameter exit	2.584	2.797	2.996	3.182	3.358	3.525
deviation = $\beta_2^* - \beta_2$	9.7	12.1	10.6	9.3	8.0	8.0
<u>Stator 6</u>						
diameter inlet	2.584	2.797	2.996	3.182	3.35	3.525
incidence = $\alpha_2^* - \alpha_2$	-10.15	-10.25	-10.45	-10.8	-11.35	-12.0
distance to minimum loss angle of attack $\Delta\alpha = \alpha_{min} - \alpha_2$	-3.5	-4.3	-3.8	-3.3	-2.6	-1.9
critical Mach number	0.6173	0.6349	0.6291	0.6202	0.5985	0.5740
throat/pitch area ratio (o/τ)	0.7071	0.7484	0.7397	0.7246	0.6793	0.6195
Reynolds number	52,200	57,700	60,400	61,200	61,400	58,300
loading criteria:						
$\Delta P/Q = \dfrac{P_3 - P_2}{1/2\ \rho_2 C_2^2}$	0.324	0.324	0.314	0.304	0.294	0.267
D factor $= 1 - \dfrac{C_3}{C_2} + \dfrac{\tau}{b}\ \dfrac{\Delta C_u}{2\ C_2}$	0.446	0.378	0.380	0.385	0.395	0.453
pressure loss coefficient						
$Zp = \dfrac{P_{o_{2A}} - P_{o_{3A}}}{1/2\ \rho_2 C_2^2}$	0.1310	0.0627	0.0601	0.0601	0.0601	0.1295
diameter exit	2.672	2.878	3.070	3.251	3.423	3.586
deviation = $\alpha_3^* - \alpha_3$	11.7	10.75	11.0	11.9	13.4	15.4

TABLE 7

Compressor Blade Stress Summary

Stage	Unrestored Gas Bending Stress, psi	Centrifugal Stress at 50, 000 rpm, psi
1	700	10, 000
2	800	10, 000
3	600	9, 000
4	600	9, 000
5	700	9, 000
6	700	9, 000

The compressor blades are twisted and a centrifugal untwist moment is applied at design conditions. The stress associated with the untwist is about 5000 psi. The combined blade stress, including the untwisting moment at the design conditions and the 20 per cent overspeed conditions, is well below the allowable stress for the titanium alloy.

The blades are retained in the shaft by dovetails which were also designed with a generous design margin. The dovetail of the fifth stage of the compressor is the most critical. The dovetail attachment stresses in this stage are summarized in Table 8.

TABLE 8

Dovetail Stresses in Compressor Fifth-Stage Blade

Stress, psi	Allowable Stress, psi	Stress Type
13, 000	47, 000	combined bending and tensile
19, 000	69, 000	maximum bearing stress on dovetail shoulder
4, 000	42, 000	shearing stress in dovetail
6, 000	58, 000	tensile stress in dovetail neck

The compressor blades have a flutter margin in torsion frequency of approximately 2. 5 and they have about twice this margin in bending. The first, second, and third blade natural frequencies in bending and the first and second in torsion are summarized in Table 9 at design speed. Since Stages 4 and 5 were practically the same as Stages 3 and 6, the natural frequencies of Stages 4 and 5 are not listed. The centrifugal stiffening effects on the natural frequencies of the blades are small.

TABLE 9

Compressor Blade Natural Frequencies at 50,000 rpm

Stage	First Bending, cps	Second Bending, cps	Third Bending, cps	First Torsion, cps	Second Torsion, cps
1	5070	21,900	46,400	12,400	34,900
2	4330	19,600	46,000	14,300	39,500
3	5370	25,500	51,200	15,900	45,000
6	5770	27,700	52,900	15,300	53,500

The blades have natural frequencies removed from major sources of excitation. The major sources of excitation are the four inlet struts and the twelve inlet guide vanes. At design speed the wakes from these members produce some excitation at 3333 cps and 10,000 cps, frequencies well removed from the natural frequency of any of the blades. The stator vanes also produce some excitation. The wakes of the first stage stators excite the second-stage blades at 16667 cps and the other blades at this same frequency to a lesser extent. The 24 vanes in the following stages produce wake excitation at 20,000 cps primarily affecting the third through sixth-stage blades. The airfoils were designed to avoid natural frequencies which correspond to the sources of excitation.

Inlet and Exit Ducting Design

To provide space for the thrust and journal bearings and associated instrumentation and support systems, the diameter of the inlet-duct gas path is larger than the corresponding diameter in the compressor. The inlet passage converges to limit the growth of the wall boundary layer in an effort to prevent excessive end wall loss in the compressor. Four struts provide support for the inner section of the inlet. Twelve inlet guide vanes follow the struts and the inlet guide vane design is defined in Tables 5 and 6. A long inlet guide vane chord was selected to provide higher Reynolds numbers.

The geometry of the exit duct and scroll for the turbine-compressor package is presented in Figure 8. The gas is diffused and turned to the radial direction in the duct and then it flows into the scroll. The gas leaves the scroll through a single duct not shown in Figure 8. The exit scroll serves as a settling chamber to provide uniform back pressure circumferentially on the compressor. The predicted pressure distributions along the walls of the exit duct shown in Figure 8 are presented in Figure 9. The estimated loss of the diffuser and scroll is shown in Figure 3.

Off-Design Performance

The estimated performance of the compressor at a variety of speeds and gas flows is presented in Figures 10 and 11. These data were developed for compressor design inlet temperature and pressure levels and if they are applied at significantly different conditions some Reynolds number effects can be anticipated.

IV. DESCRIPTION OF COMPRESSOR RESEARCH PACKAGE

The compressor research package was designed to provide a convenient means of evaluating the aerodynamic performance of the Brayton-cycle axial-flow compressor. A cross-sectional drawing of the compressor research package is presented in Figure 12. The argon enters through the inlet cone and duct assembly, flows through the inlet case, through the six stages of blades and stators, and exhausts through the exit diffuser and scroll. Individual photographs of these parts are shown in Figures 13 through 18. The scroll shown in Figure 12 is a mirror image relocation of the aerodynamic scroll design shown in Figure 8, to provide access for instrumentation. The compressor blades are attached to the rotor by dovetails and the rotor is a bolted assembly (Figure 19). The rotor is supported by two ball bearings axially loaded against each other by a wave washer and mounted in titanium spring mounts (Figure 20) which incorporate oil film damping. The bearings are jet oil lubricated. The bearing compartments are sealed by carbon face seals (Figure 21) and a labyrinth seal (Figure 22). The compartments include breather fittings as well as oil inlet and scavenge ports. The compressor is driven through a flexible coupling (Figure 23).

The compressor research package employs the same blading used in the turbine-compressor package. The inlet section geometry is also identical to the turbine-compressor but, as can be seen in Figure 12, the exit scroll is relocated. This modification permits access for traverse instrumentation. The exit diffuser geometry is identical to the turbine-compressor diffuser.

The purpose of the compressor research package was to provide a means of measuring the aerodynamic performance of the Brayton-cycle axial-flow compressor. The overall performance can be measured by pressure and temperature instrumentation mounted in the bosses provided. Detailed interstage instrumentation was provided to aid in the assessment of the performance of each stage of the six-stage compressor. Table 10 summarizes the instrumentation incorporated in the package.

TABLE 10

Aerodynamic Instrumentation Provisions

Location	Static Pressure Taps	Other Provisions
plane ahead of four inlet struts		six 3/8-inch dia. holes for fixed probes
leading edge plane of inlet guide vanes	four in inner wall and four in outer wall	

TABLE 10 (Cont'd)

Location	Static Pressure Taps	Other Provisions
trailing edge plane of inlet guide vanes	four in inner wall and four in outer wall	
plane ahead of Rotors 1 through 6	three in outer wall	
plane ahead of Stators 1 through 6	three in outer wall	
leading edge plane of Stators 1 through 6	one in inner wall of each stator assembly	one radial traverse boss in each stator
plane downstream of Stator 6	four in outer wall and four in inner wall	ten total pressure probes and ten total temperature probes
exit diffuser	total of twelve spaced at one-inch intervals in two rows about 180 degrees apart	
scroll exit	four	four 3/8-inch dia. holes for fixed probes

The compressor research package is shown in Figure 24 with the outer case removed to show some of the instrumentation lines. The lines feed upstream (down in Figure 24) and terminate in the instrumentation turrets shown. Since the compressor research package is small, a method of connecting instrumentation lines that occupied minimum space was required. Heat-shrinkable plastic tubing was employed to seal the joints in the pressure instrumentation tubing. Appendix 1 presents a more detailed description of this method of connecting tubing.

In order to provide for more detailed surveys of the flow in the first stage of the compressor, two alternate configurations were provided. The package can be assembled without the first-stage stator and without the remaining stages by utilizing the alternate rotor shown in Figure 25. When this configuration is selected, a radial traverse boss downstream of the blades permits detail traversing. The second alternate configuration includes the first stage rotor and stator

but the remaining stages are not included. The alternate rotor required for this configuration is shown in Figure 26. To provide for flow surveys when testing the first stage, three traverse bosses are located downstream of the stator.

The rotor of the compressor research package consists of a drum with broached slots which retain the blades. The drum is held at the ends by disks which are retained by a tie-bolt. Ball bearings are located outboard of the disks to support the rotor. The ball bearings have an inner diameter of 25 millimeters and an outer diameter of 47 millimeters. They are made of AMS-6444 steel with silver-plated steel cages. The bearings are preloaded against each other to assure thrust loading under all operating conditions. A wave washer at the front bearing outer race provides a thrust load of about 30 pounds on each bearing at design operating conditions. Each bearing is cooled and lubricated by MIL-L-7808 lubricant or by an appropriate oil with similar characteristics at the operating conditions. A thermal map is presented in Figure 27 showing the predicted operating temperatures at the design conditions with an oil inlet temperature of 80°F. Three iron-constantan thermocouples are located in the housing of each bearing to monitor bearing outer-race temperatures. Oil is metered to each bearing through two 0.031-inch diameter orifices, resulting in an oil flow rate of 1.0 lb/min for each bearing. Bearing oil compartment design parameters are presented in Table 11.

TABLE 11

Bearing Compartment Design Parameters

	Front	Rear
oil supply pressure, psia	13	19
bearing compartment pressure, psia	4	10
rear labyrinth seal		
radial clearance, inch	-	0.007
leakage flow, lb/sec of air	-	0.005

The DN factor for the bearings (bearing inner diameter multiplied by the design speed) is 1,250,000 mm rpm, which represents an adequate design for this application. Operating at design conditions with an unbalance of 0.010 ounce-inches at each bearing and a total thrust load of 90 pounds, the rear ball bearing, the most highly loaded, has a predicted B10* fatigue life of at least 200 hours.

* The B10 life is the predicted operating time to failure of 10 per cent of the bearings of a given type in a given application

The interfaces between the argon and the bearing compartments are sealed by carbon face seals held in contact with a rotating plate by a spring. O-rings serve as the static secondary seal. The bearing compartment pressure can be set in the course of the particular test to any value above 2 psia. Whenever practical, the bearing compartment pressure should approximately correspond to compressor inlet pressure in order to reduce the pressure drop across the carbon face seals. The oil should be supplied at a pressure of 8 to 10 psi above the bearing compartment pressure. The drive end of the shaft is sealed with a 5-lip staggered labyrinth seal having a radial clearance of 0.007 inch. The labyrinth seal was selected for this location to reduce the parasitic power consumption. This seal incorporates an oil slinger to centrifuge oil from the seal area.

The environmental heat losses assuming no insulation are shown in Table 12.

TABLE 12

Gas Path Heat Loss

exit scroll	1096 Btu/hr
exit diffuser	324
case	112
total loss	1532 Btu/hr
power input to the compressor	76,000 Btu/hr
per cent heat loss (no insulation)	2.01

These heat losses do not include the heat generated in the bearings and seal that is carried away by the oil. As indicated in the table, if the package were not insulated, the heat loss would be approximately 2 per cent of the compressor input power, which would affect the measured compressor efficiency. Therefore, Pratt & Whitney Aircraft recommends that the rig be insulated.

The blade tip clearances and stator inner seal clearances are fairly small (0.007 and 0.006 inch, respectively). To avoid the possibility of contact between rotating and stationary parts, positive location of the parts and a minimum number of connections are required. Logically the bearings would be mounted in a solid housing. However, the critical speed of such an arrangement was calculated near the design speed. Therefore, the bearings are mounted in springs which permit radial motion while restraining axial motion. The bearing mount springs are restricted to 0.0015 inch of radial motion and the radial gap between the spring and the housing is filled with oil to provide

damping. The bearing mount springs were designed to provide a spring rate of 16, 000 pounds/inch. The predicted rigid-body critical speeds were at 12, 000 and 18, 000 rpm. These speeds are below the probable operating range of the compressor research package, from 20, 000 to 59, 100 rpm. The bent-shaft critical speed was predicted to be about 100, 000 rpm which provides ample margin above the maximum speed.

The static structure and rotating parts were conservatively designed and have ample design margins. The titanium bearing mount springs are limited to 0. 0015 inch of radial deflection. The stress at this deflection was calculated to be 18, 000 psi. The fatigue limit for the material at the operating temperature including a factor for notch sensitivity is 22, 000 psi. Rotor stresses are at acceptable levels at all operating conditions. The calculated disc drum tangential stress is 35, 800 psi at 60, 000 rpm, providing yield and burst margins of 1. 68 and 1. 95, respectively. Rotor end hub tangential stress is 12, 700 psi at 60, 000 rpm providing yield and burst margins in the neighborhood of 5.

V. TEST PROGRAM

A. Introduction

A test program was conducted at Pratt & Whitney Aircraft to evaluate the mechanical dynamic performance of the compressor research package. No aerodynamic tests were conducted at Pratt & Whitney Aircraft. The aerodynamic testing of the Brayton-cycle compressor is planned to be conducted at the Lewis Research Center.

B. Test Facility

The test stand used for testing the compressor research package is shown in Figures 28 and 29. The test was controlled remotely from the control room shown in Figure 30. The compressor was driven by a 400-horsepower electric dynamometer through a 20.7 to 1 stepup gearbox. The oil lubrication system consisted of motor-driven supply and scavenge pumps, a reservoir, strainer and filter, and control valves. The bearing compartments were vented to the ambient environment.

Vibration pickups (Consolidated Electrodynamics Corporation Type 4-H8-0001) were used to measure the vibration of the static cases at the inlet case rear flange and at the exhaust scroll rear flange. Measurements were made for vibration in both the horizontal and vertical directions. Signals from the pickups were read on meters designed by Pratt & Whitney Aircraft and capable of measuring vibrations with amplitudes up to 0.0025 inch.

Rotor speed was sensed by two Electro-Products Laboratories Model 3016 magnetic speed pickups. The outputs of the pickups were read on two Dynapar Company Dynacounters.

Temperatures of the bearings and the lubricating oil at the inlet and outlet were sensed by thermocouples, with the thermocouple output being read on Brown potentiometers.

C. Mechanical Dynamic Test

The compressor research package was tested over the full speed range to 60,000 rpm to determine the dynamic mechanical characteristics of the research package. In order to permit observation of the dynamic characteristics of the rotor, the blades and vanes were not included in the assembly. Instead, Bentley eddy-current proximity probes were installed in the first and fifth-stage rotor seal areas to measure rotor dynamic motion. Two proximity probes were installed ninety degrees apart circumferentially at each location. Also, pairs of proximity

probes were installed at each end of the drive coupling as shown in Figures 31 and 32.

The compressor research package was tested at speeds up to 60,000 rpm. At the exit scroll case, vibration in the order of 0.00005 inch amplitude was noted at 38,800 rpm. Amplitudes of 0.0001 inch were recorded in the vertical plane at both ends of the research package at 52,000 rpm. At 60,000 rpm, vibratory amplitudes of 0.0001 to 0.0002 inch were indicated at both ends of the rig. The vibration at 60,000 rpm is believed to be, in part, due to input from the gear box. At other speeds the case vibration was not measurable.

Thermocouples were located at the bearing housings to monitor outer race temperatures. The bearing temperatures increased with speed and stabilized rapidly. Some representative bearing temperatures with an oil inlet temperature of 55°F are shown in Figure 33.

The rotor motions, as recorded by the proximity probes and displayed on oscilloscopes, are presented in Figures 34 through 40. The "static" traces shown in Figures 34 and 38 were produced by rotating the rotor by hand so that they correspond to essentially a static condition. The irregularities in the traces are due to surface finish of the rotor. These surfaces are machined to standard quality and were not specifically designed for use with these probes. The trace at the front of the machine indicated runout of the rotor at this position which is acceptable for normal compressor operation. Figures 34 and 35 indicate very little change in the traces from the static condition to 38,000 rpm. In the speed range between 38,000 and 44,000 rpm, the trace for the front probes oscillated between the static trace and a somewhat smaller trace which is shown in Figure 36. The orbits remain consistent from above 44,000 rpm to just under 60,000 rpm. From 57,000 to 60,000 rpm some increase in the rotor orbit at the rear was indicated, probably due to input from the gearbox. Absence of the expected critical speeds in the research package is attributed to the oil present in the radial clearance gap at each spring. The oil forms a squeeze film type of bearing which provides damping and may affect the equivalent spring rate of the system. In general, no indications were observed that would limit the operation of the compressor research package.

The bearing housing, Figure 20, is a flexible structure designed to provide a radial spring rate of about 16,000 pounds per inch. The radial motion of the support is restricted to 0.00015 inch maximum and the restricted space contains oil which provides damping. Originally, a steel bearing support was designed and fabricated and then redesigned bearing supports were constructed of titanium. Although Figure 20 shows a steel mount, the changes made in the redesign to the titanium mount would almost be indistinguishable visually. The mechanical dynamic test assembly included the steel bearing supports.

On disassembly, the front bearing support was found to have failed at the bearing end of each of the eight inner axial beams. A photograph of the failed part is shown in Figure 41. The spring was examined and fatigue was established as the basic cause of the failure. Figure 42 is a photograph of a typical beam indicating a fatigue failure progressing from the sides of the beam. Fatigue cracks were found in the forward end of the beams and Figure 43 is typical of these cracks. The bearing mount spring was analyzed to determine if the material conformed to the requirements. The material composition, hardness, and grain structure were within the specifications. Figure 44 is a microphotograph of one beam adjacent to the fracture. The rear bearing mount spring which is similar to the front spring was inspected and no cracks were indicated.

The predicted maximum vibratory stress in the steel mount is about 25,000 psi, while the fatigue limit including a notch factor for the steel is 20,000 psi. Therefore, the steel mount could be expected to fail if the mount deflected through the full range. The titanium bearing mount has a fatigue limit at 22,000 psi, while the maximum stress with the spring deflected through the full range is 18,000 psi. Therefore, the titanium bearing mounts are expected to be satisfactory. The compressor research package was assembled and delivered to the National Aeronautics and Space Administration with titanium bearing mounts.

D. Bearing Mount Spring Constant

The spring constants of a steel mount and a titanium mount were measured. The bearing mounts were mounted in a fixture and were loaded by applying known weights. The mount deflections were measured by a dial indicator. Load-deflection data taken for a steel bearing mount is shown on Figure 45. The spring rate is 13,300 pounds per inch as compared to the predicted spring rate of 16,400 pounds per inch. This result is not unusual, as the predicted spring rate is often somewhat higher than the actual value. The spring constant of a titanium bearing mount was measured and the load - deflection results are shown in Figure 46. A spring constant of 13,700 pounds per inch was measured which is in good agreement with the measured spring rate of the steel bearing mount.

APPENDIX 1

Pressure Tubing Seals

APPENDIX 1

Pressure Tubing Seals

The interstage pressure instrumentation requires tubing that can be connected and disconnected during assembly and disassembly. In order to maintain alignment of the compressor research package, an outer casing is employed. As a result, the space available for instrumentation tubing is limited and a method of connecting tubing that uses minimum space was required. Figure 24 provides some indication of the space available and the number of instrumentation tubes involved.

Heat-shrinkable plastic tubing was investigated as a means of connecting the pressure lines. The basic components of a tubing joint are shown in Figure 47. The tubing ends to be joined are deburred and polished. A stainless steel sleeve covers the joint to provide mechanical strength. The plastic tubing covers the sleeve and extends approximately 1/2 inch beyond the ends of the sleeve. Heat is applied to the plastic tubing by the heat gun shown in Figure 48. When the plastic is heated it shrinks onto the sleeve and tubing, forming a seal.

Two candidate plastics were evaluated for this application: a polyvinylide fluoride and a polytetrafluoroethylene. Initially joints were made of both materials and bubble-tested for leaks after heating for 5 hours at 350°F. The polytetrafluoroethylene was eliminated when two of three sample joints failed in the bubble tests. The polyvinylide fluoride was satisfactory.

Eight sample joints using the polyvinylide fluoride were thermally cycled from room temperature to 300°F thirty times. The joints were tested for leaks with a mass spectrometer helium leak detector. Eight other sample joints were heated for 16 hours at 350°F and leak-checked with the mass spectrometer. No unacceptable leakage was measured for any of these joints. The maximum helium leak rates were 10^{-8} cc per second at room temperature and 10^{-6} cc per second at 300°F.

The polyvinylide fluoride plastic heat-shrinkable tubing provides a useful compact seal for application in the compressor research package.

APPENDIX 2

Figures

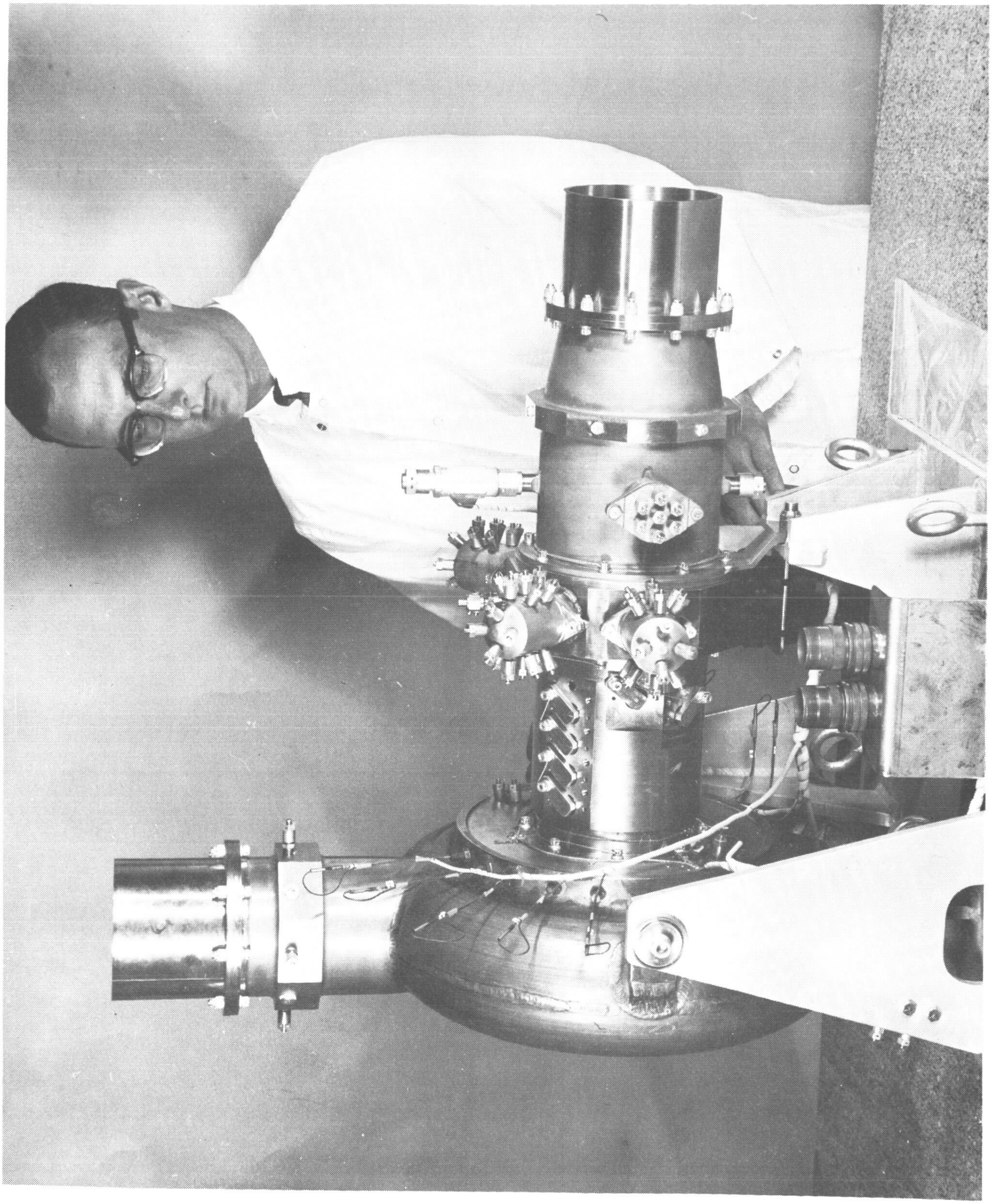

Figure 1 Compressor Research Package CN-6393

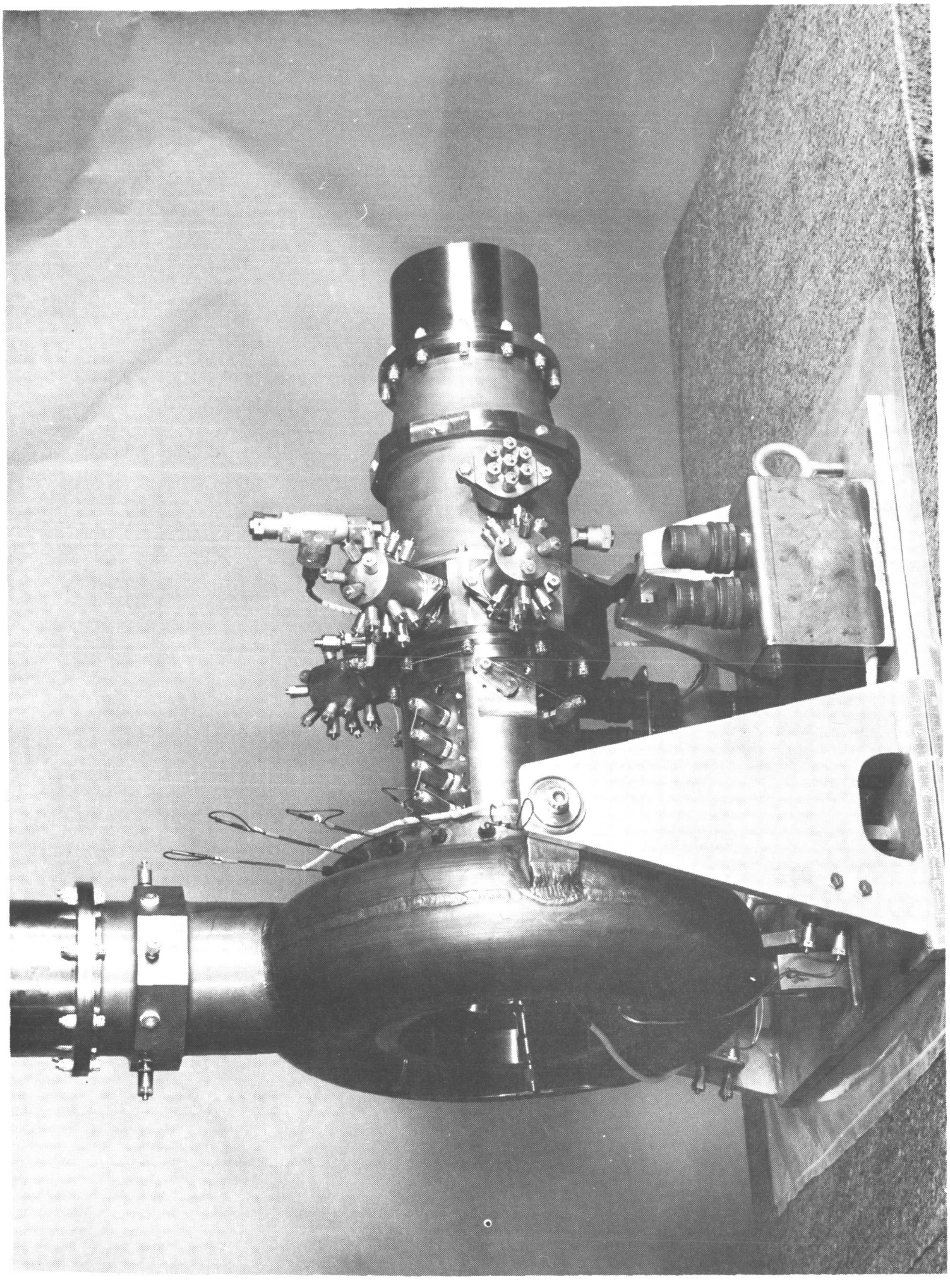

Figure 2 Compressor Research Package CN-6391

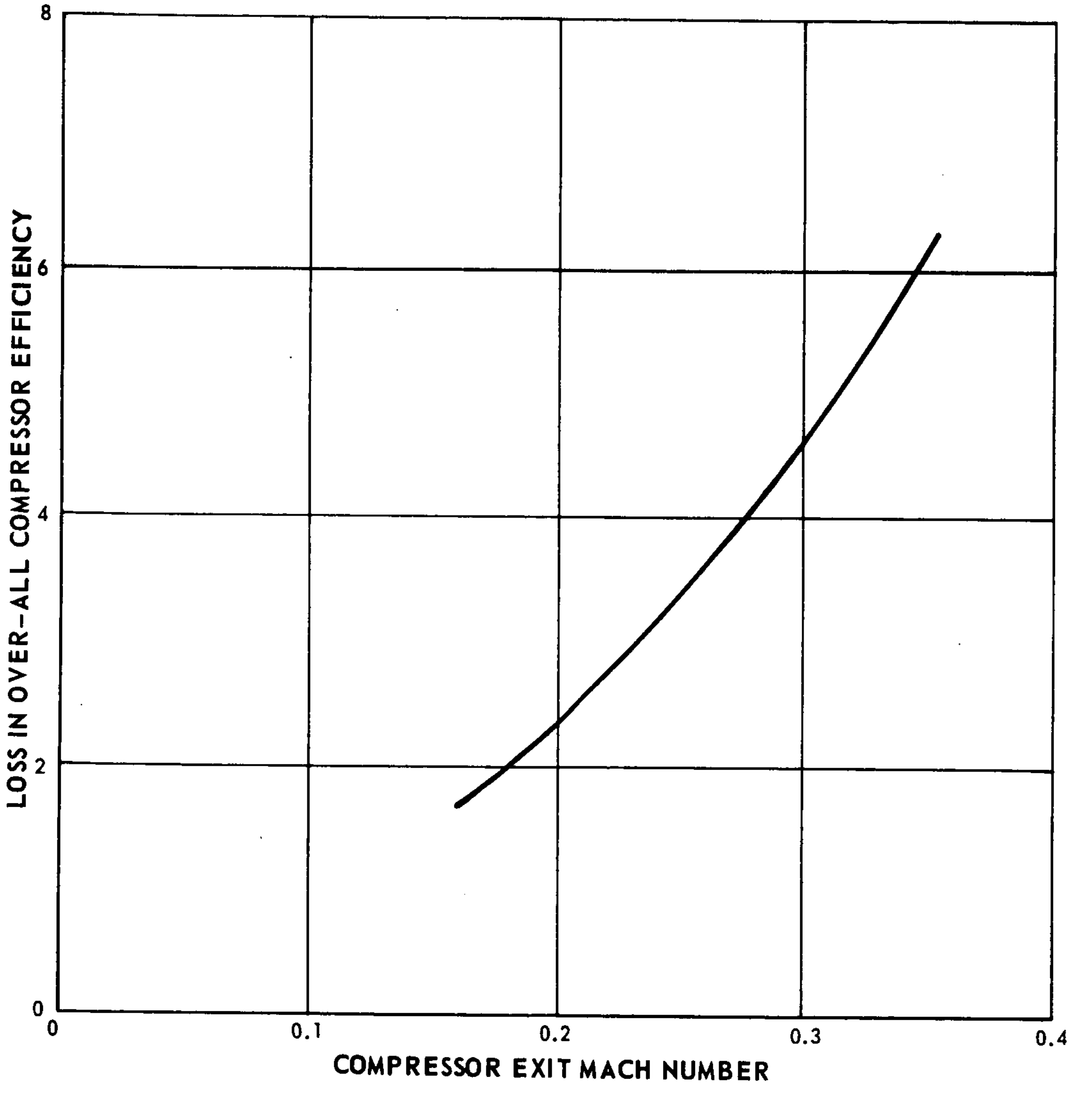

Figure 3 Compressor Exit Diffuser and Scroll Losses

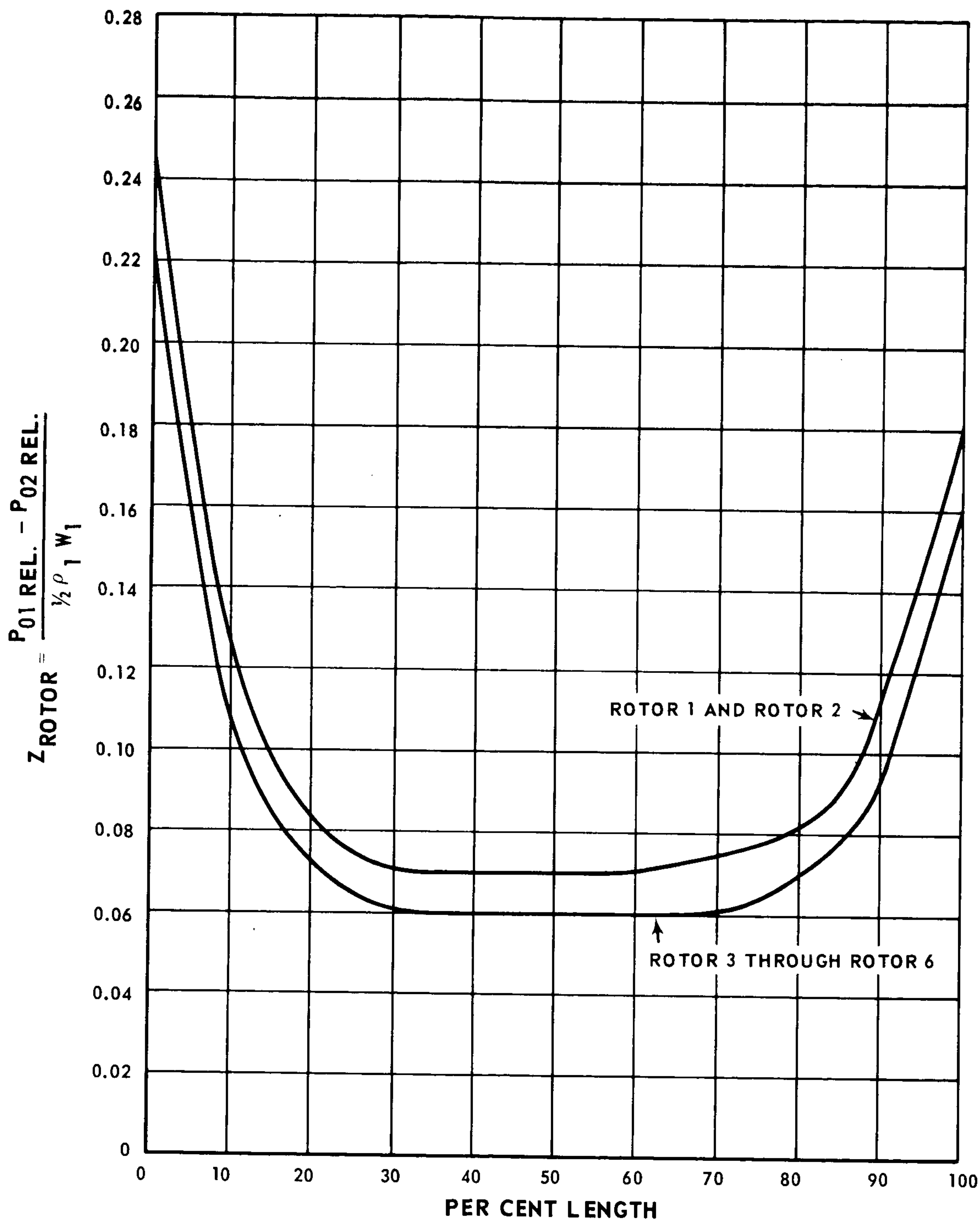

Figure 4 Rotor Loss Distribution of Six-Stage Compressor

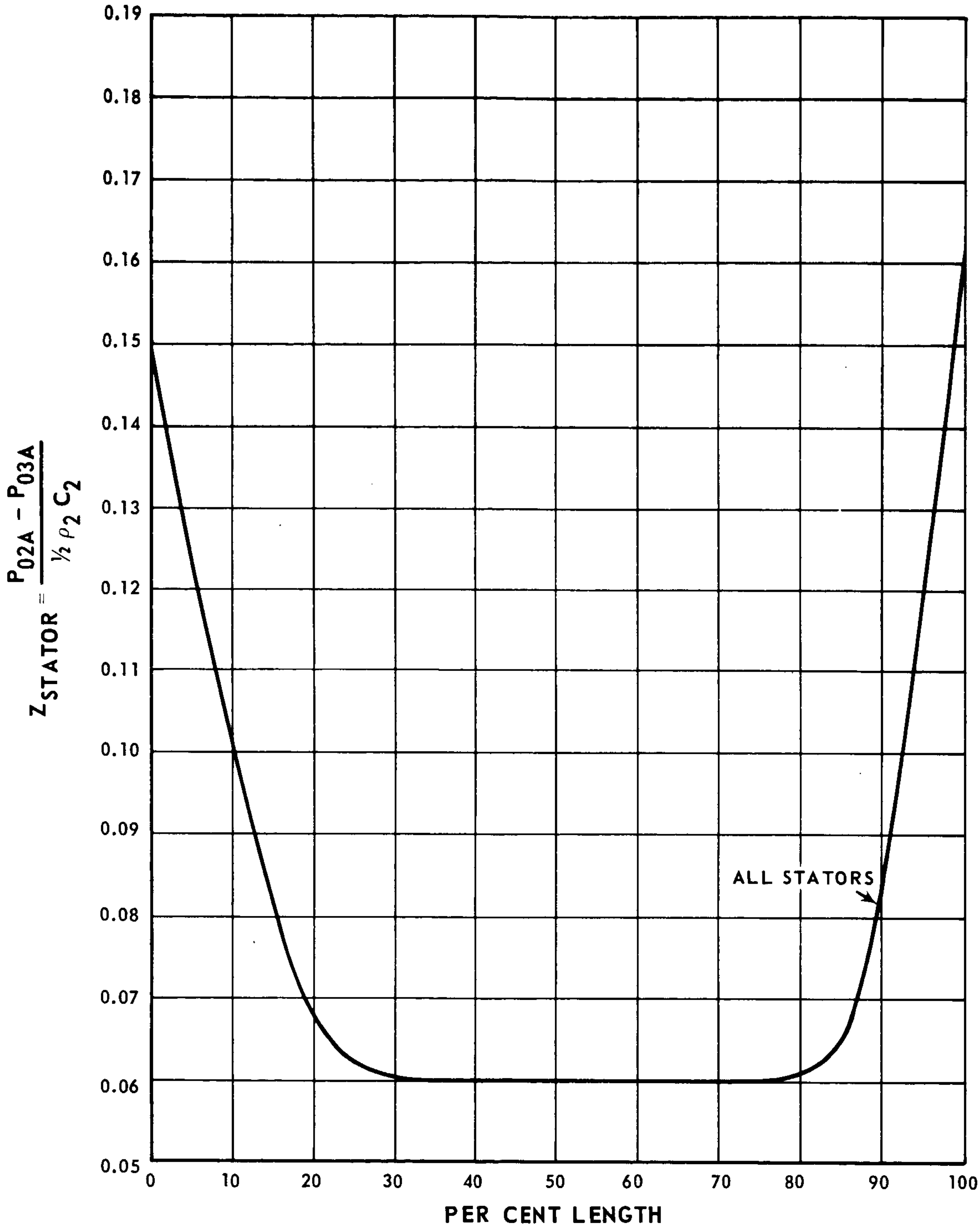

Figure 5 Stator Loss Distribution of Six-Stage Compressor

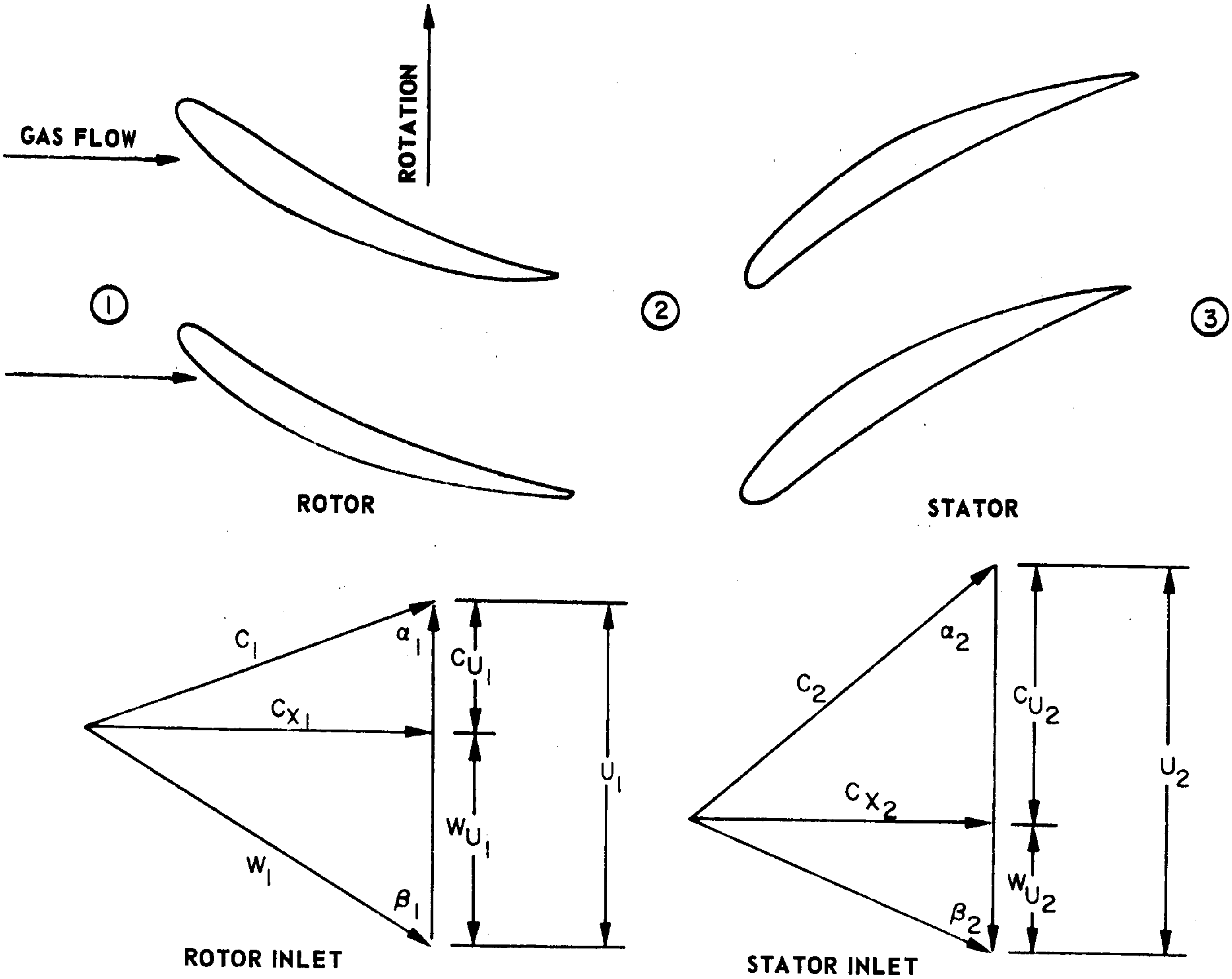

subscripts refer to circled station numbers above

C = absolute component of velocity, ft/sec
W = relative component of velocity, ft/sec
C_x = axial component of velocity, ft/sec
C_u = tangential component of absolute velocity, ft/sec
W_u = tangential component of relative velocity, ft/sec
α = angle of absolute component of velocity, degrees
β = angle of relative component of velocity, degrees
U = wheel speed, ft/sec
θ = turning angle, degrees $\beta_2 - \beta_1$, $\alpha_3 - \alpha_2$

Figure 6 Compressor Velocity Triangle Nomenclature

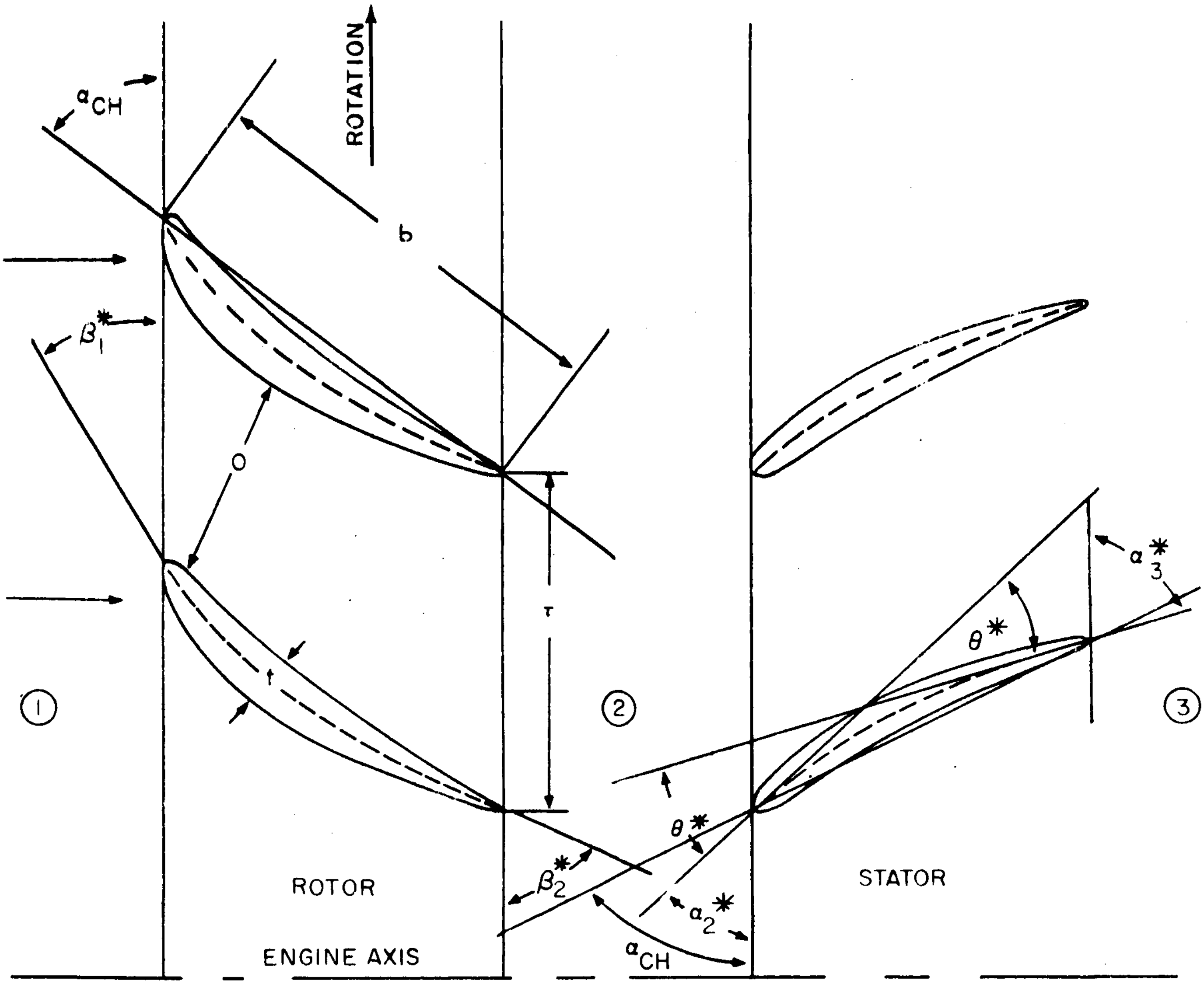

β_1^* , α_2^* = angle between a tangent to airfoil mean line at leading edge and a plane perpendicular to engine axis

β_2^* , α_3^* = angle between a tangent to airfoil mean line at trailing edge and a plane perpendicular to engine axis

θ^* = airfoil camber $\beta_2^* - \beta_1^*$, $\alpha_3^* - \alpha_2$

b = chord, distance between extremes of airfoil mean line

α_{ch} = angle between chord line and a plane perpendicular to engine axis

τ = spacing between adjacent airfoils

t = maximum airfoil thickness

circled number = station

Figure 7 Compressor Airfoil Nomenclature

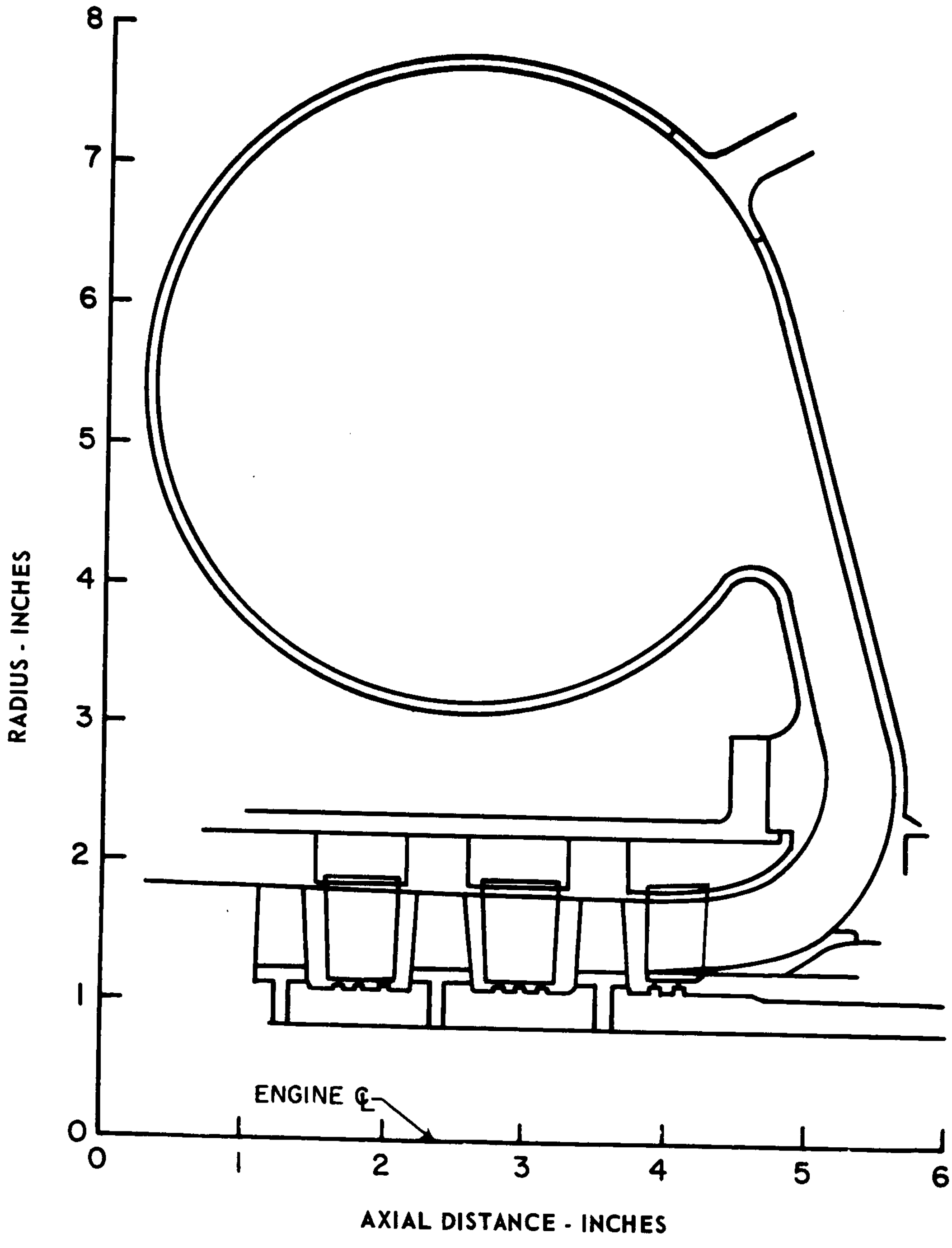

Figure 8 Exit Diffuser and Scroll Design

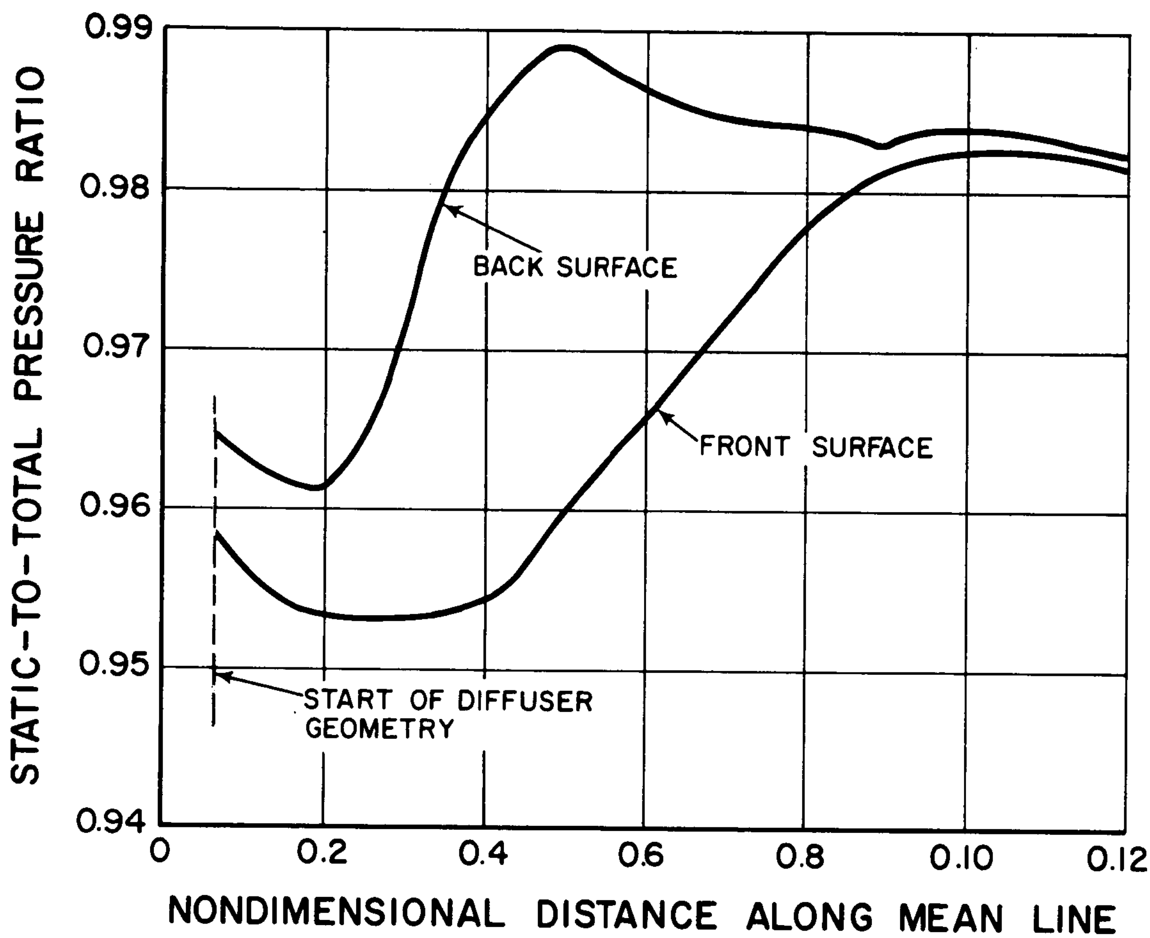

Figure 9 Exit Diffuser Static Pressure Distribution

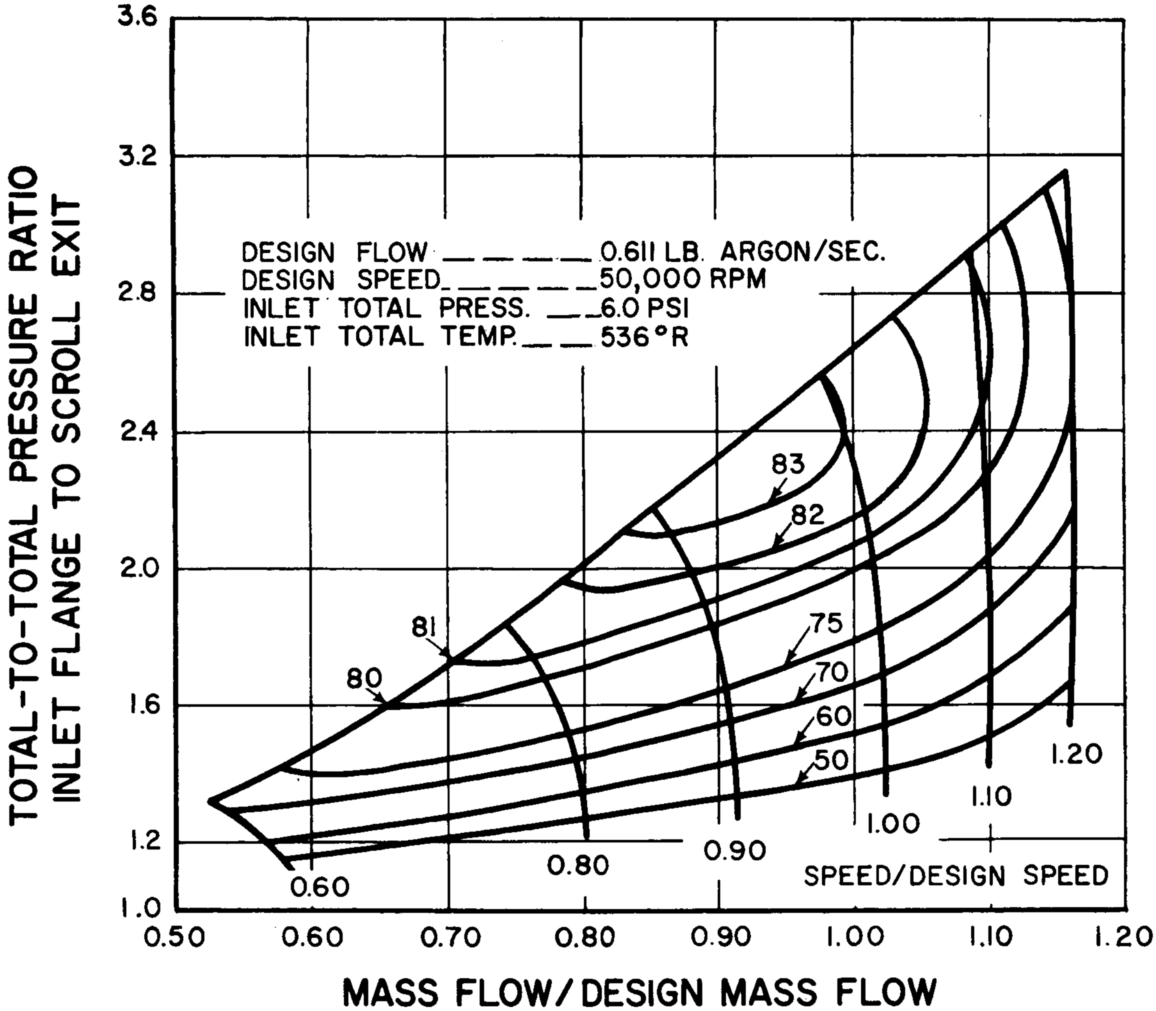

Figure 10 Estimated Compressor Efficiency from Inlet Flange to Scroll Exit Flange

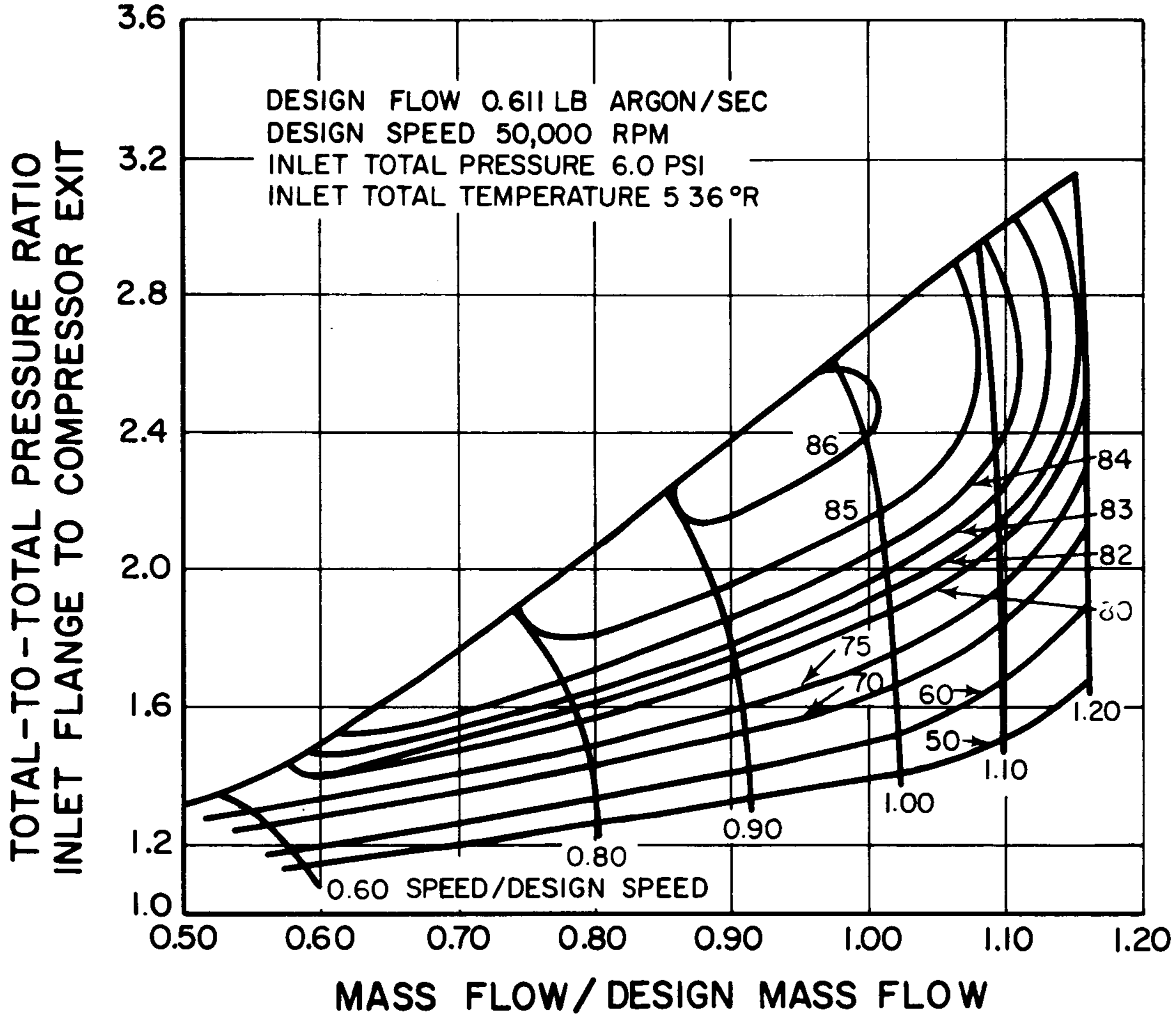

Figure 11 Estimated Compressor Efficiency from Inlet Flange to Compressor Exit

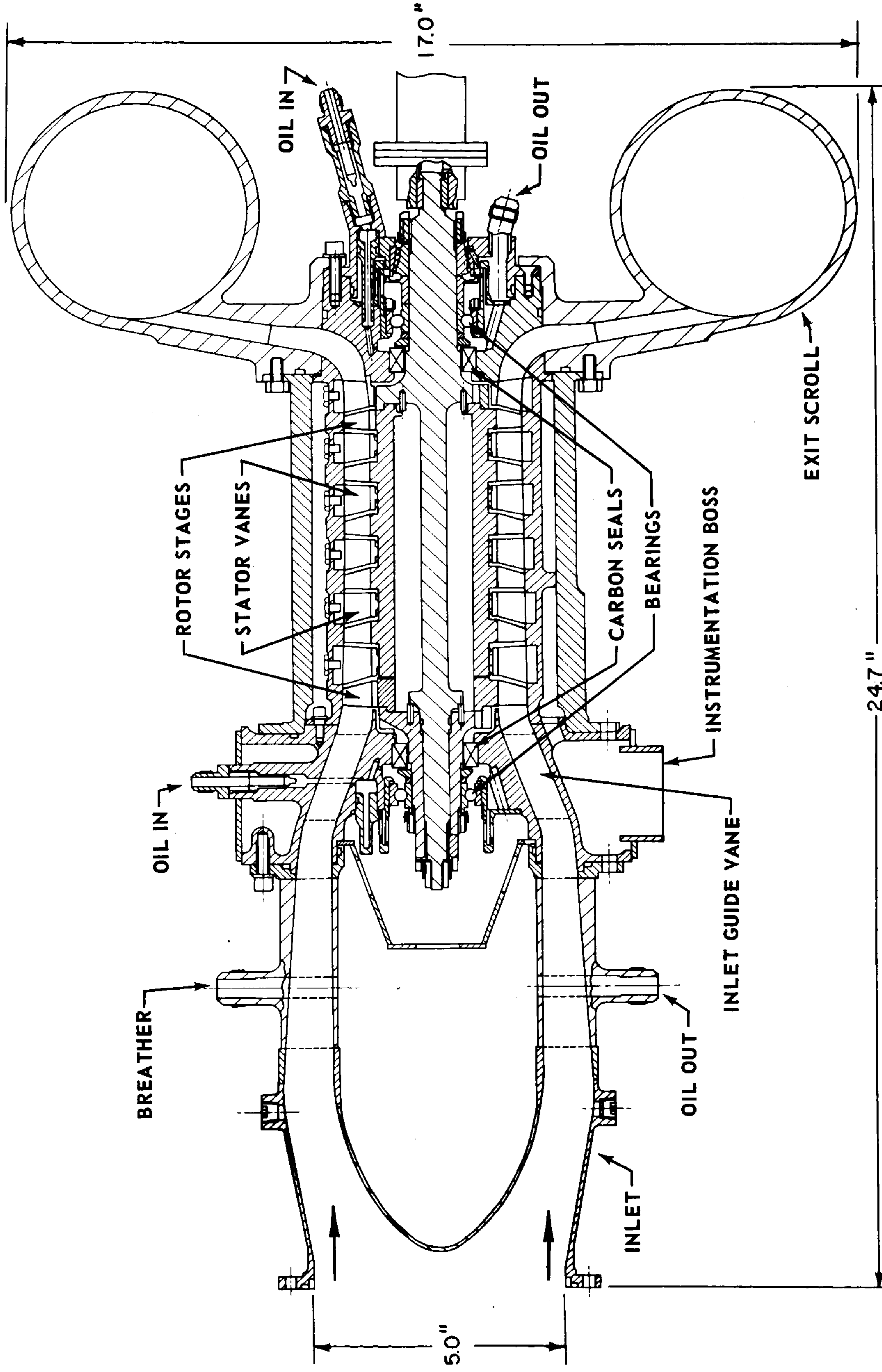

Figure 12 Cross-Section of Compressor Research Package M-38705

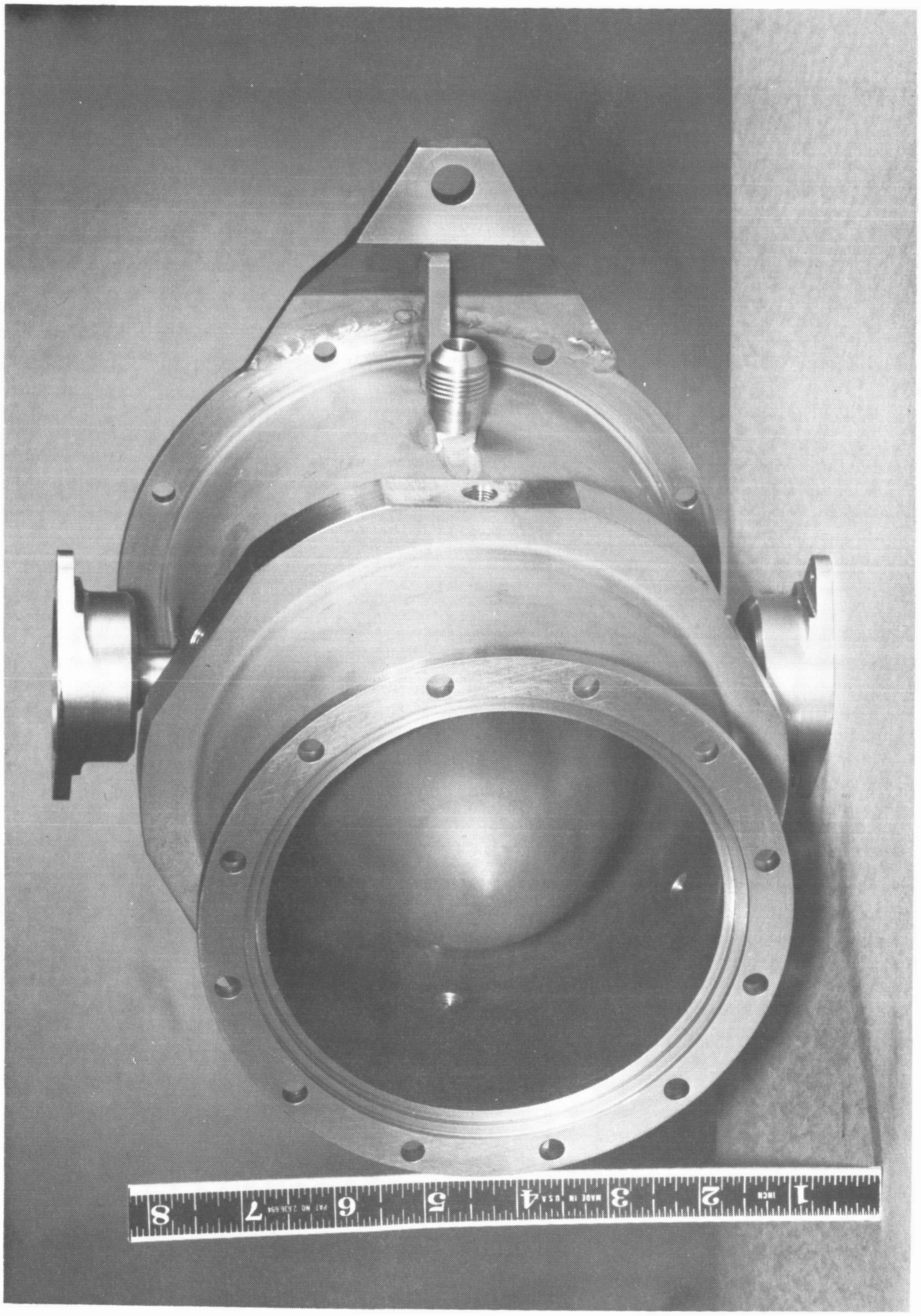

Figure 13 Inlet End of Inlet Cone and Duct Assembly XP-57192

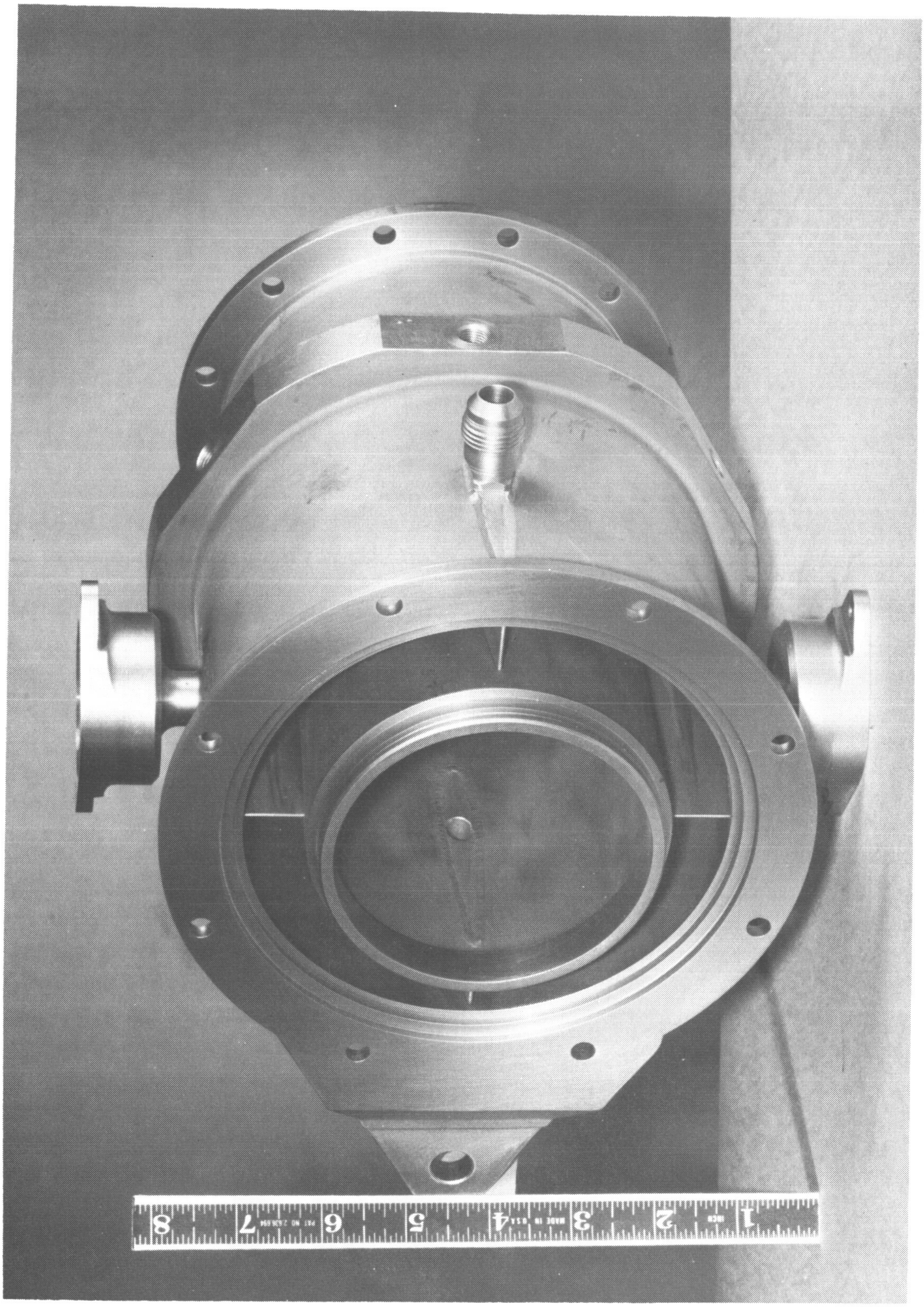

Figure 14 Exit End of Inlet Cone and Duct Assembly XP-57191

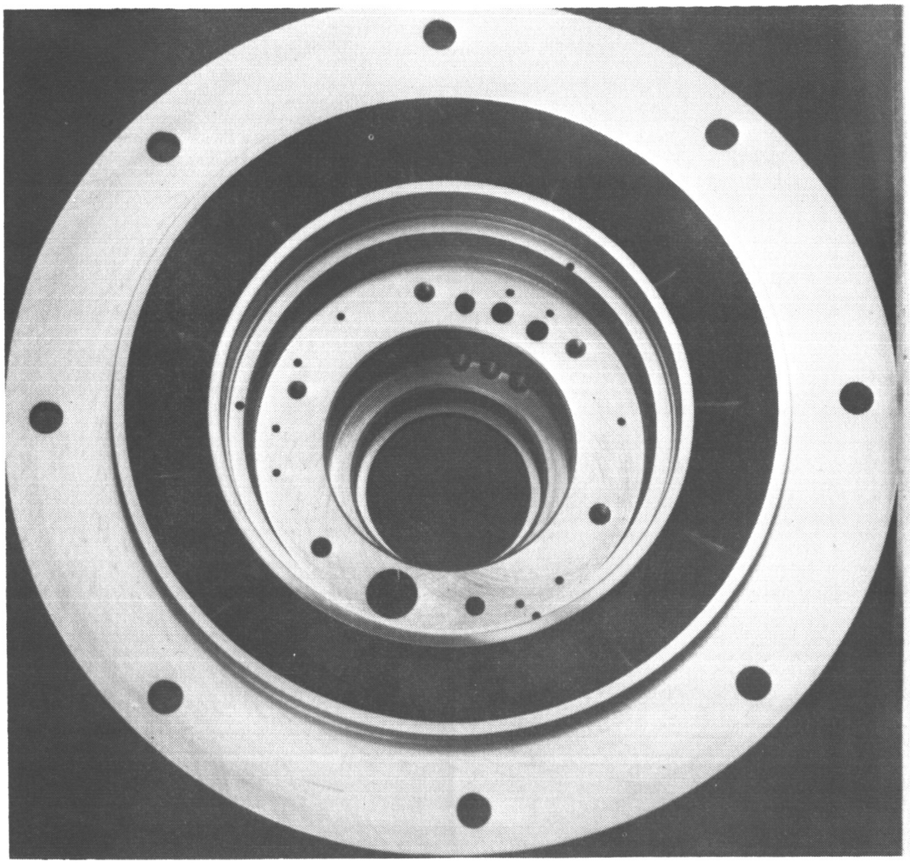

Upstream End

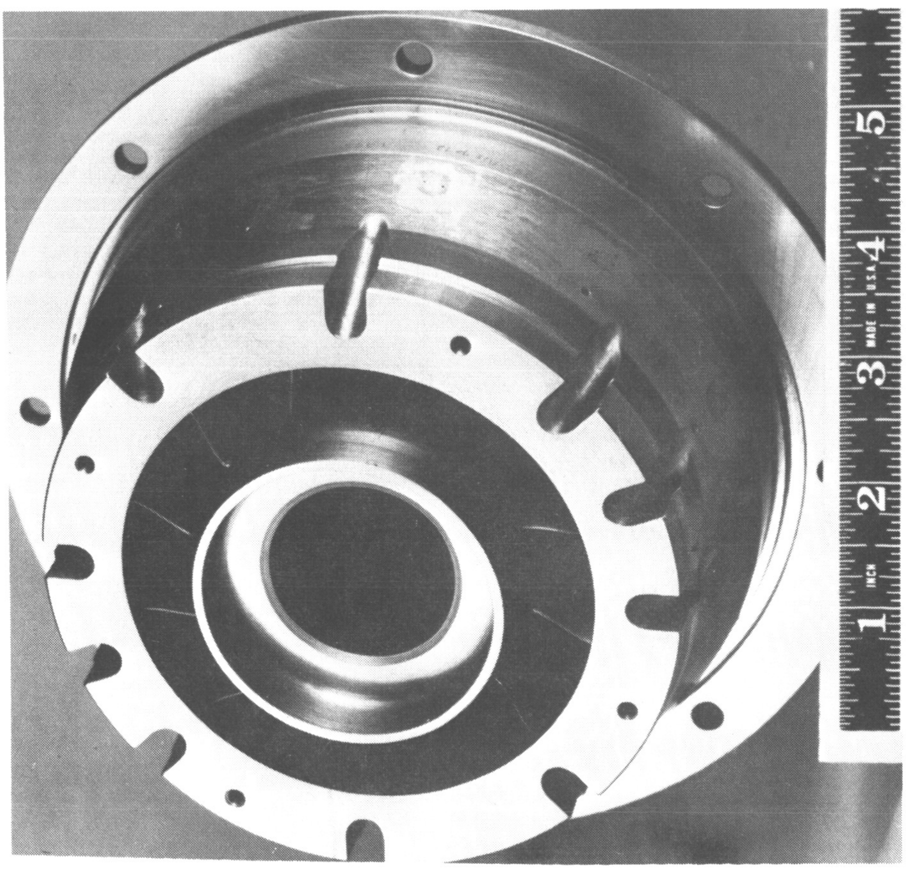

Downstream End

Figure 15 Inlet Case M-36223

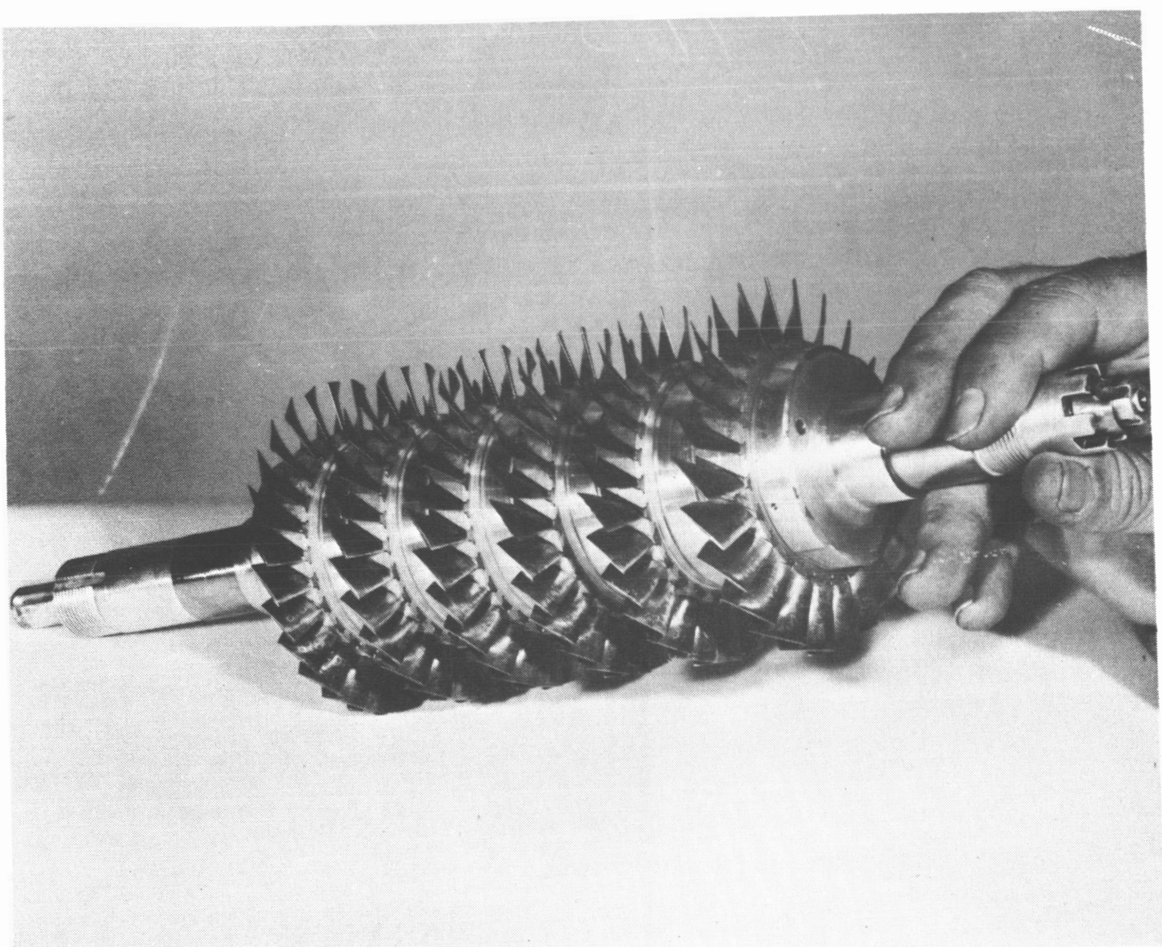

Figure 16 Rotor M-38004

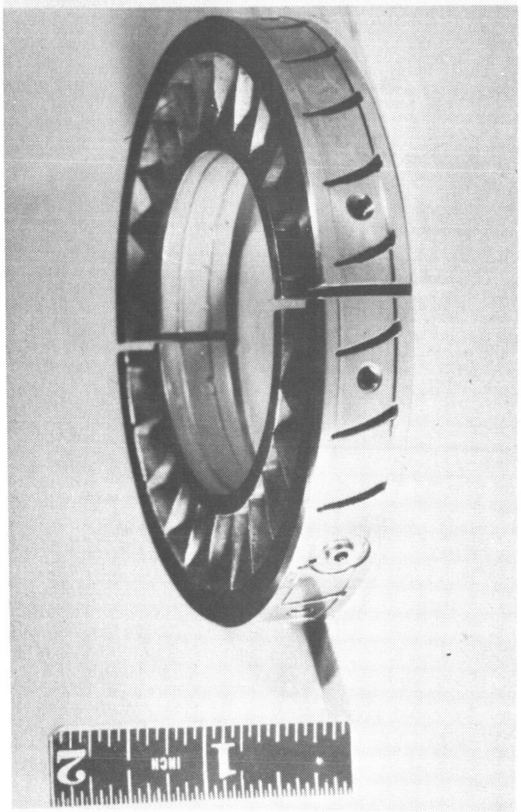

Third Stage
Trailing Edge View

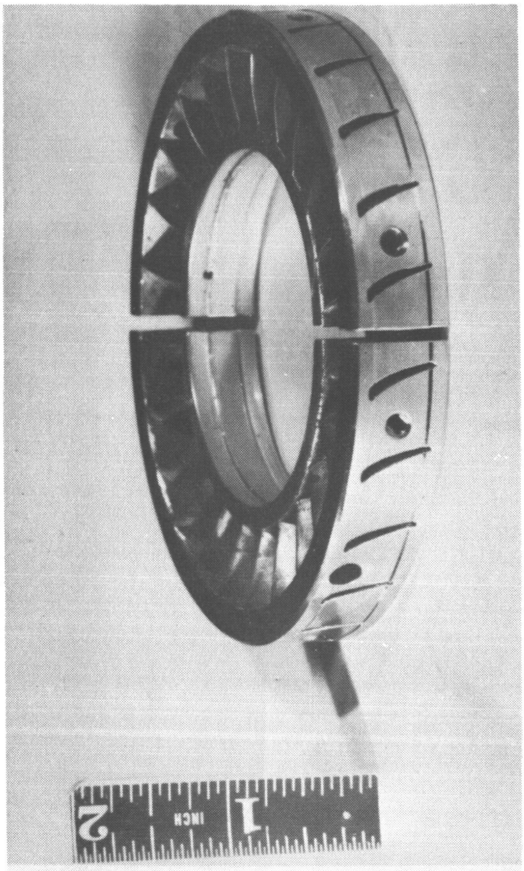

Fifth Stage
Leading Edge View

Figure 17 Vane and Shroud Assemblies M-37299

Figure 18 Exit Diffuser and Scroll X-21132

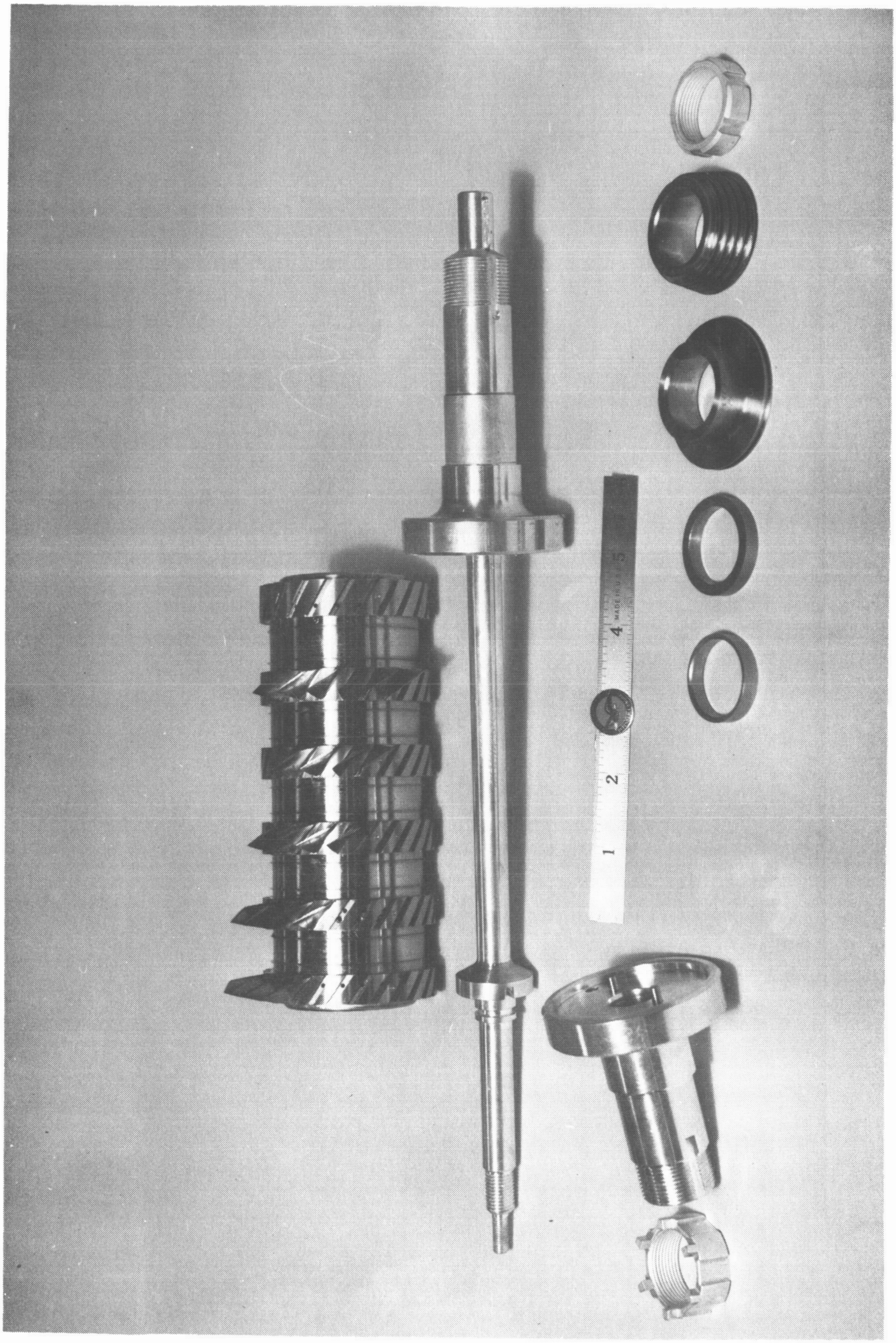

Figure 19 Detail Parts for Rotor Assembly X-20469

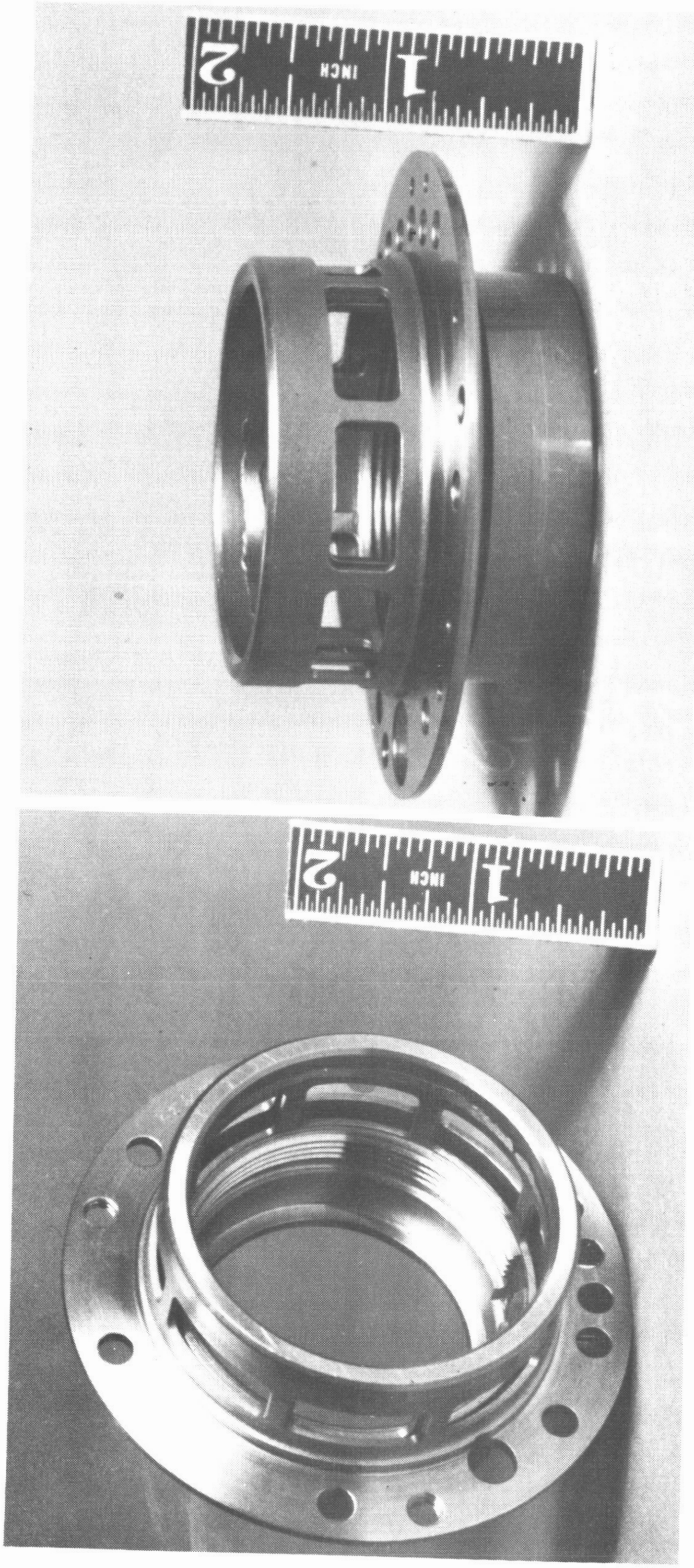

Figure 20 Bearing Housing M-36221

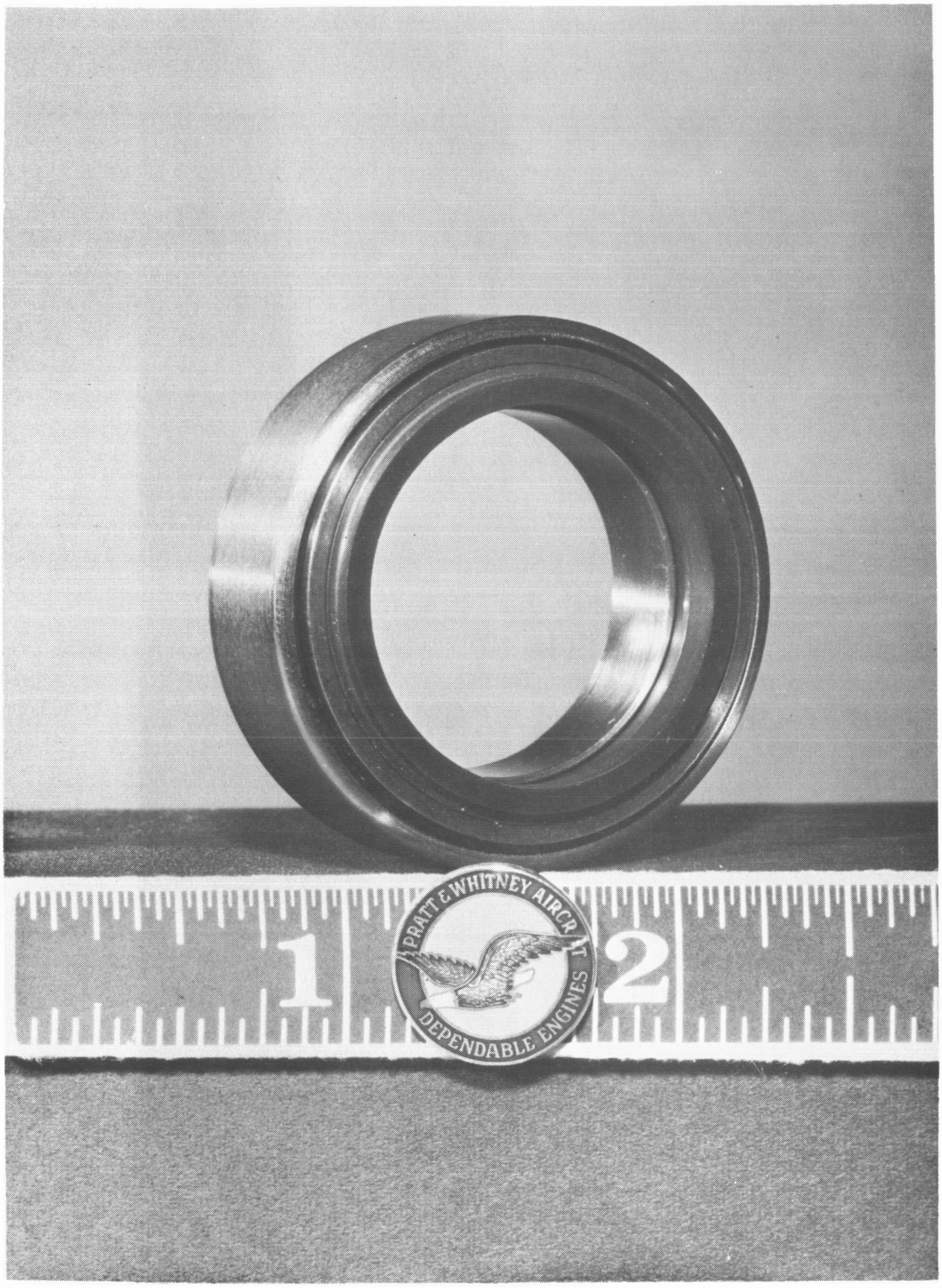

Figure 21 Carbon Seal XP-57077

Inboard View

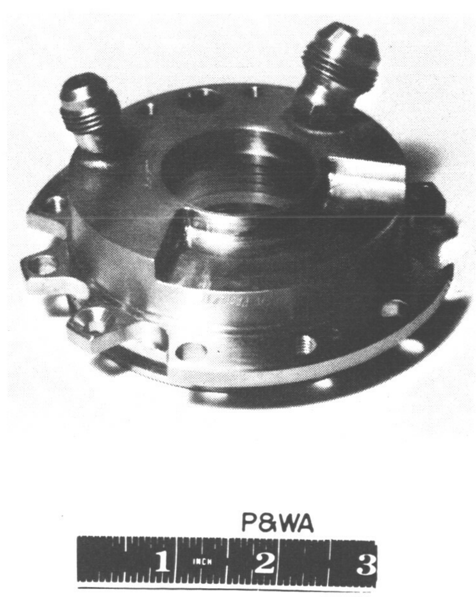

Outboard View

Figure 22 Labyrinth Seal Housing M-36225

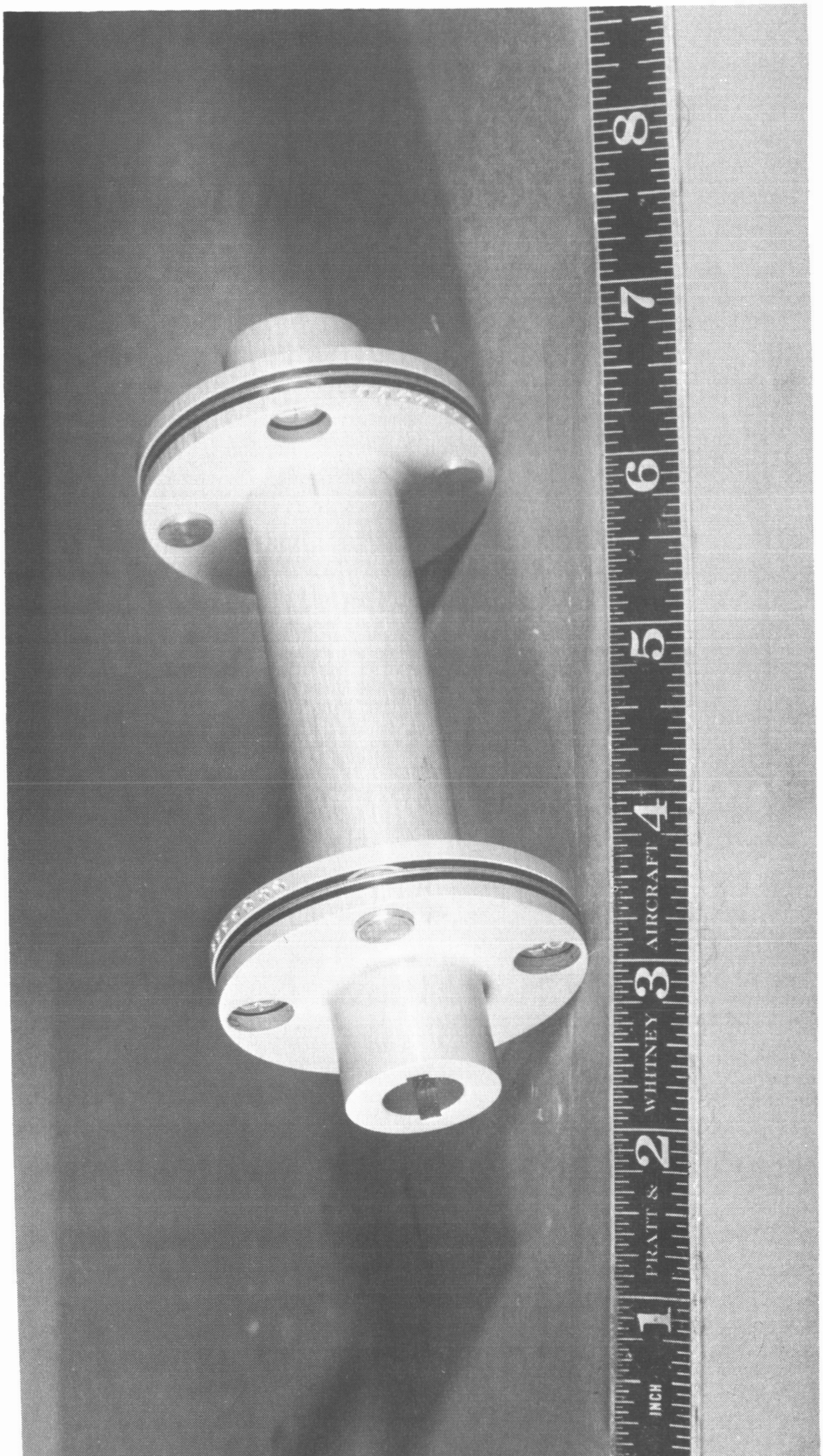

Figure 23 Drive Coupling XP-54886

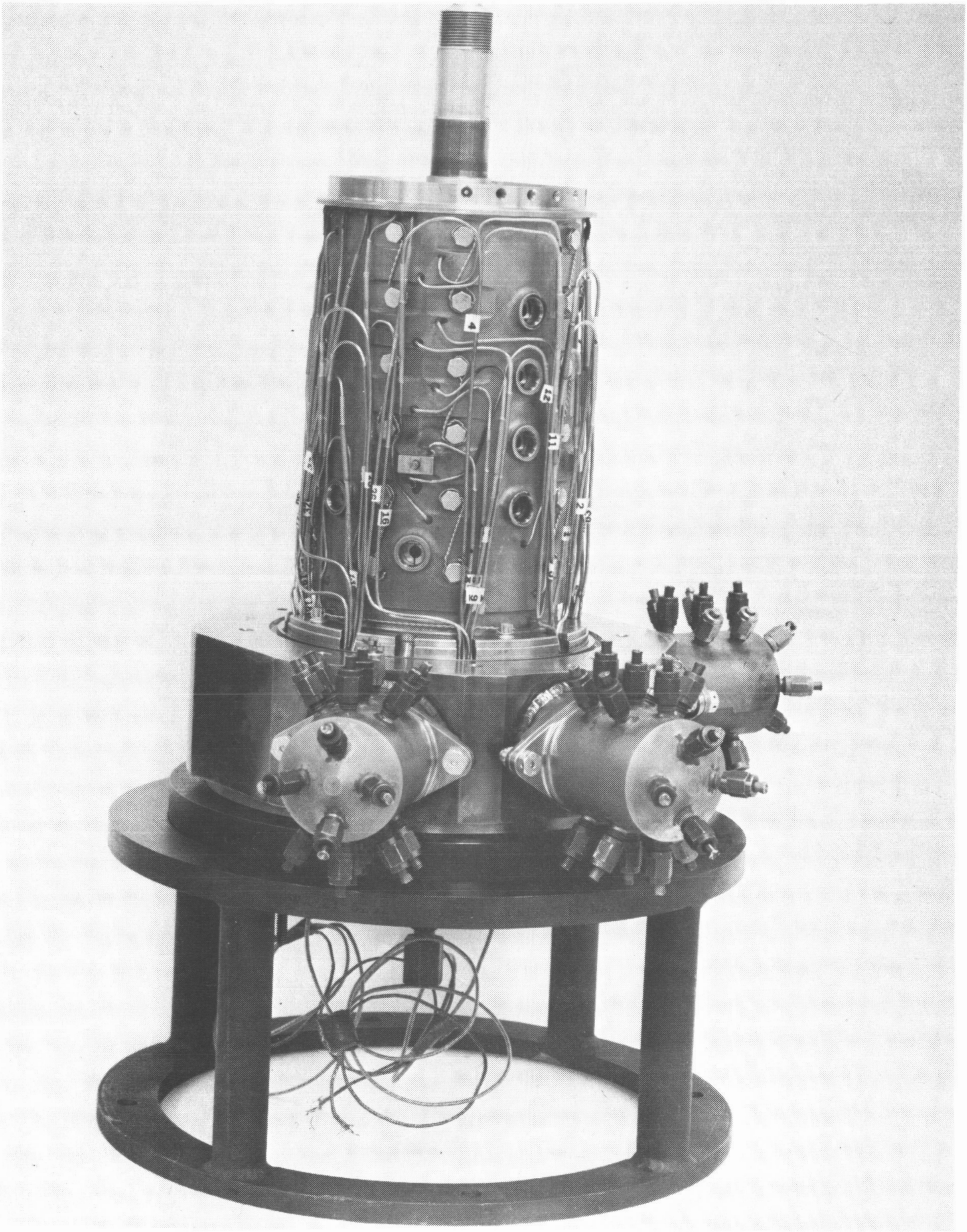

Figure 24 Compressor Assembly Showing Shrink-Fit Joints in Instrumentation Lines X-22309

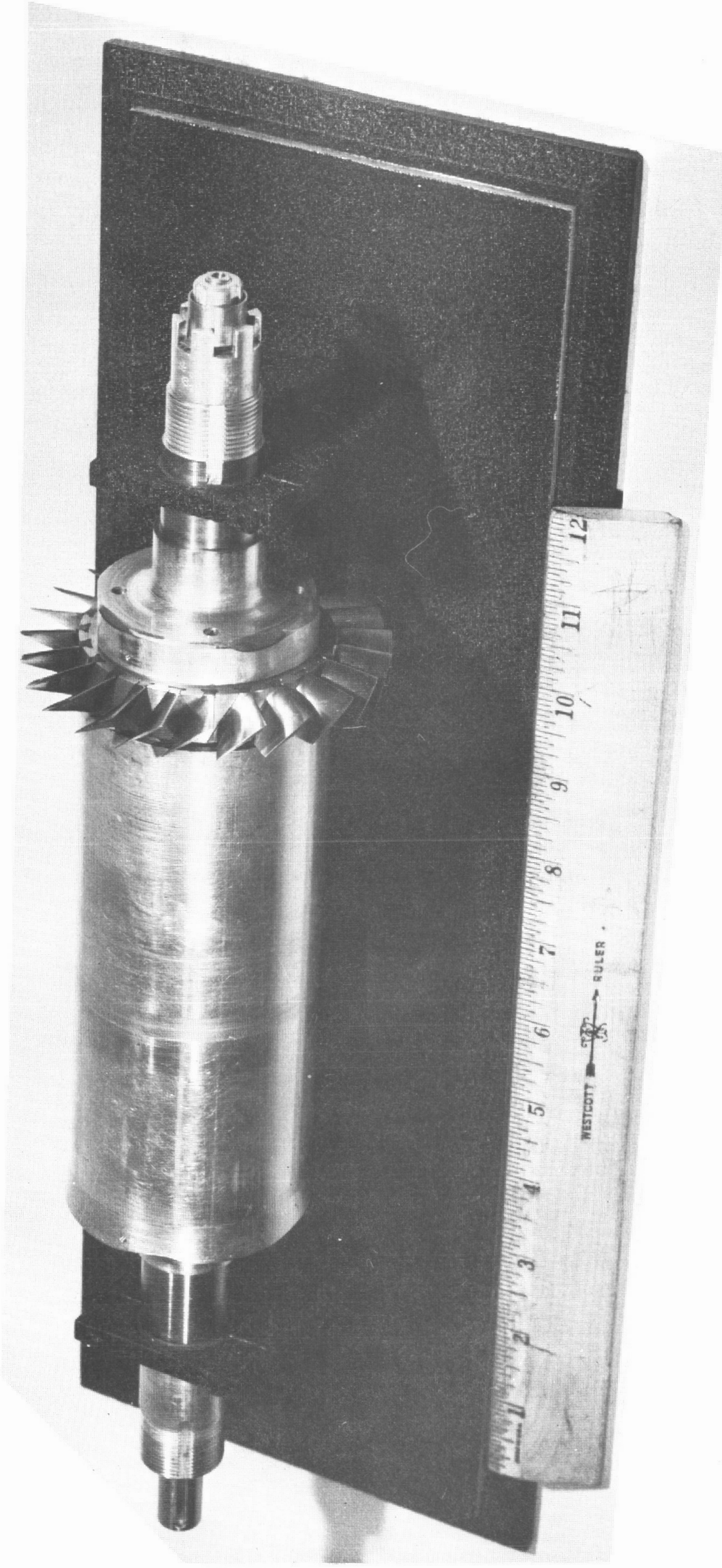

Figure 25 Alternate Rotor for Testing First-Stage Blades X-21877

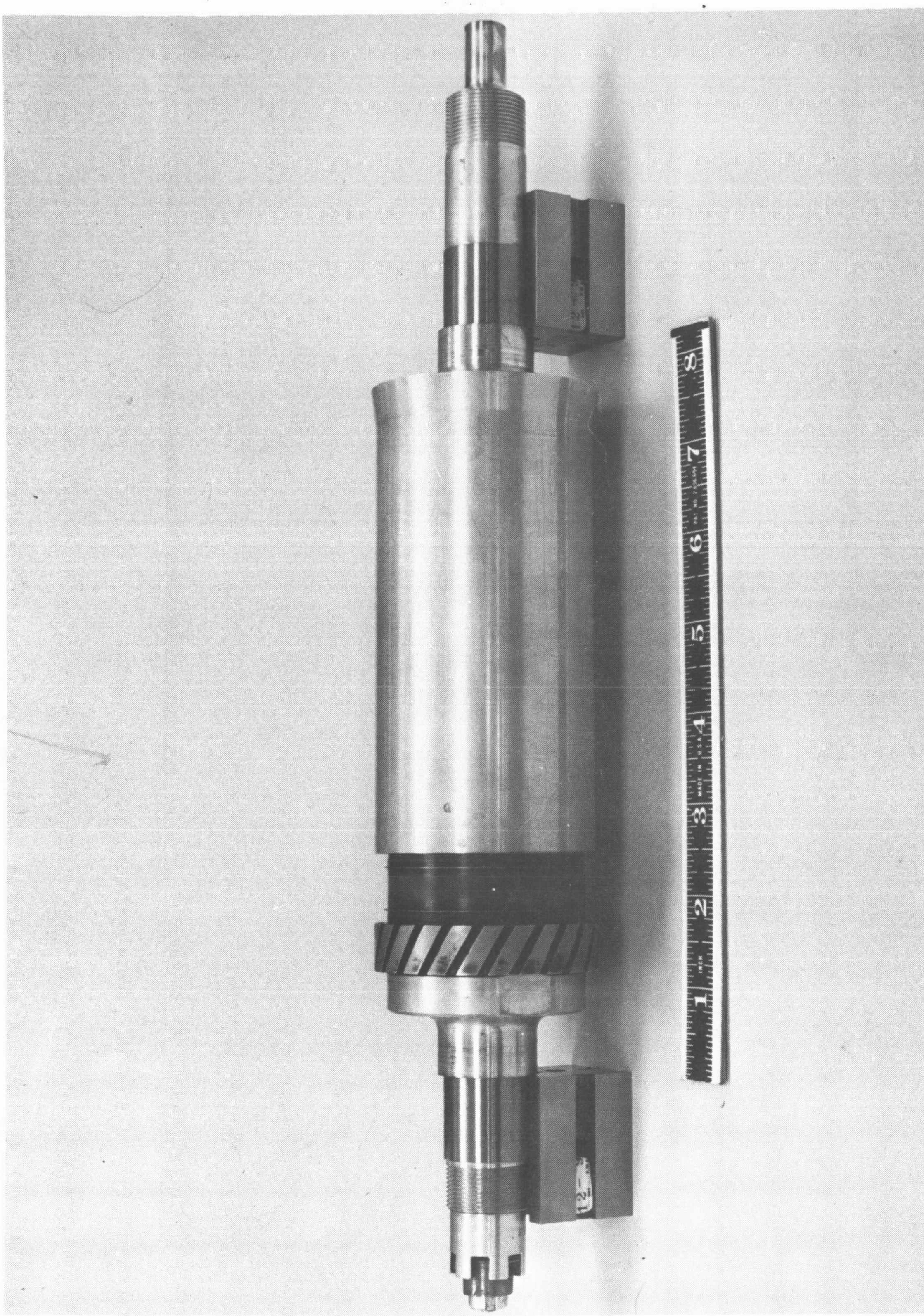

Figure 26 Alternate Rotor for Testing First-Stage Blades and Stator X-22165

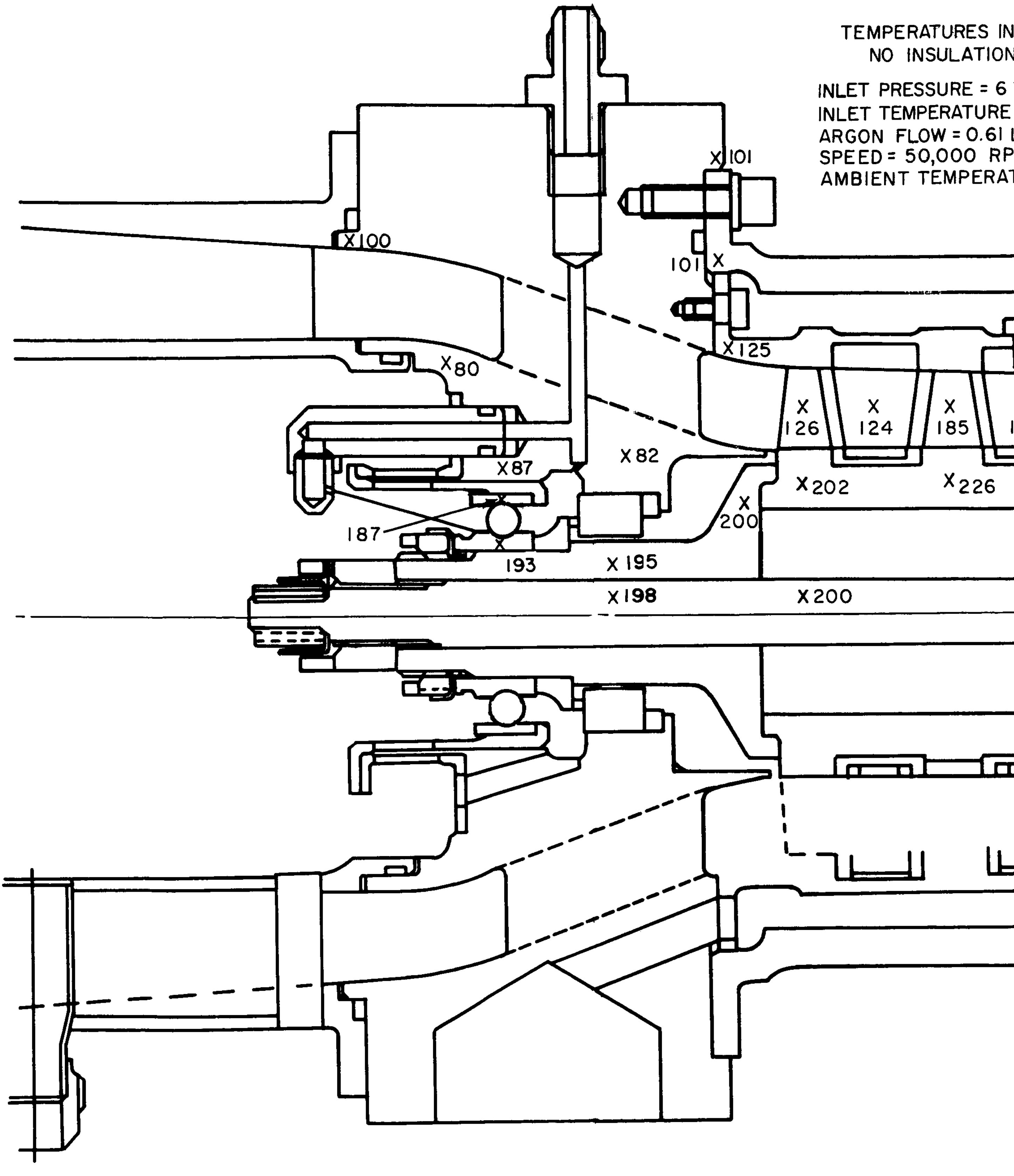

Figure 27 Temperature Map of Compressor Research Package

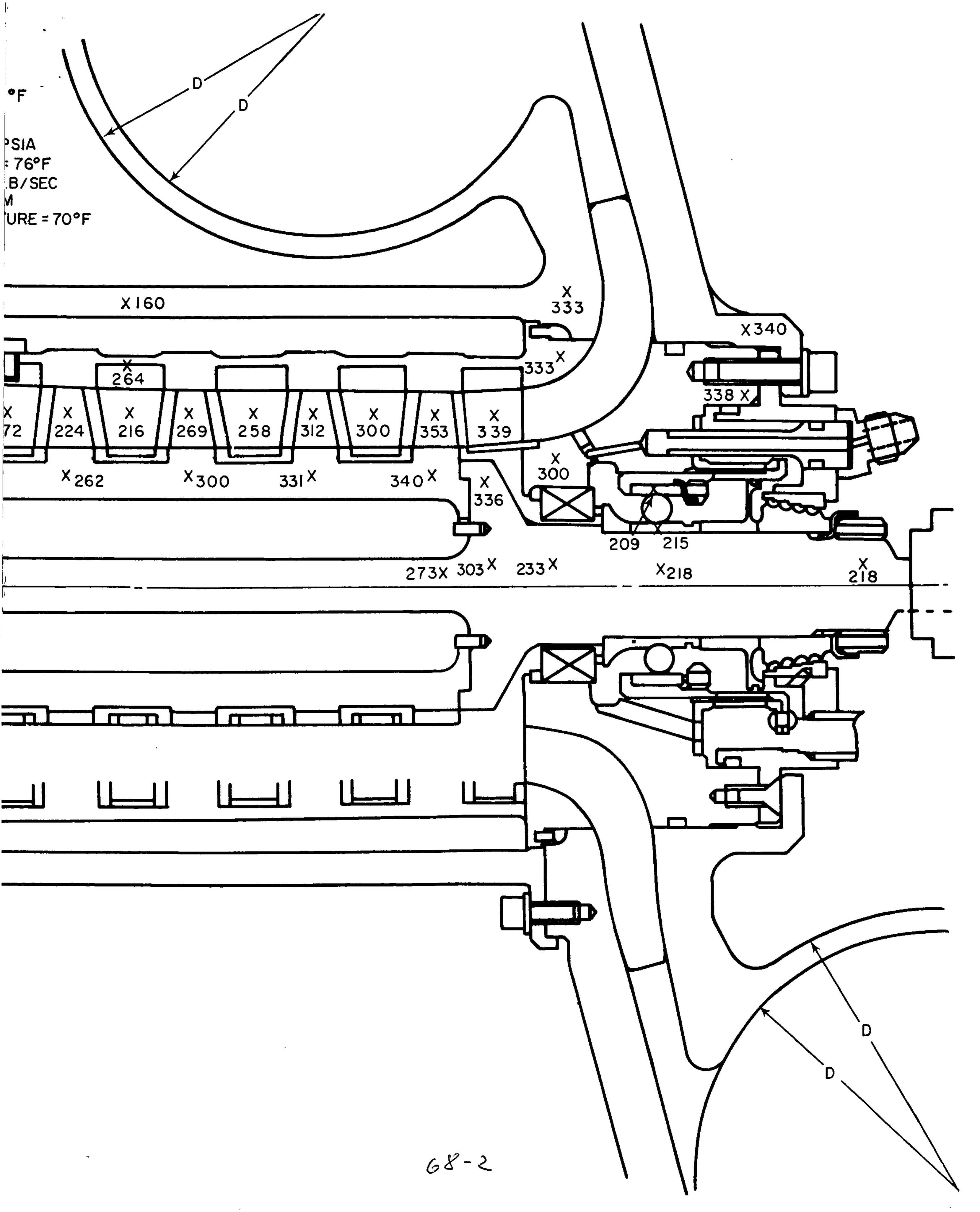

°F
PSIA
= 76°F
LB/SEC
M
TURE = 70°F
D
D
X 160
X 333
333 X
X 340
338 X
X 264
X 72
X 224
X 216
X 269
X 258
X 312
X 300
X 353
X 339
X 262
X 300
331 X
340 X
X 336
X 300
209
215
273 X
303 X
233 X
X 218
X 218
D
D

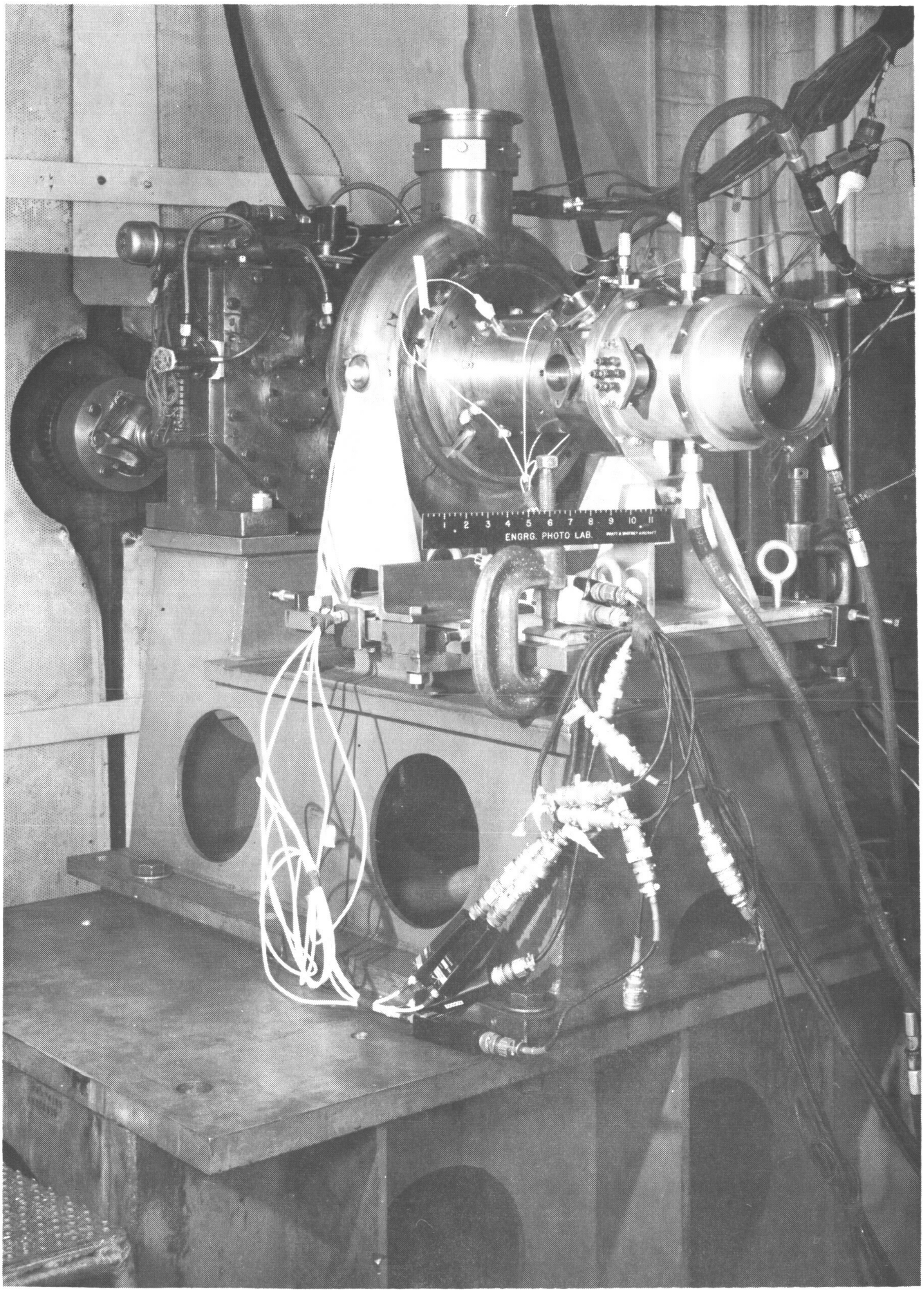

Figure 28 Compressor Research Package Mounted for Rotor Dynamic Test

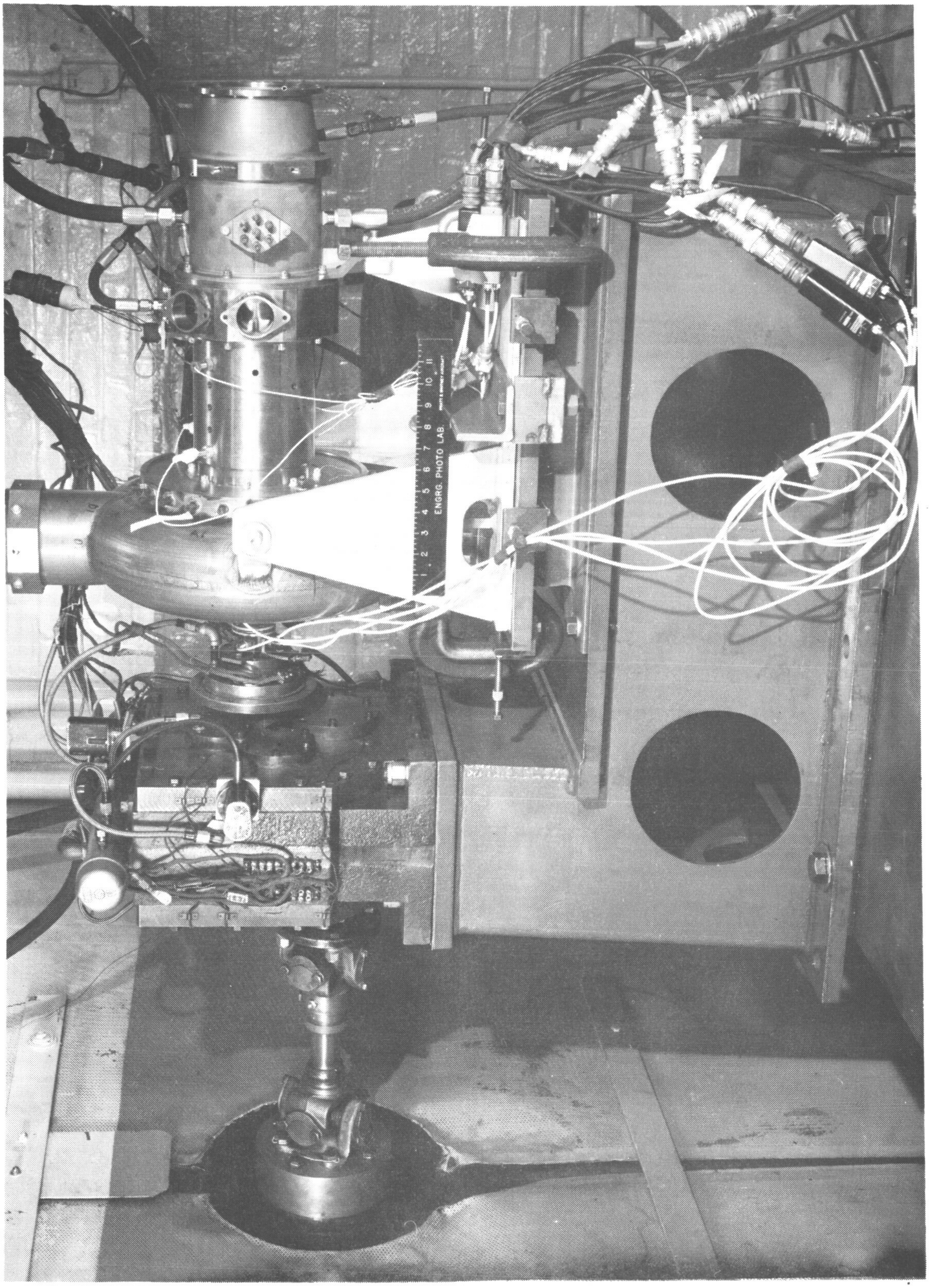

Figure 29 Compressor Research Package Mounted for Rotor Dynamic Test XP-63029

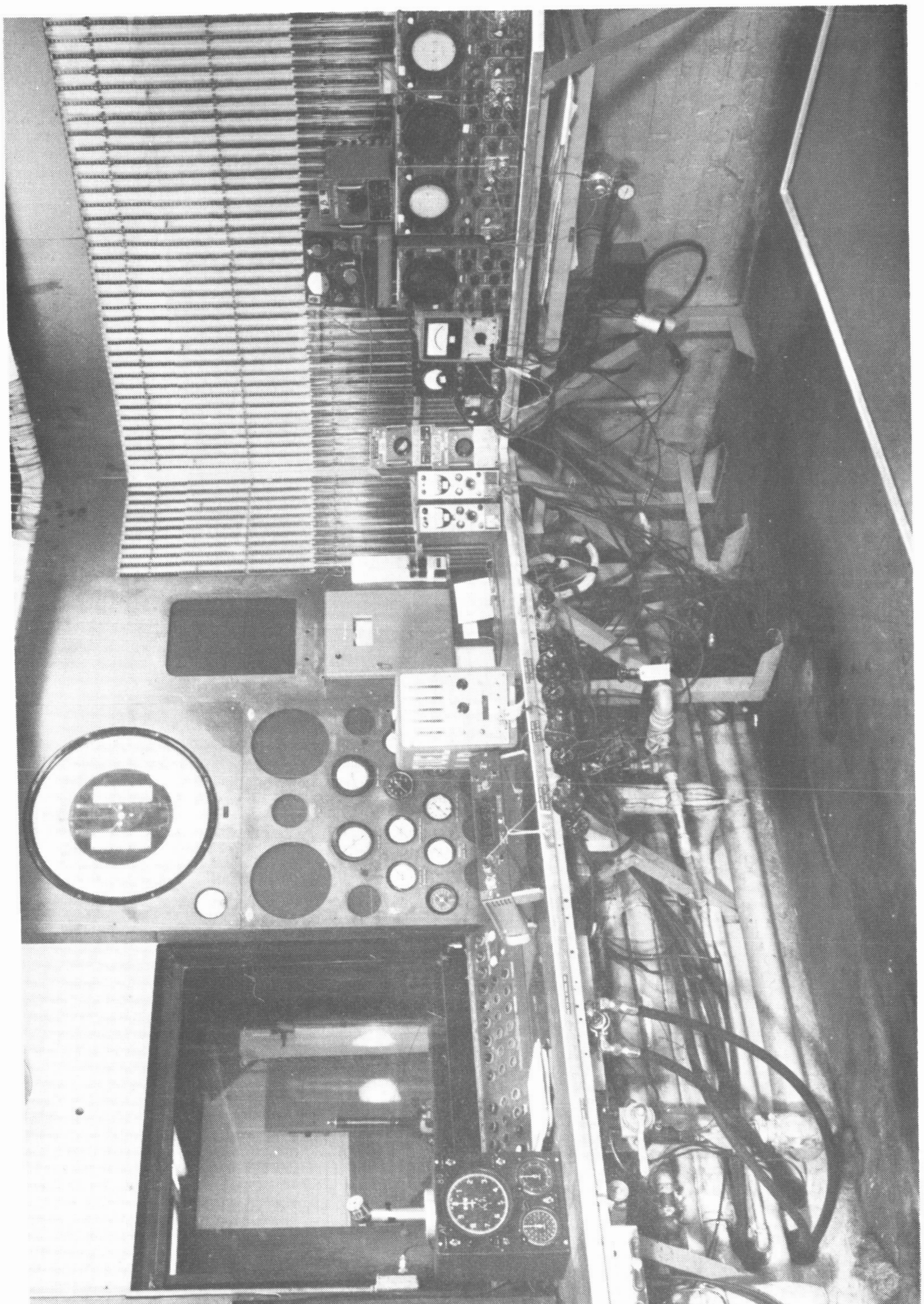

Figure 30 Control Room Used for Test M-37154

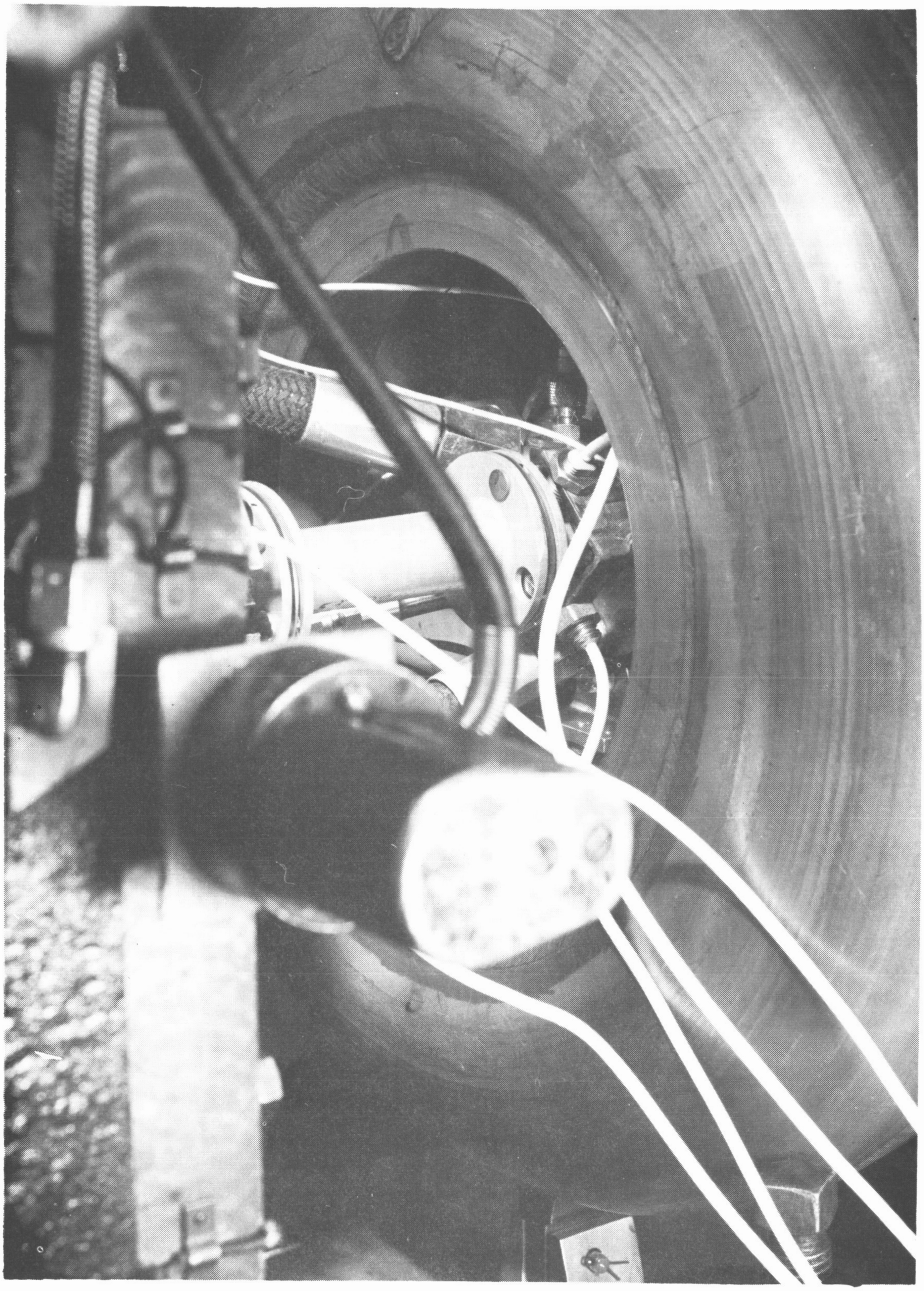

Figure 31 Proximity Probes at Compressor End of Coupling XP-63032

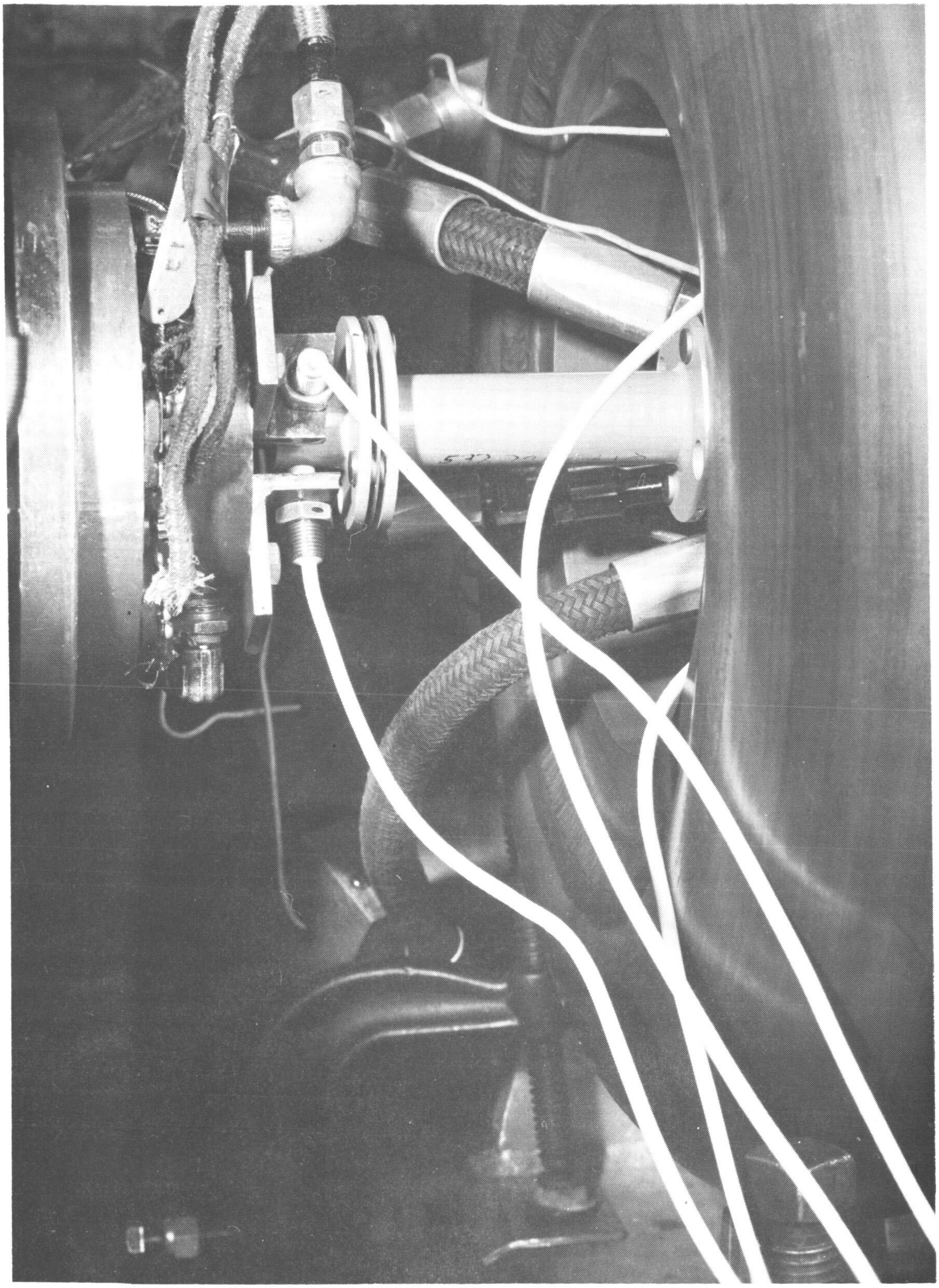

Figure 32 Proximity Probes at Gearbox End of Coupling XP-63031

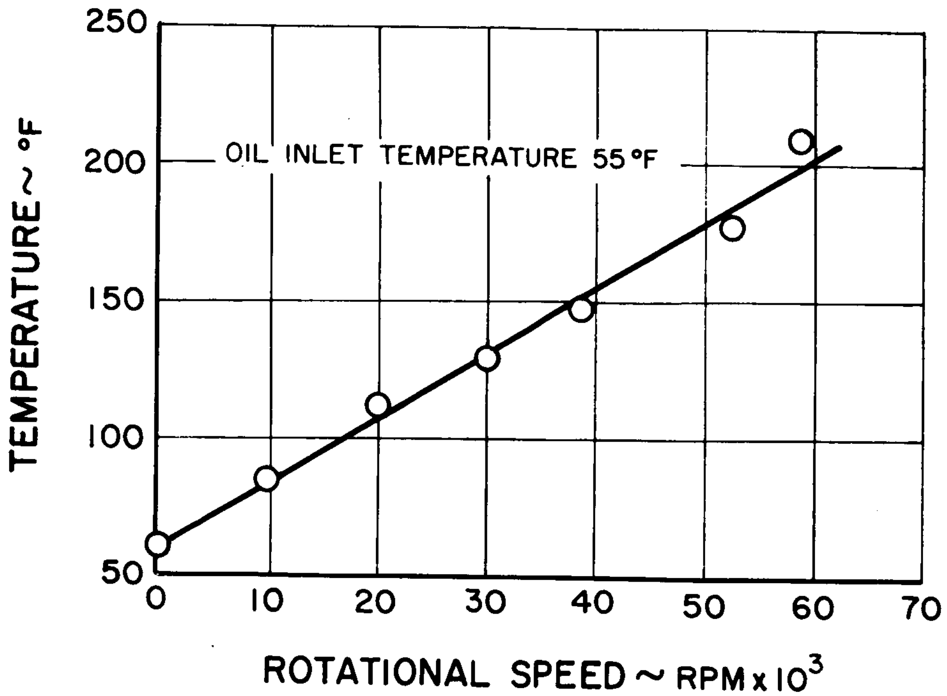

Figure 33 Representative Bearing Temperatures

Front Rear

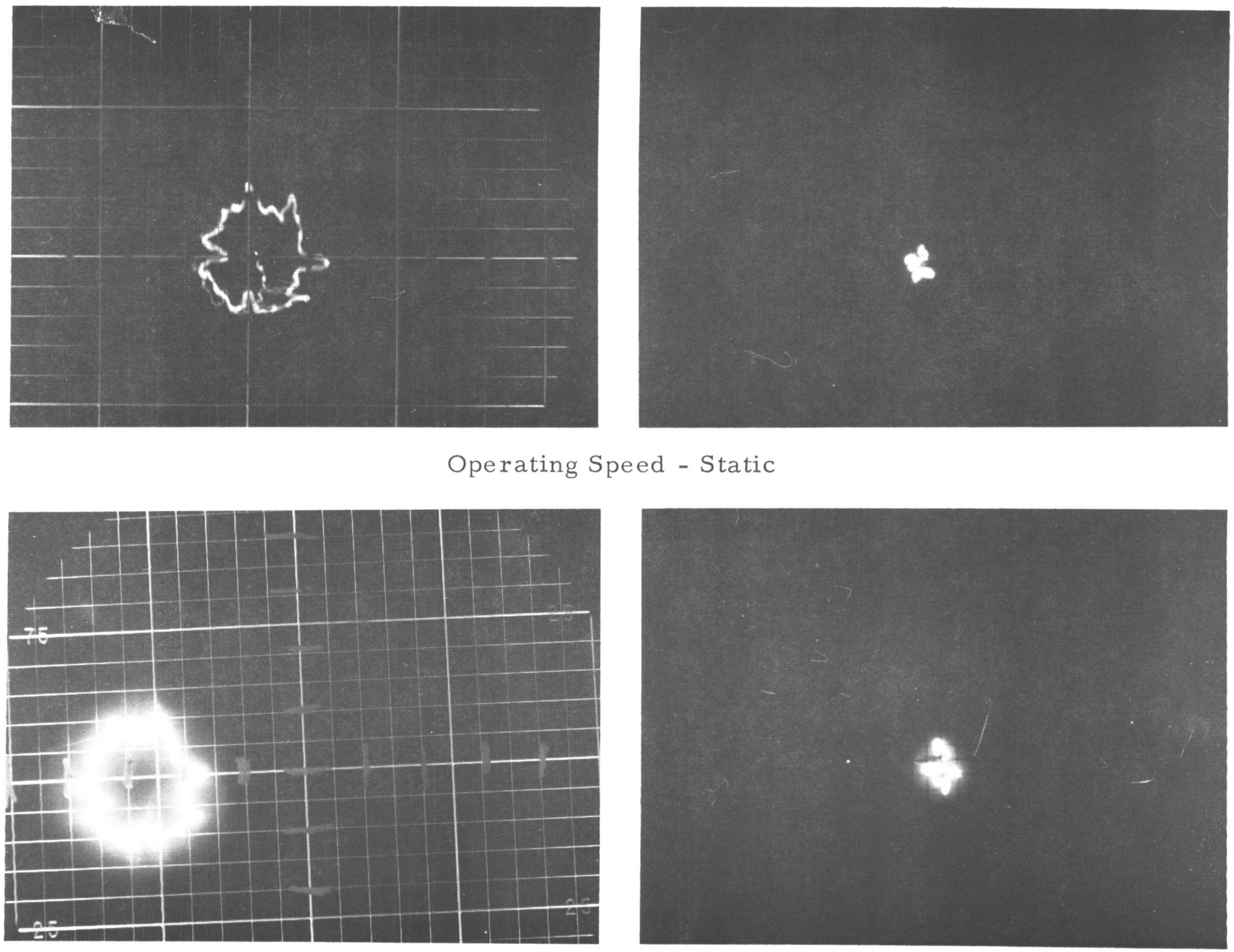

Operating Speed - Static

Operating Speed - 9,260 rpm

Figure 34 Compressor Research Package Proximity Probe Data.
Compressor Rotor Traces

Front

Rear

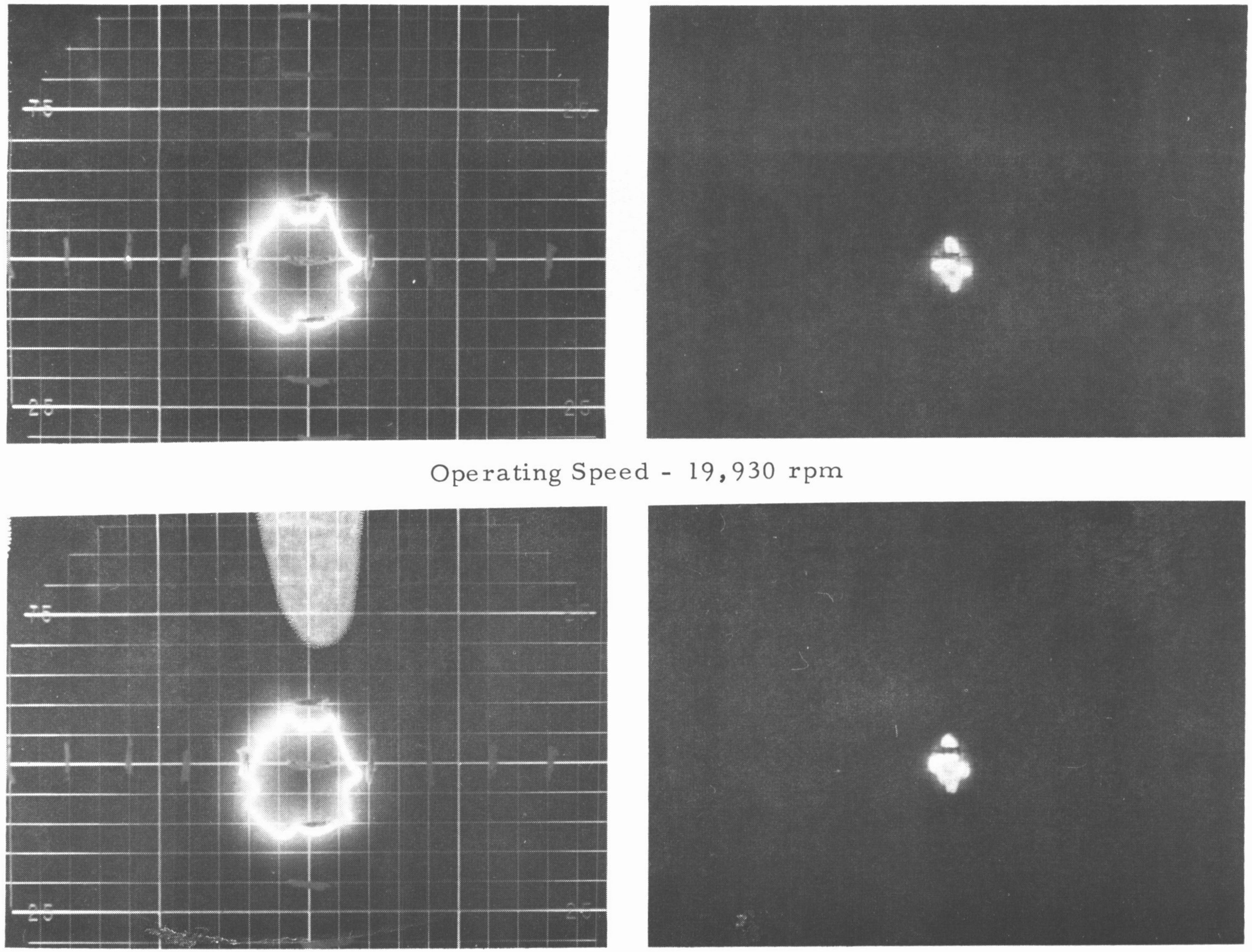

Operating Speed - 19,930 rpm

Operating Speed - 29,960 rpm

Figure 35 Compressor Research Package Proximity Probe Data. Compressor Rotor Traces

Front

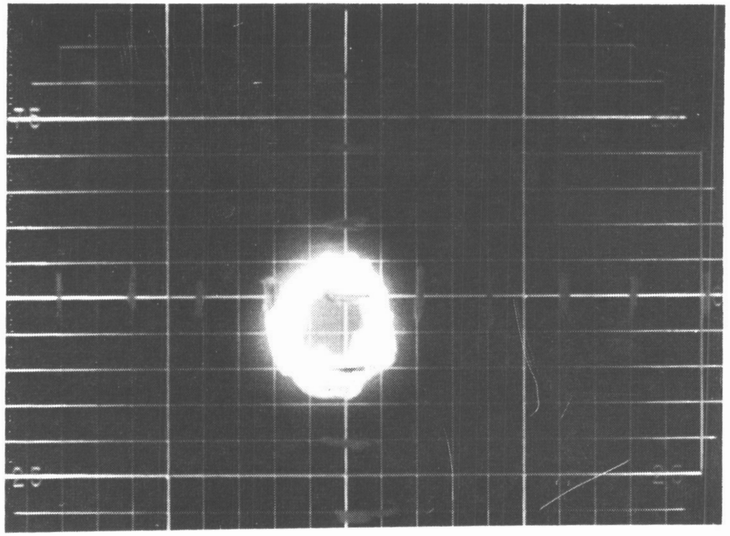

Operating Speed - 38,880 rpm

Rear

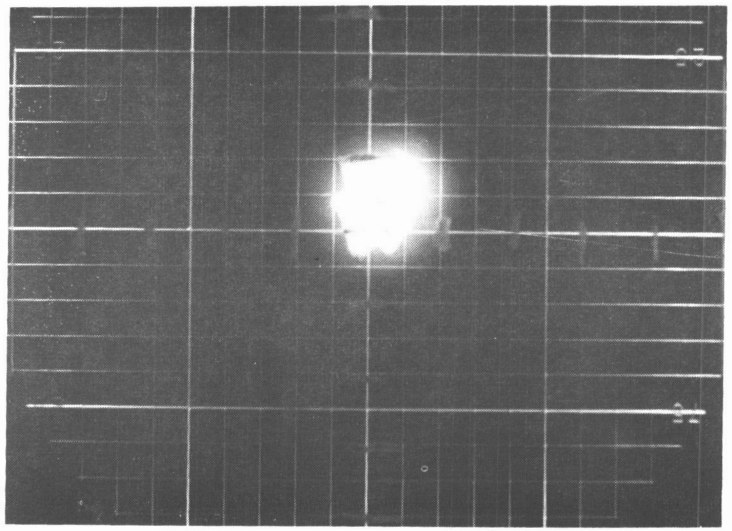

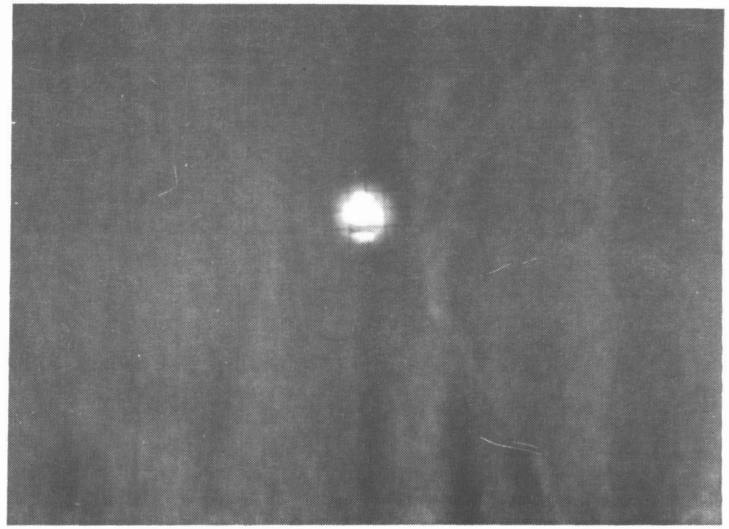

Operating Speed - 44,010 rpm

Figure 36 Compressor Research Package Proximity Probe Data. Compressor Rotor Traces

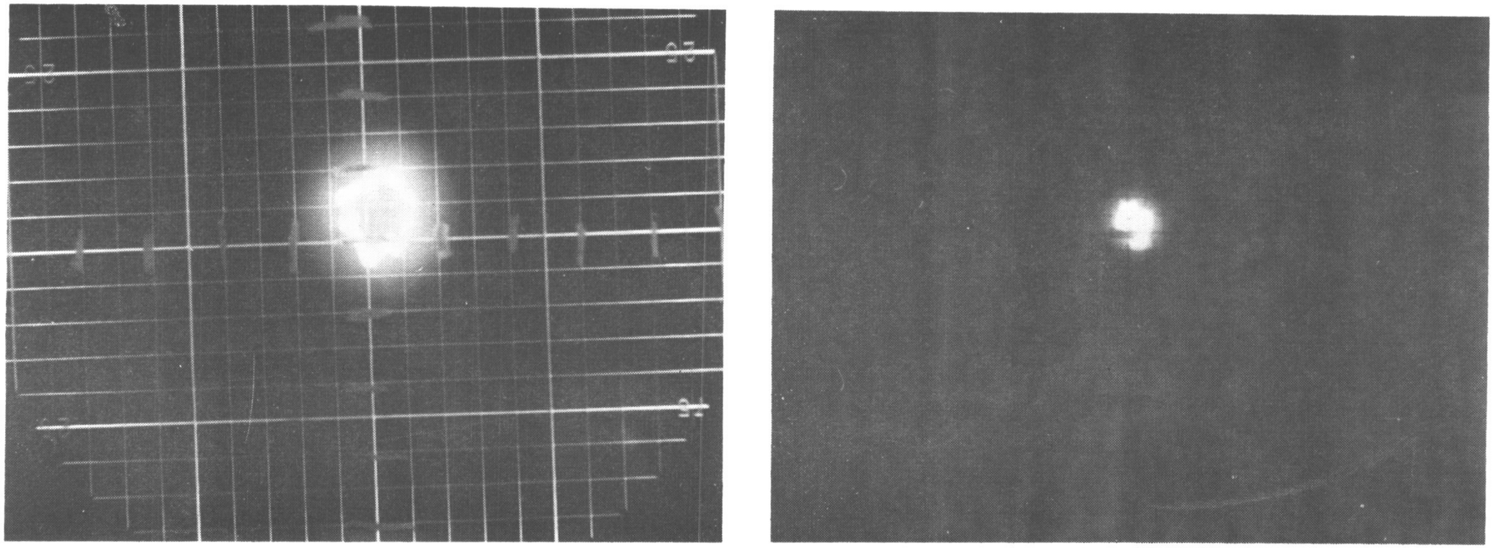

Operating Speed - 52,500 rpm

Figure 37 Compressor Research Package Proximity Probe Data. Compressor Rotor Traces

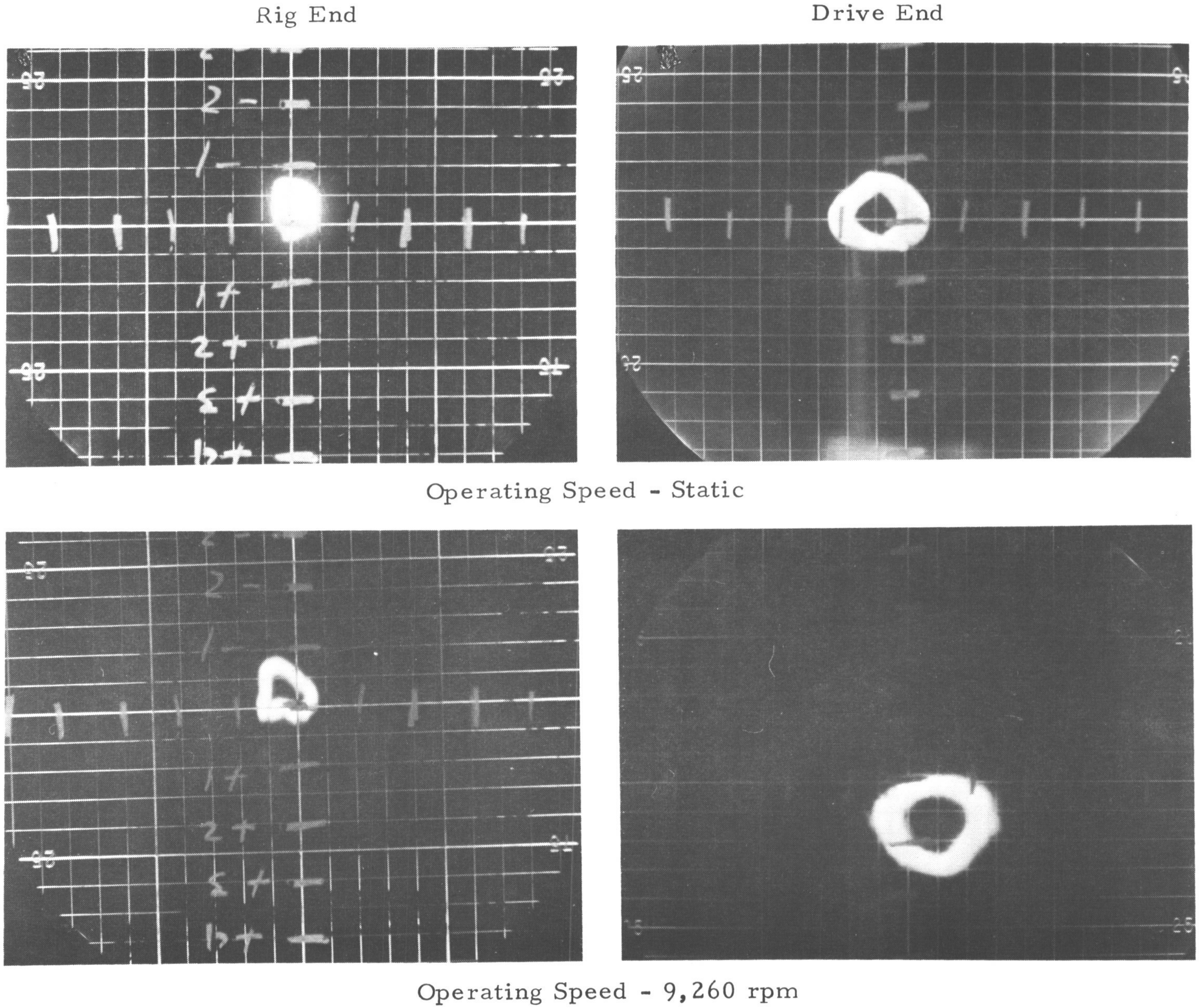

Figure 38 Compressor Research Package Proximity Probe Data. Drive Coupling Traces

Rig End Drive End

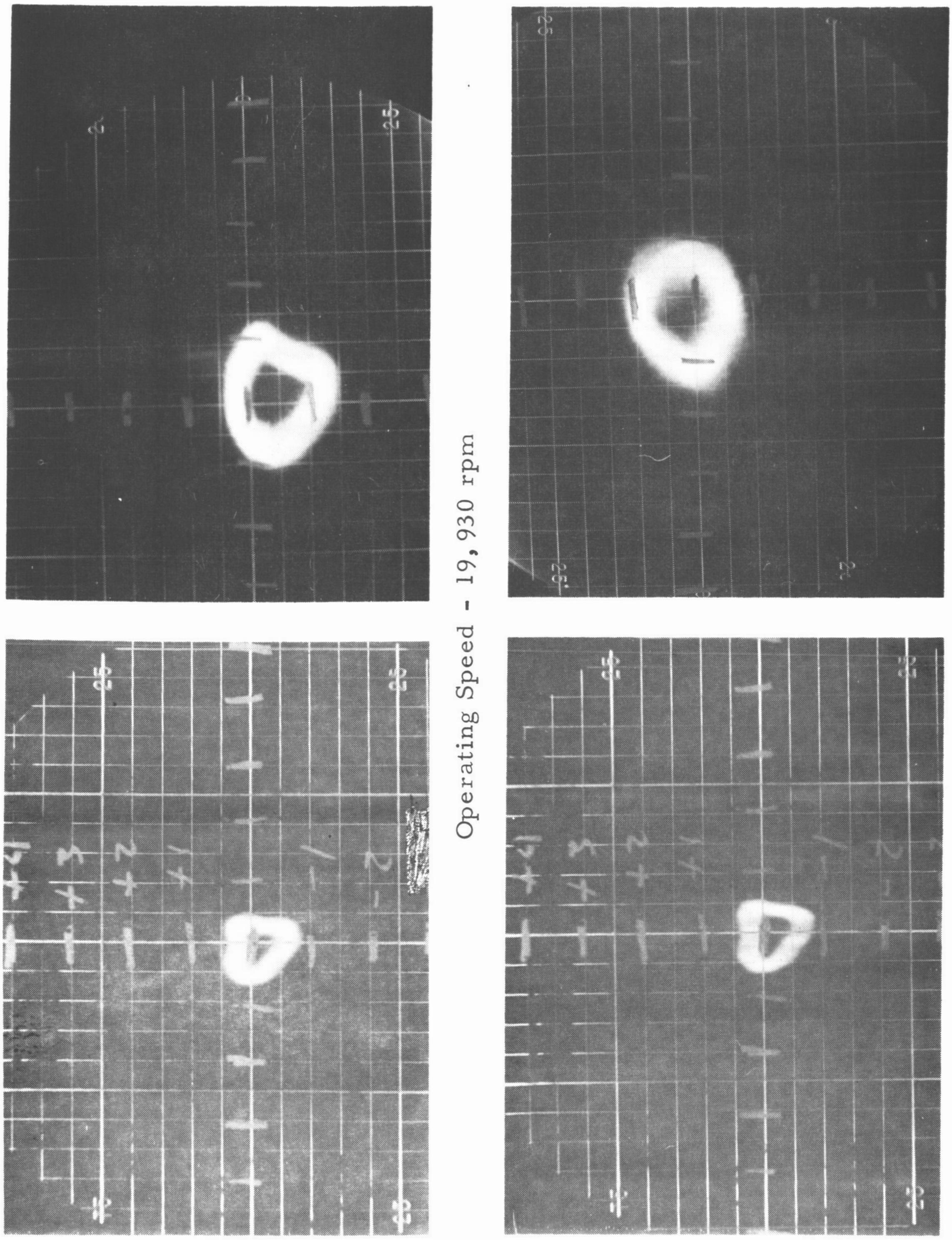

Operating Speed - 19,930 rpm

Operating Speed - 29,960 rpm

Figure 39 Compressor Research Package Proximity Probe Data. Drive Coupling Traces

Drive End

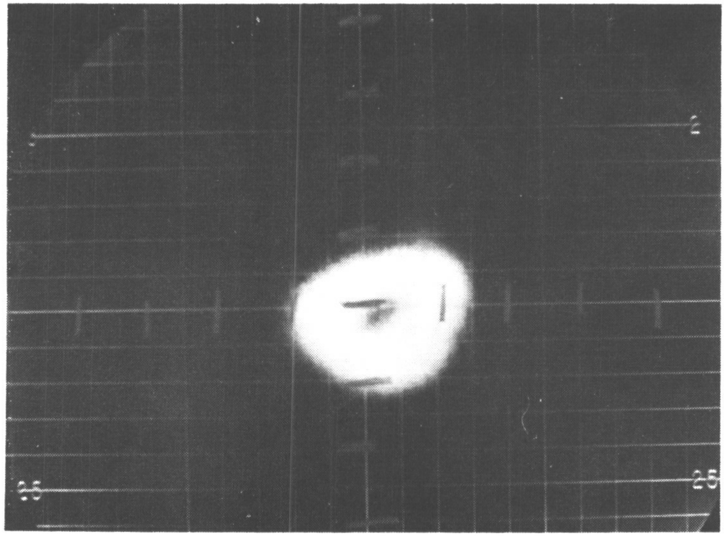

Operating Speed - 52,500 rpm

Figure 40 Compressor Research Package Proximity Probe Data. Drive Coupling Traces

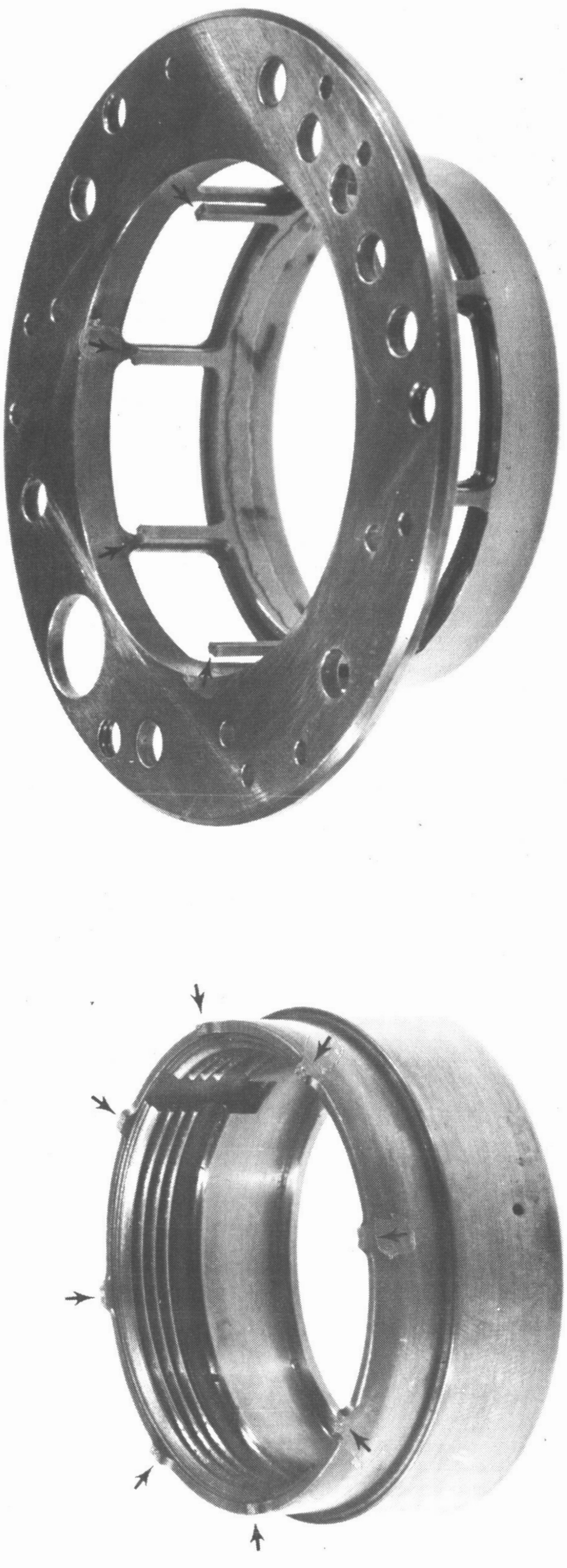

Figure 41 Front Bearing Mount Spring Showing Failure of Eight Axial Beams
XP-64229

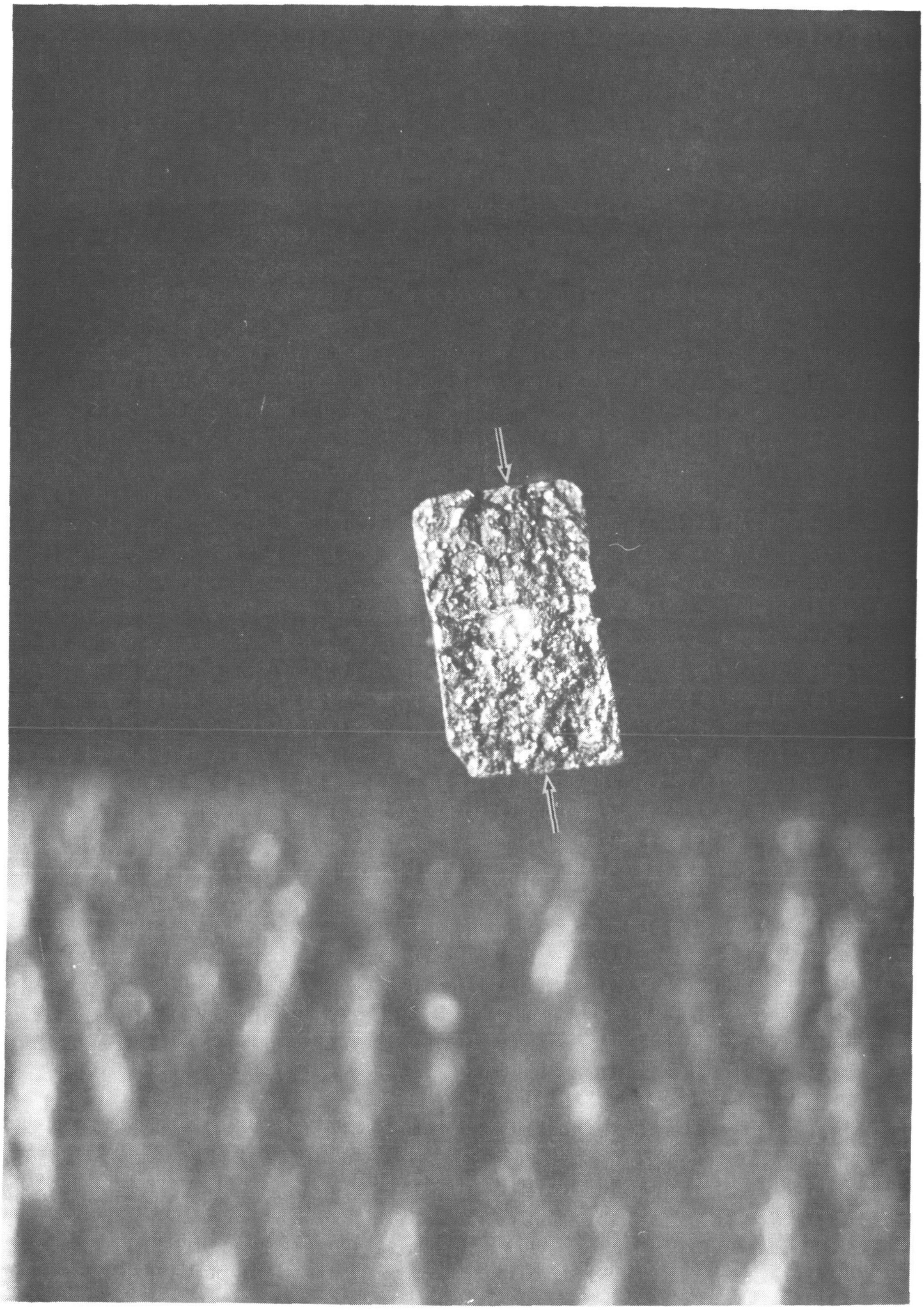

Figure 42 Closeup of Typical Beam Fracture Showing Fatigue Failure Progressing from Origins (Arrows) H-57708

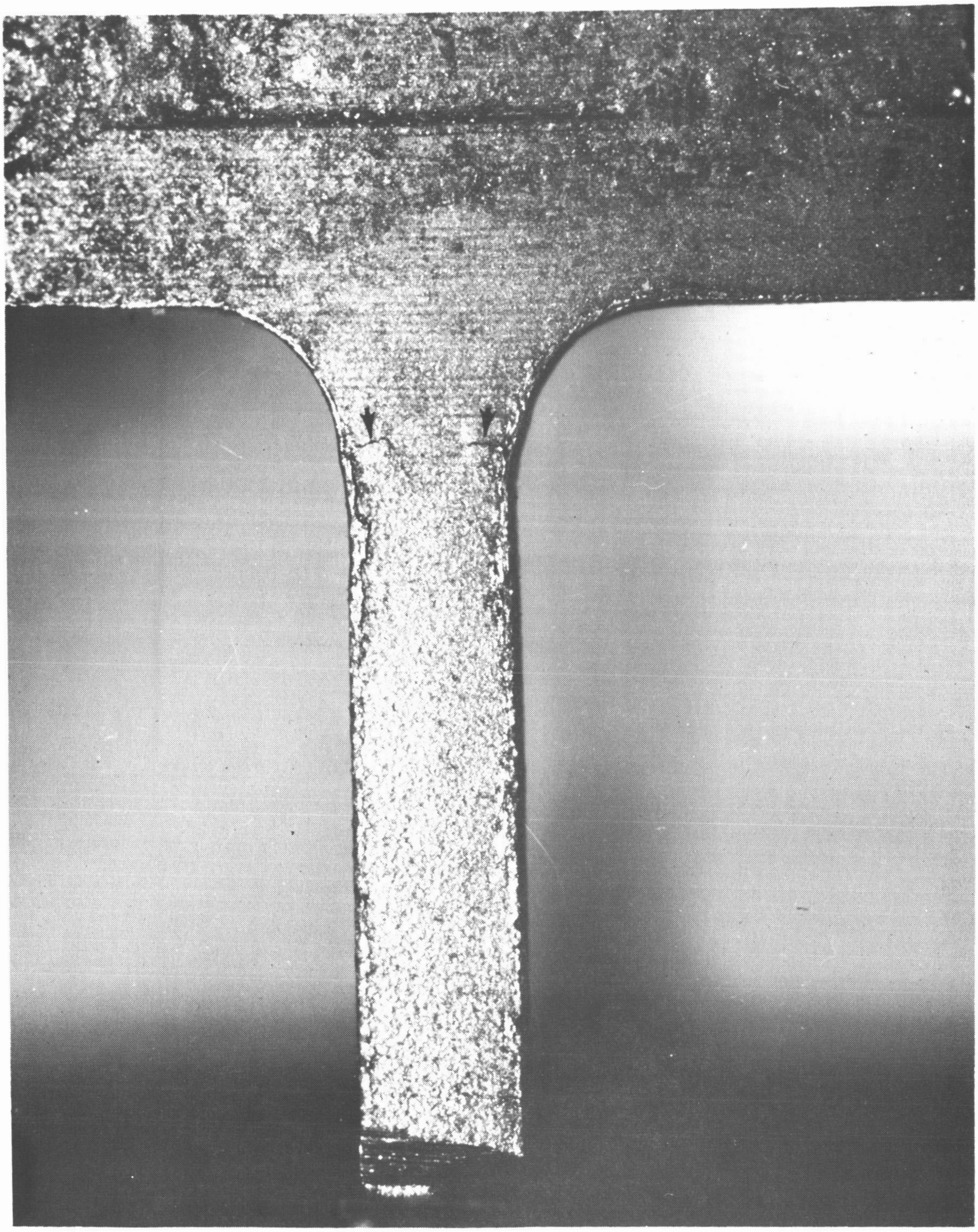

Figure 43 Closeup of Typical Failed Beam Showing Circumferential Cracks (Arrows) at Forward End of Beam H-57709

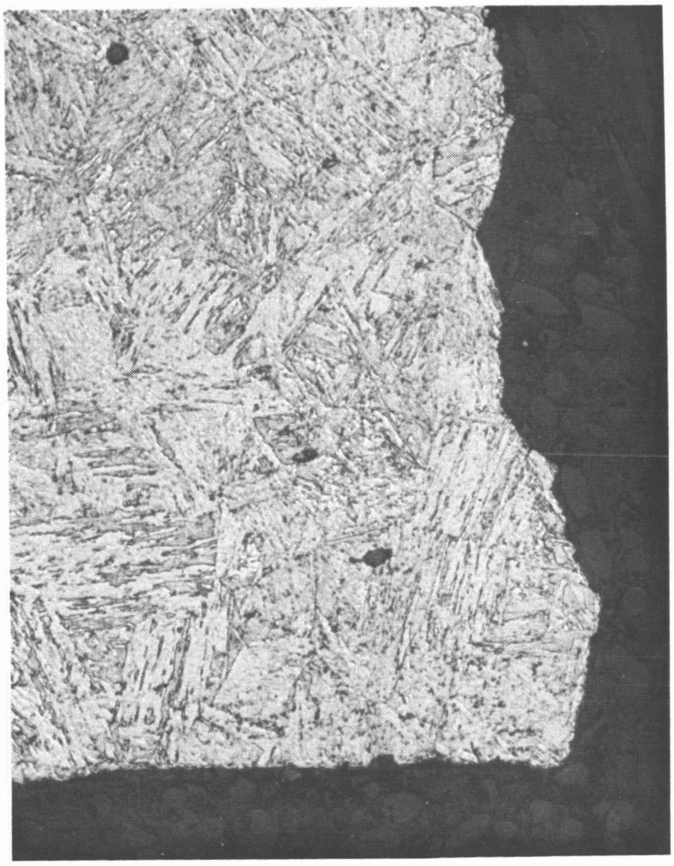

Mag: 325X

Figure 44 Photomicrograph of Beam at Location of Failure. Material AMS 5613. Hardness Rockwell C29 to 31

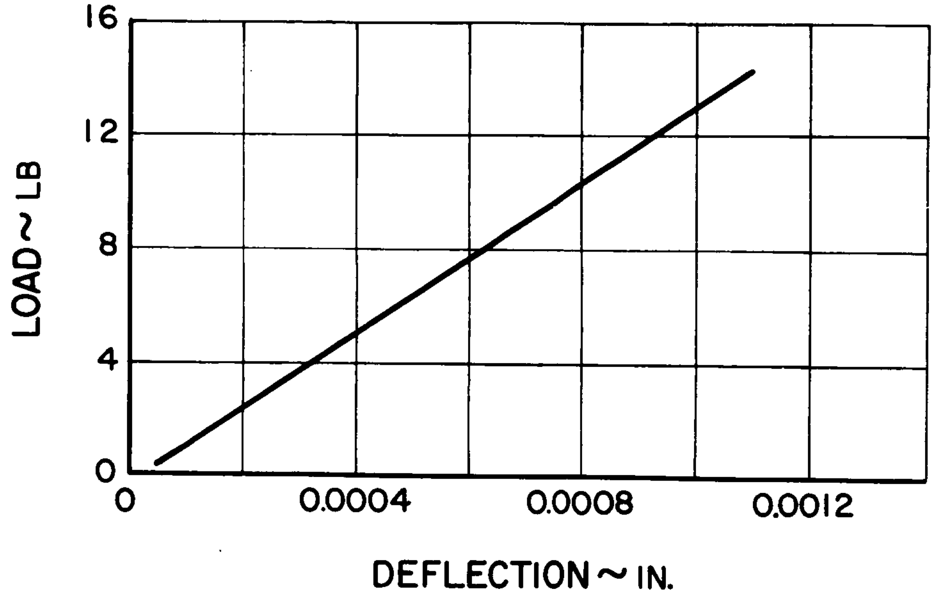

Figure 45 Deflection Rate for Steel Bearing Mount

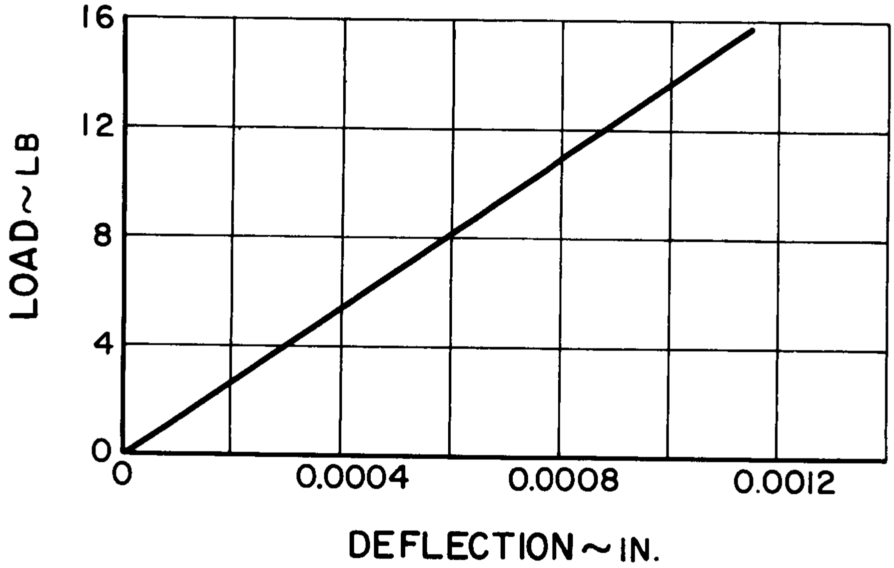

Figure 46 Deflection Rate for Titanium Bearing Mount

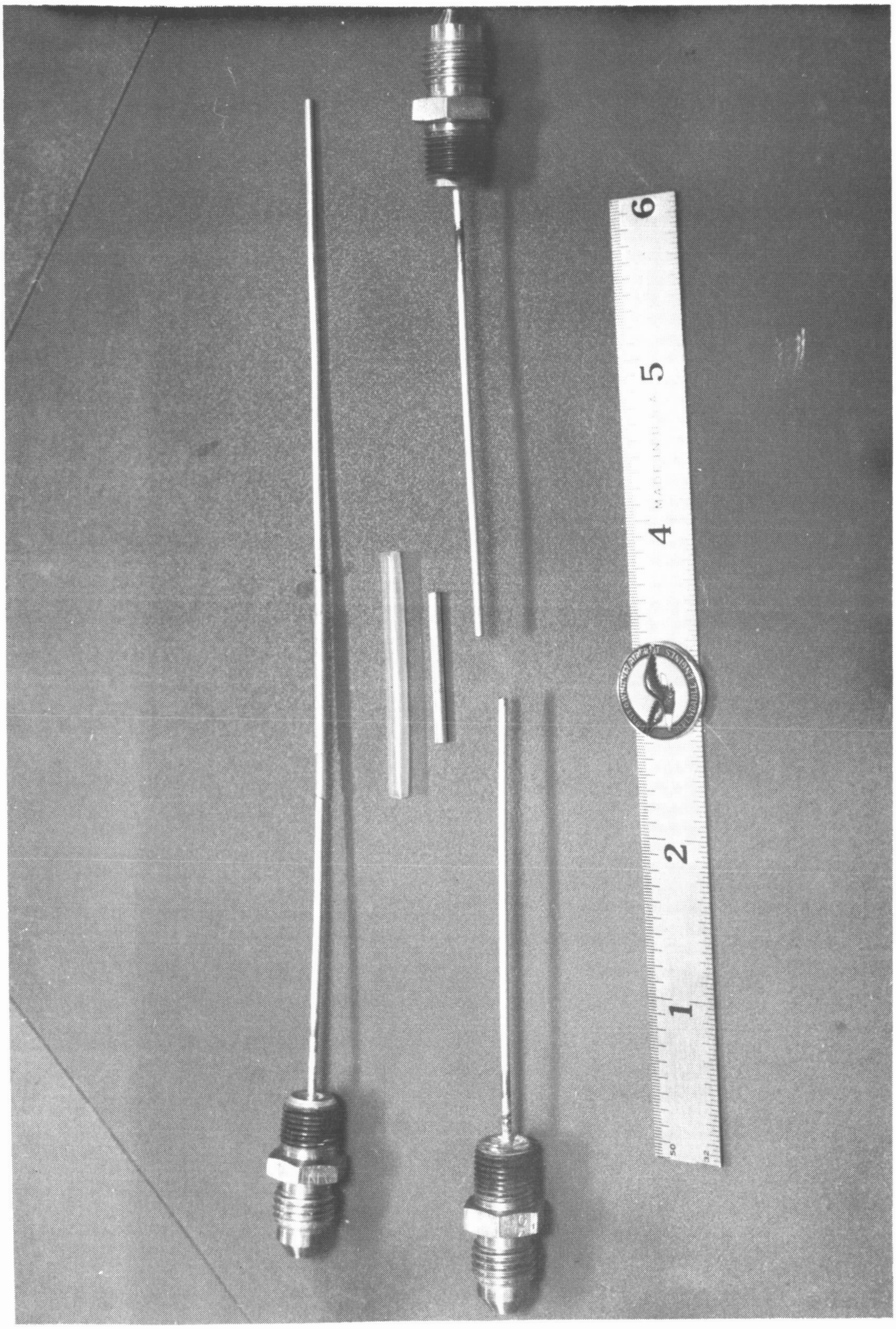

Figure 47 Shrink Tube Test Specimen X-20384

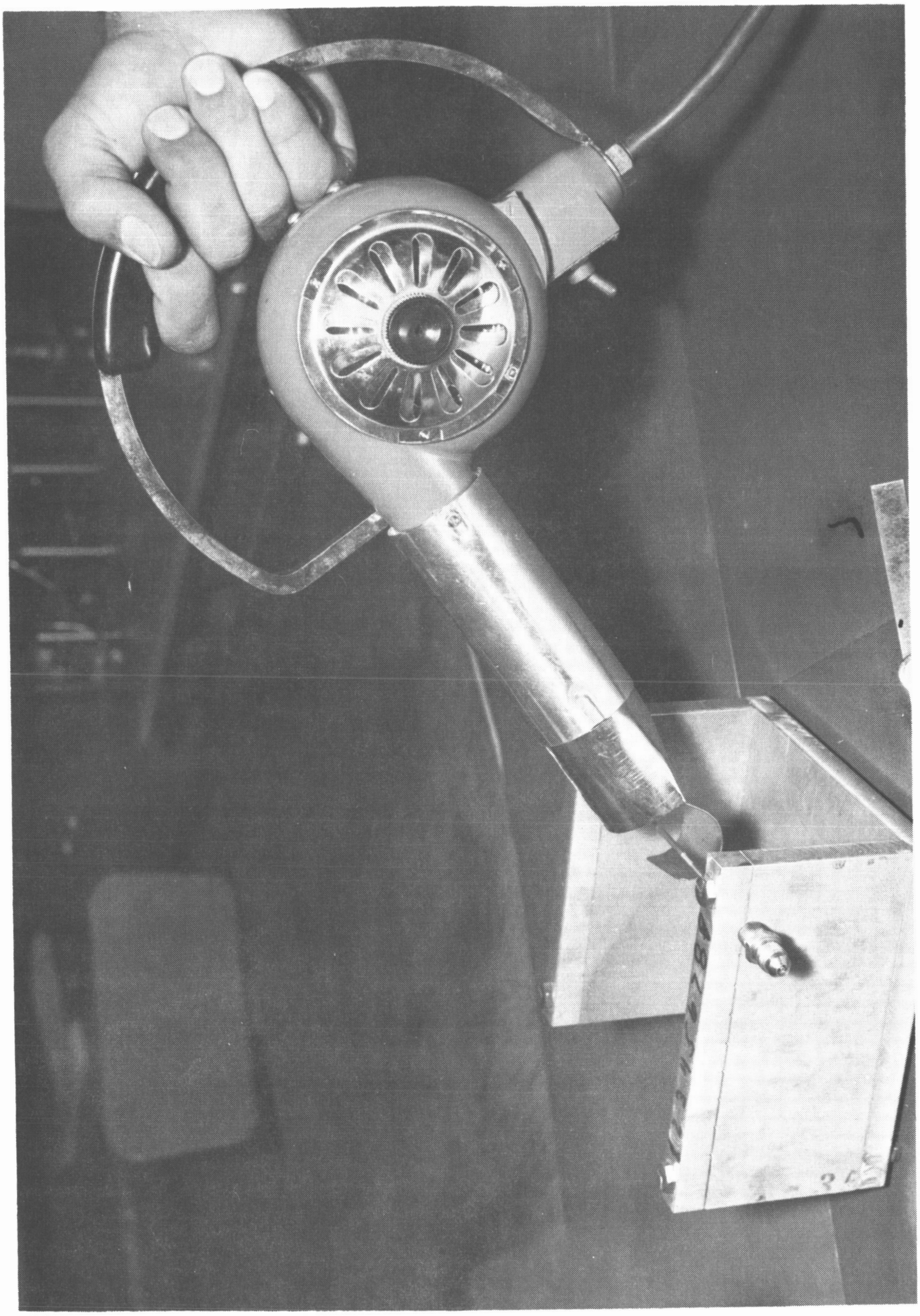

Figure 48 Shrink Tube Being Heated X-20386

Distribution List
Contract NAS3-4179

National Aeronautics and Space Administration
Washington, D. C. 20546
Attention: Dr. Fred Schulman, RNP 1
Herbert D. Rochen, RNP 1
S. V. Manson, RNP 1
Arvin Smith, RNW 1

National Aeronautics and Space Administration
Lewis Research Center
21000 Brookpark Road
Cleveland, Ohio 44135
Attention: Jack A. Heller, MS 500-201 1
J. E. Dilley, MS 500-309 1
P. E. Foster, MS 3-19 1
Dr. B. Lubarsky, MS 500-201 1
D. G. Beremand, MS 500-201 1
J. H. Dunn, MS 500-201 1
J. P. Joyce, MS 500-201 1
H. B. Tryon, MS 500-201 1
I. I. Pinkel, MS 5-3 1
W. L. Stewart, MS 77-2 1
H. E. Rohlik, MS 77-2 1
C. L. Ball, MS 5-9 2
W. A. Benser, MS 5-9 1
D. C. Guentert, MS 500-201 1
D. T. Bernatowicz, MS 500-201 1
T. A. Moss, MS 500-201 1
V. F. Hlavin, MS 3-14 1
E. R. Tysl, MS 5-9 1
F. J. Dutee, MS 21-4 1
R. Y. Wong, MS 77-2 1
M. J. Hartmann, MS 5-9 1
Report Control Office, MS 5-5 1
Reliability & Quality Assurance Office, MS 500-203 1
Library, MS 60-3 2

NASA Ames Research Center
Moffett Field, California 94035 1
Attention: Library

NASA Flight Research Center
P.O. Box 273, Edwards, California 93523
Attention: Library 1

NASA Goddard Space Flight Center
Greenbelt, Maryland 20771
Attention: Library 1

NASA Langley Research Center
Langley Station, Hampton, Virginia 23365
Attention: Library 1

NASA Manned Spacecraft Center
Houston, Texas 77058
Attention: Tony Redding, 1
Library, 1

NASA Marshall Space Flight Center
Huntsville, Alabama 35812
Attention: Library 1

NASA Western Operations Office
150 Pico Boulevard
Santa Monica, California 90406
Attention: Library 1

NASA Jet Propulsion Laboratory
4800 Oak Grove Drive
Pasadena, California 91103
Attention: Library 1

National Aeronautics and Space Administration
Scientific & Technical Information Facility
P.O. Box 33, College Park, Maryland 20740
Attention: Acquisitions Branch, SQT-34054 1 + 1 repro

NASA Lewis Research Center Resident Office
Pratt & Whitney Aircraft
West Palm Beach, Florida 33402
Attention: George K. Fischer 1

U.S. Army Engineer R&D Laboratories
Gas Turbine Test Facility
Fort Belvoir, Virginia 22060
Attention: W. Crim 1

Office of Naval Research
Department of the Navy
Washington, D. C. 20025
Attention: Dr. Ralph Roberts 1

Bureau of Naval Weapons
Department of the Navy
Washington, D. C. 20025
Attention: Code RAPP 1

Bureau of Ships
Department of the Navy
Washington, D. C. 20025
Attention: G. L. Graves 1

Air Force Systems Command
Aeronautical Systems Division
Wright-Patterson Air Force Base, Ohio 45433
Attention: Library 1

Wright-Patterson Air Force Base, Ohio 45433
Attention: Robin Chasman, APFL 1
George Thompson, APFL 1

Institute for Defense Analyses
400 Army - Navy Drive
Arlington, Virginia 22202
Attention: Library 1

University of Pennsylvania
Power Information Center
Room 2107
3401 Market Street
Philadelphia, Pennsylvania 19104 1

Massachusetts Institute of Technology
Cambridge, Massachusetts 02139
Attention: Library 1

University of Virginia
Department of Mechanical Engineering
Charlottesville, Virginia 22903
Attention: Dr. E. J. Gunter, Jr. 1

Aerojet General Corporation
Azusa, California 91703
Attention: Library 1

AiResearch Manufacturing Company
The Garrett Corporation
402 South 36th Street
Phoenix, Arizona 85034
Attention: R. Bullock 1
Library 1

AiResearch Manufacturing Company
The Garrett Corporation
9851 Sepulveda Boulevard
Los Angeles, California 90009
Attention: Library 1

Bendix Research Laboratories Division
Southfield (Detroit), Michigan 48232
Attention: Library 1

The Boeing Company
Aero-Space Division
Box 3707, Seattle, Washington 98124
Attention: Library 1

Borg-Warner Corporation
Pesco Products Division
24700 North Miles Road
Bedford, Ohio 44014
Attention: Library 1

Consolidated Controls Corporation
15 Durant Avenue
Bethel, Connecticut 06801
Attention: Library 1

Continental Aviation & Engineering Corporation
12700 Kercheval Avenue
Detroit, Michigan 48215
Attention: Library 1

Curtiss-Wright Corporation
Wright Aero Division
Main and Passaic Streets
Woodridge, New Jersey 07075
Attention: Library 1

Douglas Aircraft Company
3000 Ocean Park Boulevard
Santa Monica, California 90406
Attention: Library 1

Franklin Institute Laboratories
Benjamin Franklin Parkway at 20th St.
Philadelphia, Pennsylvania 19103
Attention: Otto Decker 1

General Dynamics Corporation
16501 Brookpark Road
Cleveland, Ohio 44142
Attention: Library 1

General Electric Company
Flight Propulsion Laboratory Division
Cincinnati, Ohio 45215
Attention: Library 1

General Electric Company
Mechanical Technology Laboratory
Schenectady, New York 12301
Attention: Library 1

General Electric Company
Missile & Space Vehicle Department
3198 Chestnut Street
Philadelphia, Pennsylvania 19104
Attention: Library 1

General Motors Corporation
Indianapolis, Indiana 46206
Attention: Library 1

Lear Siegler, Inc.
3171 S. Bundy Drive
Santa Monica, California 90406
Attention: Library 1

Lockheed Missiles & Space Company
P.O. Box 504, Sunnyvale, California 94088
Attention: Library 1

Mechanical Technology Incorporated
968 Albany-Shaker Road
Latham, New York 12110
Attention: Library 1

North American Aviation, Inc.
Space and Information Systems Division
Downey, California 90241
Attention: Library 1

Northern Research & Engineering Company
219 Vassar Street
Cambridge, Massachusetts 02139
Attention: Library 1

Solar Division of International Harvester
2200 Pacific Highway
San Diego, California 92112
Attention: Library 1

Space Technology Laboratories, Inc.
One Space Park
Redondo Beach, California 90278
Attention: Library 1

Sunstrand Denver
2480 West 70th Avenue
Denver, Colorado 80221
Attention: Library 1

Thompson-Ramo-Wooldridge Accessories Division
23555 Euclid Avenue
Cleveland, Ohio 44117
Attention: Library 1

Union Carbide Corporation
Linde Division
P.O. Box 44, Tonawanda, New York 14152
Attention: Library 1

United Aircraft Research Laboratory
East Hartford, Connecticut 06108
Attention: Library 1

Westinghouse Electric Corporation
Astronuclear Laboratory
P.O. Box 10864, Pittsburgh, Pennsylvania 15236
Attention: Library 1

Williams Research
Walled Lake, Michigan 48088
Attention: Library 1